NTNU

Norwegian University of
Science and Technology

Condition Assessment of Service Aged Medium Voltage Cable Joints During Load Cycling

Ingeborg Bjurholt

Master of Energy and Environmental Engineering
Submission date: June 2018
Supervisor: Frank Mauseth, IEL
Co-supervisor: Sverre Hvidsten, SINTEF Energi

Norwegian University of Science and Technology
Department of Electric Power Engineering

Problem Description

A significant part of the Norwegian medium voltage cable distribution system is older than the expected lifetime of 30 years. Generally, cable accessories have a shorter expected lifetime than the cable. In case of heat-shrink joints installed in the 80's, many service failures have occurred due to over-heating of the metallic connector. The condition of the insulation of the joints can be assessed by partial discharge measurements or dielectric spectroscopy. For joints and terminations, field grading materials (FGM) are often used to achieve the wanted field distribution to avoid local field enhancement and partial discharges. The dielectric properties of the FGM is influenced by the frequency of the applied voltage as well as the service conditions such as humidity and temperature.

The project will be mainly experimental and focus on the effect of load cycling on service aged MV cable joints. It is of interest to compare PD measurements on-line and off-line at 50 and 0.1 Hz in addition 50 Hz measurements under load-cycling.The PDs should also be localised using acoustic PD measurements. Break-down testing should also be performed at the end of the testing for estimation of the rest life-time. Finally, a dissection of joint should be performed to find the exact location and reasons for the measured PDs.

The work will be a continuation of previous project/master works in 2016/17.

Preface

This master thesis was carried out at the Norwegian University of Science and Technology(NTNU), Department of Electrical Power Engineering in the spring semester of 2018. The thesis is a part of a research project with SINTEF Energy Research, Energi Norge, Nexans and 11 Norwegian electric utilities.

First and foremost, I want to thank my supervisors, associate professor Frank Mauseth at NTNU and senior research scientist Sverre Hvidsten at SINTEF Energy. It has been such an interesting year, and that is all thanks to you.

Thanks should also be given to Morten Flå, Bård Almås, Jan Arne Ervik, Arild Følstad, Kristian Thinn Solheim, Espen Eberg, Henrik Enoksen and Morten Lund Torkildsen.

I want to express my gratitude to my friends and office mates. And to my family, who I could never have done this without. Finally, a massive shout-out to Fredrik, who really should have dumped me like a month ago.

Trondheim, June 2018
Ingeborg Bjurholt

Abstract

In order to be able to take maximum advantage of the remaining lifetime of the components in the distribution network, utilities need to know the condition of the equipment as accurately as possible. When partial discharges (PD) are measured in medium-voltage cable systems, it is often chosen to disconnect the cable length and use voltage sources with frequencies of 0.1 or 50 Hz. Temperature dependence of the conductivity in the joints' field grading materials, as well as expansion and contraction of materials could potentially cause PD characteristics to be load dependent. This again means the method and time of testing may affect the results and subsequent assessment of the equipment's condition. There are few studies available in the literature where XLPE cable joints from service are characterised by PD during load cycling.

The purpose of this master thesis is to study PD activity during load cycling of field aged cable joints at 50 Hz. PD measurements are also performed at 0.1 and 50 Hz in room temperature to simulate the conditions during off-line testing. The insulation resistance of the test objects will be measured through both tests.

The conditions during on-line and off-line PD measurements have been simulated in the laboratory, where three phases from a field-age joint have been tested. During the "off-line" measurements, the inception voltage was measured with 0.1 and 50 Hz voltages in room temperature. The measurements were performed with and without voltage conditioning (50 Hz, 6 kV for 1 hour) prior to the PD measurements. On-line measurements were simulated by use of load cycling to temperatures in intervals up to 65 °C and voltage conditioning. The inception voltage of the joints was measured at stable temperature. PDs were recorded at 6 kV during the cooling of the test objects to investigate whether the PD sources are temperature dependent.

Towards the end of the experimental work, PDs in the joints were localised acoustically. Then, the break-down voltages were measured, before the dissection of the joints ended the experimental work.

The PDs that were measured appear to depend more on voltage frequency than joint temperature. In room temperature, inception voltages of 3-6 kV and 1-1.5 kV were measured at 0.1 Hz with and without conditioning, respectively. When PDIV was measured at 50 Hz in room temperature, the results were between 5.7 and 7.1 kV without and 6.1-7.6 kV with conditioning. No clear trend of inception voltages was observed when the temperature was increased. With the exception of one (very high) PDIV, all inception voltages measured during load cycling are between 6.0 and 7.1 kV, i. e. in the same range as measured at 50 Hz voltage in room temperature. The break-down voltages of the joints were found to be 65, 65 and 50 kV.

The inception voltages measured at 0.1 Hz are all less than or equal to the operating voltage, and highly dependent on how recently voltage has been applied to the joint. Based on this, it might be concluded that the measurement results at 0.1 Hz can be difficult for the utility to interpret, thus increasing the risk of misdiagnosis. On the other hand, the off-line measurement results at 50 Hz provide a realistic impression of the condition of the joints, and are also a good representation of the conditions under operation. This is confirmed by the measured break-down voltages.

Weibull analysis of the PD measured during cooling showed a decreasing number of PD sources in 2 of 3 cases. In the joint where a constant number of PD sources were identified during cooling, approximately the same number of sources was detected acoustically. Dissection of the joints after break-down voltage testing showed that 2 out of 3 failures were thermal and that all punctures occurred at the semiconductor cut-off. Traces of discharge spots and ageing due to water ingress were observed by use of microscope.

These findings indicate that the discharge sources may be temperature dependent, but that more investigations are necessary before any conclusions can be drawn.

Sammendrag

For å kunne utnytte levetiden til distribusjonsnettets komponenter maksimalt, er det ønskelig å få best mulig vurdering av utstyrets tilstand ved bruk av tilstandskontroll. Når delutladninger (PD) måles i mellomspente kabelanlegg, velges det ofte å ta kabellengden ut av drift og bruke spenningskilder med 0,1 aller 50 Hz spenning. Temperaturavhengighet av ledningsevnen i skjøters feltstyring, samt utvidelse og sammentrekning av materialer gjør at delutladningenes amplitude og antall kan variere med lastforholdene. Dette gjør igjen at valg av metode og måletidspunkt vil kunne påvirke målinger og tilstandsvurderingen. Det er få studier tilgjengelig i litteraturen der PEX-kabelskjøter fra drift er karakterisert med PD under lastsykling.

Formålet med denne masteroppgaven er å studere PD-aktivitet under lastsykling av feltaldrede skjøter ved 50 Hz. I tillegg gjøres målinger ved 0,1 og 50 Hz, samt motstandsmålinger («megging») ved romtemperatur for å etterligne forholdene ved en off-line-måling.

Forholdene under on-line og off-line PD-målinger har blitt simulert i laboratoriet der tre faser fra en feltaldret skjøt har blitt testet. Under «off-line» målingene ble tenn- og slukkespenning målt med 0,1 og 50 Hz spenning ved romtemperatur. Målingene ble utført med og uten spenningskondisjonering (50 Hz, 6 kV i 1 time) i forkant av PD-måling. «On-line» målinger ble simulert ved bruk av lastsykling til temperaturer i intervaller opp mot 65°C og spenningskondisjonering. Skjøtenes tenn- og slukkespenning ble målt ved stabil temperatur. For å undersøke om utladningskildenes temperaturavhengighet, ble PD også målt ved driftsspenning på 6 kV under nedkjøling av skjøtene.

Mot slutten av det eksperimentelle arbeidet ble det gjennomført akustisk lokalisering av PD, deretter ble skjøtenes gjennomslagsspenning målt, før de til slutt ble dissekert.

Resultatene viser at spenningens frekvens har mer betydning for nivå av tennspenning, enn skjøtens temperatur. I romtemperatur måles det tennspenninger på 1-1,5 kV uten kondisjonering og 3-6 kV med kondisjonering ved 0,1 Hz. Ved 50 Hz ble det målt tennspenninger mellom 5,7 og 7,1 kV uten- og 6,1-7,6 kV med kondisjonering. Det ble ikke observert noen klar trend i tennspenning når temperaturen ble økt. Med unntak av en (svært høy) måling, ligger alle tennspenningene i området mellom 6,0 og 7,1 kV, altså i samme område som hva som ble målt med 50 Hz spenning i romtemperatur. Skjøtenes gjennomslagsspenning ble målt til 65, 65 og 50 kV.

Tennspenningene målt ved 0,1 Hz er alle like eller mindre enn driftsspenning, og svært avhengige av om skjøten nylig har blitt påtrykt spenning. Basert på dette kan det konkluderes at måleresultatene ved 0,1 Hz kan være vanskelige å tolke, og dermed gi feil i tilstandsvurderingen. På den andre siden gir de «off-line» måleresultatene ved 50 Hz et realistisk inntrykk av skjøtenes tilstand, og en god representasjon av forholdene under drift. Dette ble bekreftet av de målte gjennomslagsspenningene.

Weibull-analyse av delutladningene som ble målt under nedkjøling viser i 2 av 3 tilfeller at antall utladningskilder synker med skjøtens ledertemperatur. I tilfellet der et konstant antall PD-kilder ble målt under nedkjøling ble ca. like mange kilder detektert akustisk. Dissekering av skjøtene etter test av gjennomslagsspenning viste at 2 av 3 gjennomslag var termiske, og at alle punkteringer skjedde ved halvlederavtaket. Spor etter utladningsområder og aldring som et resultat av vann, ble observert ved hjelp av et mikroskop.

Funnene peker mot at utladningskildene kan være temperaturavhengige, men at det kreves flere undersøkelser før noe kan konkluderes sikkert.

Contents

1 Introduction **1**

1.1 Background . . . 1
1.2 Aim of the Master Thesis . . . 1
1.3 Experimental Work . . . 2
1.4 Thesis Structure . . . 3
1.5 Other Remarks . . . 3

2 Theory **4**

2.1 Condition Assessment . . . 4
2.1.1 Definition of Ageing . . . 4
2.2 Partial Discharges . . . 4
2.2.1 Townsend Mechanism Applied to Gaps in Cables . . . 5
2.2.2 Availability of Start Electrons . . . 6
2.2.3 Partial Discharge Inception and Extinction Voltage . . . 6
2.2.4 The ABC Equivalent . . . 7
2.2.5 The Extended ABC Equivalent . . . 7
2.2.6 Frequency Dependence of Partial Discharges . . . 8
2.2.7 Partial Discharge Measurement Principle . . . 8
2.2.8 Apparent Charge, q_a . . . 9
2.3 Cable Joints . . . 9
2.3.1 Field Grading . . . 10
2.3.2 Resistive Field Grading . . . 10
2.3.3 Effect of External Factors on the Field Grading Material . . . 12
2.4 Previous Work on PD in Loaded Cable . . . 13
2.4.1 PDIV as a Function of Temperature in a Field Aged Joint . . . 13
2.4.2 PD during Overheating of Paper Insulated Lead Covered (PILC) Belt Cables . . . 14
2.5 PD Testing of Medium Voltage Cable Joints in the Field . . . 16
2.5.1 On-line and Off-line PD Measurements . . . 16
2.5.2 PD Measurements at 50 and 0.1 Hz . . . 16
2.6 Sources of Noise . . . 17
2.7 Insulation Resistance Measurements . . . 17
2.8 Acoustic localisation of PD . . . 17
2.9 Data Analysis . . . 18
2.9.1 Phase Resolved Partial Discharge Analysis . . . 18
2.9.2 Weibull Analysis . . . 19

3 Test Object **20**
3.1 The Condition of the Test Object . . . 20
3.1.1 Measurements on Test Object while still in Service . . . 20
3.1.2 Observations of Deformation and Water Ingress . . . 20
3.2 Preparing the Test Objects . . . 21
3.2.1 Application of Aluminium Tape . . . 21
3.2.2 Re-sizing and Lugs . . . 22
3.2.3 End Terminations . . . 22
3.2.4 Thermocouples and Armaflex . . . 23
3.2.5 Preparations for Acoustic PD localisation . . . 23
3.2.6 Preparations for Break-down Voltage Testing . . . 24

4 Method **25**
4.1 Introduction . . . 25
4.2 Partial Discharge Detection Method . . . 26
4.3 Experimental Setups . . . 27
4.3.1 PD Measurements at 50 and 0.1 Hz Test Voltage . . . 27
4.3.2 PD Measurements During Current Cycling . . . 28
4.3.3 Acoustic localisation of PD . . . 29
4.3.4 Break-down Voltage Testing . . . 30
4.4 Preparation and Reference Testing of the Dummy Cable . . . 32
4.5 General Experimental Procedures . . . 33
4.5.1 Conditioning of the Test Object . . . 33
4.5.2 Partial Discharge Inception and Extinction Voltages . . . 33
4.5.3 Insulation Resistance Measurements . . . 34
4.6 Stage 1 Measuring Procedures . . . 34
4.6.1 Resistance Measurements . . . 34
4.6.2 VLF PDIV and PDEV . . . 35
4.6.3 50 Hz, 4 Minute Step Intervals . . . 35
4.6.4 50 Hz, 1 Minute Step Intervals . . . 35
4.7 Stage 2 Measuring Procedures . . . 35
4.7.1 Insulation Resistance Measurements . . . 36
4.7.2 Heating of the Joint by Resistive Losses . . . 36
4.7.3 Current Magnitudes for Temperature Cycling . . . 37
4.7.4 Partial Discharge Measurements at Stable Temperature . . . 37
4.7.5 Partial Discharge Measurements During Cooling of the Joint . . . 38
4.8 Stage 3 Measuring Procedures . . . 38
4.8.1 Acoustic PD localisation . . . 38

4.8.2 Break-Down Voltage Testing . . . 39
4.9 Estimation of Conductor Temperature . . . 39
4.10 Data Processing . . . 40

5 Results and Discussion **41**
5.1 Stage 1: "Off-line" and Reference Testing . . . 41
5.1.1 Resistance Measurements . . . 41
5.1.2 Partial Discharge Measurements . . . 41
5.2 Stage 2: Simulation of Service Conditions . . . 43
5.2.1 Insulation Resistance Measurements . . . 43
5.2.2 Stable Temperatures During Load Cycling . . . 45
5.2.3 PDIV and PDEV . . . 47
5.2.4 PD During Cooling of the Joint . . . 49
5.3 Stage 3: PD localisation, Break-Down Voltage and Dissection . . . 54
5.3.1 Acoustic Localisation of PD . . . 54
5.3.2 Break-Down Voltages . . . 56
5.3.3 Observations from Dissection . . . 56
5.4 Analysis of PDIV Measured "On-line" and "Off-line" . . . 60
5.5 Analysis of Findings About PD Sources . . . 61

6 Conclusions **62**

7 Further Work **63**

A Equipment List **67**

B Testing Aluminium Tape Glue Resistance **68**

C Initial Testing of Cycling Loads **70**

D COMSOL Simulation **71**
D.1 Introduction . . . 71
D.1.1 Description of the System being Modelled . . . 71
D.2 Building the Model: First Draft . . . 72
D.2.1 Basic Features . . . 72
D.2.2 Model Geometry . . . 72
D.2.3 Magnetic Fields Conditions and Properties . . . 73
D.2.4 Heat Transfer in Solids: Conditions and Properties . . . 74
D.2.5 Electromagnetic Heat Source . . . 74
D.2.6 Material and Their Properties . . . 75
D.2.7 Meshing . . . 76

D.2.8 Global Definitions 76
D.2.9 Solver Settings 76
D.2.10 Data Sets 76
D.3 Second Draft: Adjusting the Model to Observations 77
D.3.1 Evaluation of the first draft 77
D.3.2 Parametric Sweep of the Convective Heat Flux Coefficient 78
D.3.3 Parametric Sweep of the Thermal Insulation Thickness 78
D.3.4 Parametric Sweep of the Thermal Insulation Density 79
D.3.5 Parametric Sweep of the Heat Capacity of the Thermal Insulation 80
D.3.6 Parametric Sweep of the Thermal Insulation Thermal Conductivity 80
D.3.7 Chosen Parameters 81
D.3.8 Comparison of Simulated and Measured Temperatures at 350 A Load Cycling 81
D.3.9 Error Sources 82

E Noise Filtering of PD Streams **83**

F MATLAB Scripts **85**

G PRPD Plots of PD at 6 kV Right Before Current was Turned Off **89**
G.1 Joint 1 89
G.2 Joint 2 90
G.3 Joint 3 92

H Weibull Plots of PDs Recorded during Cooling of the Test Objects **94**
H.1 Joint 1 94
H.2 Joint 2 103
H.3 Joint 3 112

1 Introduction

1.1 Background

With an increasing share of the medium voltage cable system reaching the end of its expected lifetime, it becomes critical to know the condition of the equipment. This information enables the utilities take full advantage of the remaining lifetime of the equipment. For them, whether or not to replace equipment represents an important investment decision. This is the motivation for developing as accurate condition assessment tools as possible. Measuring partial discharges (PDs) is one such method, with which defects in the equipment can be identified.

The loading experienced by cable distribution systems varies, by time of day, day in the week and time of year. The temperature of the cable system will follow the loading due to resistive losses. An increased integration of power from renewable and intermittent sources such as wind and sun, further intensifies the load variations.

In a cable installation, the joints and end terminations are the most vulnerable to faults. This is a result of the field control challenges associated with semiconductor cut-offs. The cables that were installed in the 80's are generally joined by heat shrink joints where resistive field grading is used to redistribute the electric field in critical areas. The conductive properties of resistive field grading materials have been shown to depend on the temperature, humidity, ageing and electric field strength, [1].

PD testing of cable systems can performed as it is either on-line- in service, or off-line, coupled to an external voltage source. Voltage sources with several different frequencies are used, these are typically:

- Sine voltages with frequencies ranging from 0.1 - 50/60 Hz
- Oscillating Wave Test System (OWTS) with frequencies from 300 to 500 Hz.

Off-line PD testing is not, however, able to detect whether the PD characteristics are varying with loading conditions or not.

There are few studies in the literature about whether the PD's in XLPE cable joints depend on loading. This issue was investigated on mass impregnated distribution cables in [2].

A Condition Assessment Case The test object that will be used in this thesis is the result of a condition assessment aided reinvestment decision. When the Norwegian utility BKK renewed one of their substations, they had to determine whether the associated cable system needed to be renewed as well. Completely replacing the cable would invoke very large costs, as one would have to open up the trench it is placed in.

Very low insulation resistance measurements revealed possible defects in the cable. Localisation of PD revealed that it was most likely occurring in the middle of the cable length, where a joint was known to exist. It was therefore decided to replace the joint. New insulation resistance measurements after this showed that the cable itself was aged by water treeing, but not critically.

1.2 Aim of the Master Thesis

The main goal of this master thesis is to compare on-line and off-line PD measurements in terms of how well they describe the condition of a three-phase field aged medium voltage cable joint. This will be done experimentally.

Off-line conditions are simulated by performing PD measurements at room temperature. The test objects are excited by 0.1 and 50 Hz voltage sources. On-line measurements are simulated in the lab by load cycling and voltage conditioning, and PD is measured by application of voltage at power frequency.

When heated and cooled, the field distribution in the joint will be shifted- which could initiate PDs. If caused by malfunctions of the field grading material, PDs are likely to be located by the cut-off of the cable semiconductors.

In addition, the different layers of cable joints will expand and contract at different paces during temperature variations. This can cause temporary, or permanent delaminations, and potentially also initiate sites for PD.

A second aim of the thesis is to investigate whether the PD sources in the cable joints are, in fact, load dependent.

Consequently, these are the questions the thesis work will be designed to answer:

- How do the PDs measured "off-line" at 0.1 and 50 Hz compare to each other?
- How do the PDs measured at "off-line" conditions compare to the PDs that are measured during load cycling?
- Are the defects that cause PDs in cable joints temperature dependent?

1.3 Experimental Work

The majority of the master thesis work is experimental. It is divided into three stages, covering different aspects of the condition assessment of the cable joints. In the first stage, reference testing and "off-line" PD measurements are done. Then, online conditions are simulated by load cycling and voltage conditioning in stage 2. Here, PDs are measured at stable temperature and during cooling of the joints. The final stage focuses on identification of defects causing PD and validation of the findings from the first two stages. It comprises of acoustic localisation of the PD sources and breakdown voltage testing, followed by a dissection of the joints.

The measurements performed in the different stages are summarised below:

1. Stage 1: Reference and "Off-line" PD Measurements
   (a) Insulation resistance measurements
   (b) Measurements of PDIV and PDEV with VLF(0.1 Hz) voltage
   (c) Measurements of PDIV and PDEV with 50 Hz voltage
2. Stage 2: "On-line" PD Measurements
   (a) Insulation resistance measurements
   (b) Temperature tracking
   (c) Measurements of PDIV and PDEV at stable temperature
   (d) Recording of PDs at nominal voltage during cooling
3. Stage 3: Localisation and Destructive Testing
   (a) Acoustic localisation

(b) Testing of breakdown voltage

(c) Dissection

In addition to the experimental work, considerable effort is put into developing a COMSOL model which is used to simulate the thermal conditions in the test objects.

1.4 Thesis Structure

This thesis consists of 7 chapters. The theory that is used to develop and discuss the thesis work is presented in chapter 2. Chapter 3 introduces the test objects that were used in the thesis work along with how they were prepared. In chapter 4, the work that was done, including the setups, experimental procedures and data processing are described. The results from the work described in chapter 4 are presented and discussed in chapter 5. Each stage is treated by a separate subsection in the chapter, before the findings are analysed in light of the thesis aims. Conclusions are drawn and potential for further investigations is discussed in chapters 6 and 7, respectively.

1.5 Other Remarks

- Parts of the theory and method sections have been taken from the specialisation project that serves as a preliminary study to this work, [3].
- Unless stated otherwise, all voltages and currents in the thesis are given as Root Mean Square(RMS).
- It is assumed that the reader has knowledge equivalent to a bachelor's degree in electrical power engineering.

2 Theory

This section introduces the theory that is used in the development and discussion of the thesis.

It begins by introducing the concept of condition assessment, before partial discharges and associated models are explained. After this, the section moves on to introducing cable joints, the need for field control, and how field grading materials are affected by external factors. The section moves on to reviewing the studies that has been done on the topic previously. After this, the different methods of PD measurements in the field are discussed. Sections about the other condition assessment methods that are used in the thesis, insulation resistance measurements and acoustic localisation follows. The section ends by introducing the data analysis methods that will be used to plot the results.

2.1 Condition Assessment

Modern societies are becoming increasingly dependent on their electric power supply. High voltage power apparatus are an integral part of of the delivery of electric power. The apparatus has long service lives, but are also very expensive. Replacing the equipment because of its age, even if it is in a good condition, is very uneconomic for the utility that owns it. The ideal solution would be to replace the equipment just before its failure, which is possible if its residual life is known, [4]. Estimation of the residual life of equipment is the ultimate goal of condition assessment. This is attempted reached by help of diagnostic testing. This is challenging due to the different, and complex stresses that a power apparatus is exposed to during its service life, [4].

Diagnostic testing can be either destructive or non-destructive. During non-destructive testing, the dielectric characteristics of the material are measured. Examples of this is partial discharge, insulation resistance and tanδ measurements. Destructive testing can be used to determine the dielectric strength or lifetime of the equipment. It is performed either as a step voltage, or duration test, [5].

2.1.1 Definition of Ageing

"Ageing: Irreversible deleterious change to the serviceability of insulation systems. Such changes are characterised by a failure rate which increases with time." [6]

2.2 Partial Discharges

A partial discharge(PD) is an electric discharge that only partially bridges the insulation between the conductors. PD leads to ageing of the insulation, and can be detected, [7].

PD can be classified into three groups. These are internal discharges, surface discharges and corona discharges, [5].

- Internal discharges can cause, and be caused by treeing, occur in cavities, adhering to an electrode or completely surrounded by the insulation material.
- Surface discharges happen along gas or liquid-bounded interfaces where there are high tangential field strengths.
- Corona discharges occur around sharp points of materials that typically have a high permittivity.

The energy released by partial discharges in cavities cause the material surrounding it to erode. As erosion progresses, pits- and electric tree growth is initiated. Hence PDs are both a symptom- and a culprit of ageing in electrical equipment [5].

The gaps where the PDs in cable joints occur are typically very small. Because the Townsend mechanism is best suited to model discharges where the product of gap distance and pressure is smaller than 5 bar·mm, it is best suited to describe the PD [8].

2.2.1 Townsend Mechanism Applied to Gaps in Cables

The electric field in a cavity is the sum of two contributions. The first field component is due to the voltage applied and the geometry of the void. The second field component is a result of any space and surface charges left after previous discharges, [9].

The electric field accelerates free electrons towards the positive electrode. The distance the electron is allowed to travel, and hence the speed and energy it accumulates, before colliding with another particle, is inversely proportional to the gas density in the cavity. When a collision happens, the probability of it being ionising is proportional to the energy of the electron. This probability, per unit length in the field direction is described by Townsend's first ionisation coefficient α. The electrons after an ionising collision will be accelerated and collide once more. If this happens many times, a cascade of electrons called an electron avalanche is created[10]. Each avalanche can be detected as a partial discharge. An illustration of the development of avalanches can be seen in figure 1.

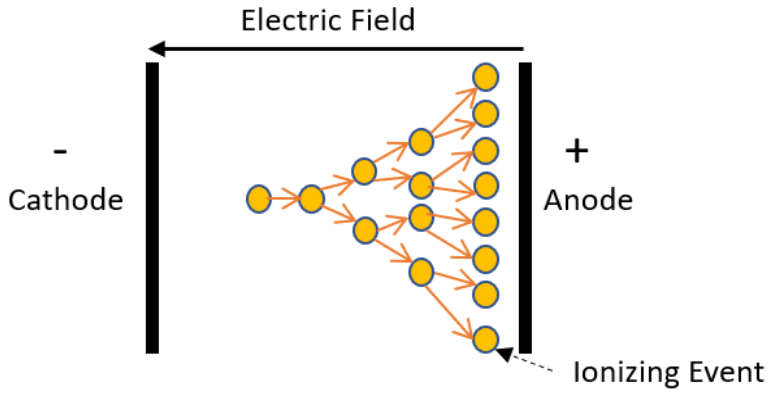

Figure 1: Illustration of the build-up of avalanches. A cascading amount of electrons are created by ionising collisions.

The voltage necessary to initiate a PD in a gap is dependent on the rate of rise of the voltage, [11]. It is also considered a function of field strength, pressure and distance. This relationship is quantified by the Paschen curve, where sparkover voltage is a function of the product of the distance between the electrodes and the gas pressure. The Pachen curve of air is given in figure 2, [10]. Due to the small size of the gaps, the area around the curve minimum is the most relevant.

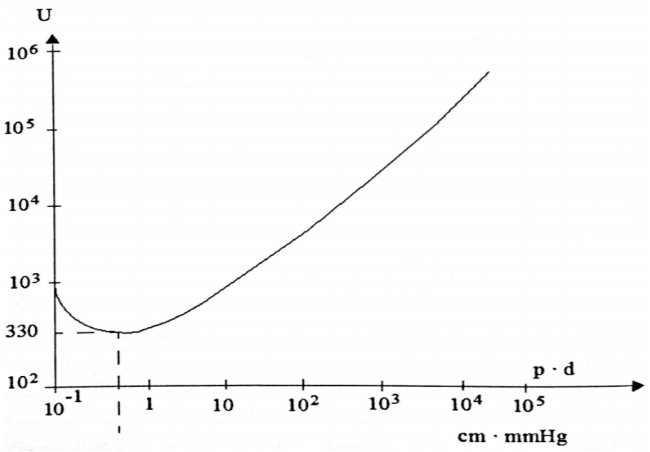

Figure 2: The Paschen curve of air illustrates how the sparkover voltage in a gap is a function of its pressure and distance [10].

2.2.2 Availability of Start Electrons

The large degree of randomness in start electron availability makes PD a highly stochastic process. The charges that are left after a discharge are deposited as either space or surface charge. The remaining electrons can act as start electrons in a new avalanche. The surface charges decay by conduction along the surface of the cavity. This happens with a time constant that depends on the surface conductivity of the void, it is given in equation 1, [9].

$$\tau_{SC} = \frac{\epsilon_0 r_c}{2\sigma_s} \tag{1}$$

Where ϵ_0 is the permittivity of vacuum, r_c is the radius of the conducting surface and σ_s is the surface conductivity. As can be seen in equation 1, the larger the surface conductivity, the faster the surface charges decay.

2.2.3 Partial Discharge Inception and Extinction Voltage

Partial discharge inception voltage (PDIV) is defined as the applied voltage where repetitive PD are first observed in the test object, when the voltage applied to the test object is increased gradually from a low voltage where PD doesn't occur, [7]. A decrease of the PDIV of a test object is typically associated with degradation of the test object, [12].

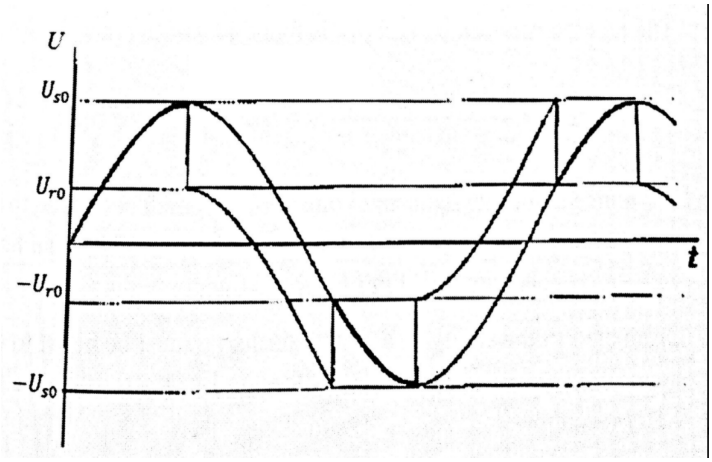

Figure 3: illustration of the voltage across the cavity at PDIV. U_{s0} is the ignition voltage and U_{r0} is the remanent voltage across the cavity after a discharge, [10].

Correspondingly, partial discharge extinction voltage (PDEV) is defined as the applied voltage where PD ceases to occur in the test object, when the voltage is gradually decreased from a higher voltage where PD is observed, [7]. PDEV is generally expected to be lower than PDIV as the discharge activity provides starting electrons to new discharges.

2.2.4 The ABC Equivalent

The ABC equivalent is the simplest way of explaining the voltage, and hence electrical field distribution within the test object. The model splits the capacitance of the test object up into three parts. C_c is the capacitance over the cavity in which the discharges occur. C_b represents the capacitance that is in a series with C_c, while C_a represents the rest of the test object. The model assumes that the capacitive impedance of the dielectric is much smaller than the resistive impedance, and hence dominates it [10].

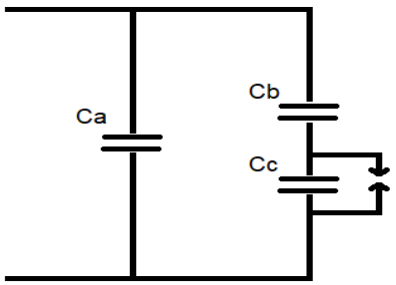

Figure 4: Illustration of the capacitances in a test object, according to the ABC equivalent model

In the case where no discharges occur, the voltage across the cavity can be found from the equivalent model;

$$V_c = \frac{C_b}{C_b + C_c} \cdot V_{applied} \tag{2}$$

2.2.5 The Extended ABC Equivalent

During the development of the ABC model, it was argued that as the reactance in the material is much smaller than the resistance, resistance becomes negligible in a parallel coupling. If, however,

the insulation resistance is low, it can't be considered negligible in a parallel coupling with the system reactance any longer. In these cases, the accuracy of the ABC equivalent model is increased if each capacitance is parallel coupled to a resistor, making up an extended ABC equivalent model. [13].

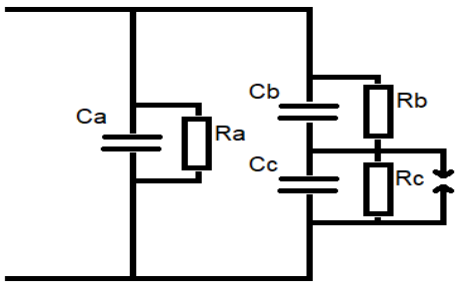

Figure 5: Illustration of the extended ABC equivalent model

Now the voltage across the cavity in the case with no occurring discharges becomes as can be seen in equation 3.

$$V_c = \frac{\frac{R_c}{j\omega C_c R_c + 1}}{\frac{R_c}{j\omega C_c R_c + 1} + \frac{R_b}{j\omega C_b R_b + 1}} \cdot V_{applied} \tag{3}$$

This makes voltage across the cavity is a function of resistance, as well as the frequency of the applied voltage. The frequency dependence of the partial discharge mechanism is explained in further detail in section 2.2.6.

2.2.6 Frequency Dependence of Partial Discharges

For a discharge to happen, it is as discussed previously, necessary to have both the required electric field and start electron in the cavity. If there are no electrons available, there will be a time lag between the breakdown strength of the electric field is reached and discharges occur. This is called the statistical time lag, Δt_{lag}. The statistical time lag causes PDs to be phase shifted forwards, and it can also cause PDs to occur at other voltages than the inception voltage level, [14].

The distortion caused by the statistical time lag is highly dependent on the frequency of the applied voltage. If Δt_{lag} is much shorter than the period of the voltage, the the lag of the discharges can be considered negligible. On the other hand, if Δt_{lag} is similar to, or larger than the voltage period, the phase and voltage level of the discharge might be shifted significantly. This can lead to larger, and fewer discharges per cycle, [14].

The relationship between the charge decay time constant (given by equation 1) and the period of the applied voltage must also be considered. If the decay time constant is larger than the voltage period, any charge will have been transported away before the next time the breakdown strength is reached. Hence, the charges won't affect the field distribution in the cavity. If, however, the decay time constant is low compared to the voltage period, there remains charges in the cavity that will alter the electric field. The result of this is a phase distortion of the discharges, whose direction depends on the field contribution of the charges.

2.2.7 Partial Discharge Measurement Principle

When a partial discharge occurs, the cavity is essentially short circuited and the voltage across it drops. This results in a second voltage drop across the terminals of the test object.

If the test object is parallel coupled to a large coupling capacitor(C_k), the capacitor compensates any voltage drop in the test object, so that the voltage across the coupling remains balanced. The compensation is in the form of a current pulse, which is proportional to the voltage drop across the test object. By inserting a measuring impedance into the path of the current pulse, the pulse can be quantified by the resulting voltage across the impedance. As the internal capacitance of the test object also supplies a current pulse, it is important that the coupling capacitance is larger than the capacitance of the test object. This ensures that the discharge magnitudes are in fact possible to detect. The measurement principle is illustrated in figure 6, ([7]).

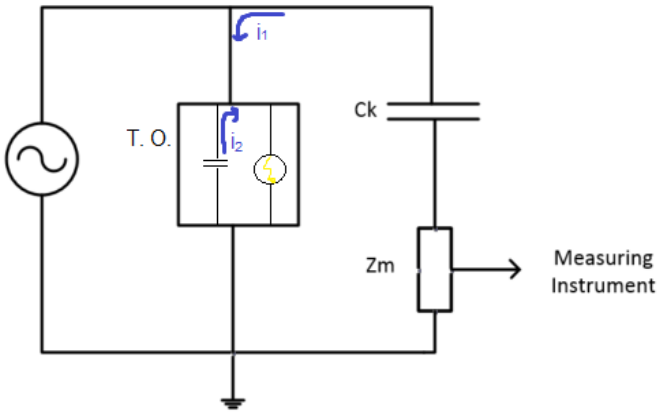

Figure 6: A simple illustration of the conventional PD measurement circuit, [7]. C_k is the coupling capacitor. I_1 and i_2 represents the compensating currents provided by the coupling capacitor and the test object's own capacitance, respectively.

2.2.8 Apparent Charge, q_a

The apparent charge, q_a, is the measurable quantity of the partial discharge magnitude. This is the charge that is transferred to the test object from the coupling capacitor in order to restore the voltage across it. The charge is found by integration of the current pulse detected by the measuring impedance, this can be seen in equation 4, [10].

$$q_a = \int \Delta i \cdot dt = \Delta V \cdot C_a \tag{4}$$

Where C_a is the capacitance across the test object.

2.3 Cable Joints

There are practical limits to how long cables can be manufactured or stored in one piece. Therefore, they are connected by joints, either in the factory, or on site.

When two cables are joined, their outer screen and semiconductors, insulation and inner semiconductors are removed. The conductors are joined in a metallic connector. If this is not done well, the result is a high contact resistance. High contact resistances can lead to significant heating, and resultant ageing of the joint, even at relatively small loads. The combination of a sharp point and large potential difference when cuts are made in the outer semiconductors will cause a very high electric field strength if no actions are taken. Therefore, some form of field control is applied across the joint, before a layer of electrical insulation. The outer screens are connected by a semiconductor and the joint is covered in a copper screen which is connected to that of the

cable's. Some form of mechanical protection and waterproofing completes the joint. Cable Joints can be built in a multitude of ways. A picture of a heat shrink joint can be seen in figure 7, [15].

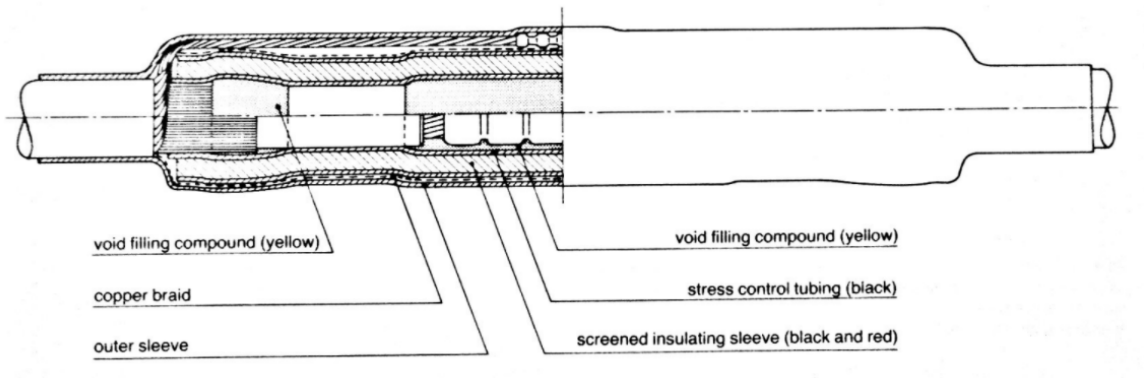

Figure 7: Illustration of the construction of heat shrink joints, [16].

2.3.1 Field Grading

The objective of field grading is to avoid too high local field strengths in the different devices. There are four different main methods [8];

1. Electrode grading, where the field strength is controlled by the electrode's geometry.
2. Epsilon grading, where the permittivity of the materials are utilised to control the field.
3. Condenser grading, where a favourable field distribution is ensured by keeping a constant capacitance around the device.
4. Resistive field grading. As this is utilised in the stress control tube in the joints that will be used as test objects in this work, it is elaborated further in section 2.3.2.

Methods 1-3 are dominated by capacitive currents and are therefore grouped as capacitive grading, while method number 4 is dominated by resistive currents.

2.3.2 Resistive Field Grading

Resistive field grading is used in both DC and AC applications. It is often much more compact than capacitive field grading. As space is limited within cables, resistive field grading is favorable to use if the conditions allow it. Resistive field grading materials consist of a thermoplastic polymeric material and filler particles that can be either conductive or semi-conductive. The field distribution in a cable termination after resistive field grading has been applied is illustrated in figure 8.

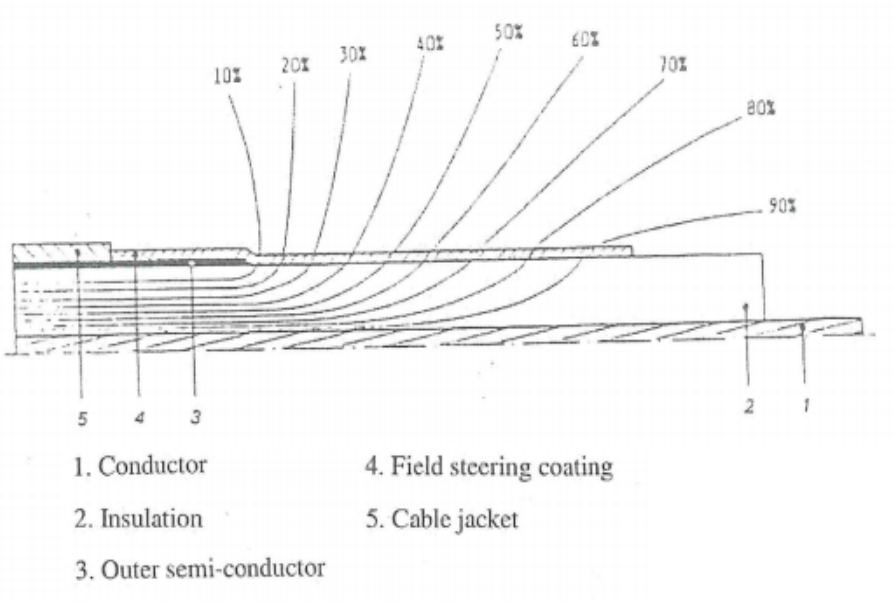

Figure 8: Equipotential field lines in a cable termination with resistive field grading [15]

Resistive field grading works by that when a large electrical stress is applied to the material, its conductivity increases tremendously [17]. The closer the stress tube is to a localised high field strength, the higher will its conductivity be, and hence the lower the resistance. The lower the resistance, the lower is the voltage dissipated, and hence the electric field in the part of the stress tube. In this way, the electric field is forced to spread. An equivalent circuit of the field grading material applied to a cable termination is presented in figure 9. This is only possible if the material has a strongly non-linear conductivity-electric field characteristic, such as the one illustrated in figure 10.

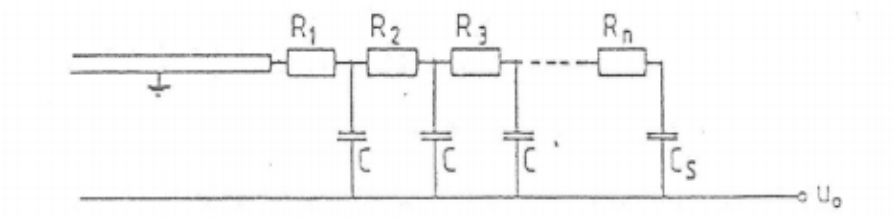

Figure 9: Equivalent circuit of resistive field grading material in a cable termination[15]

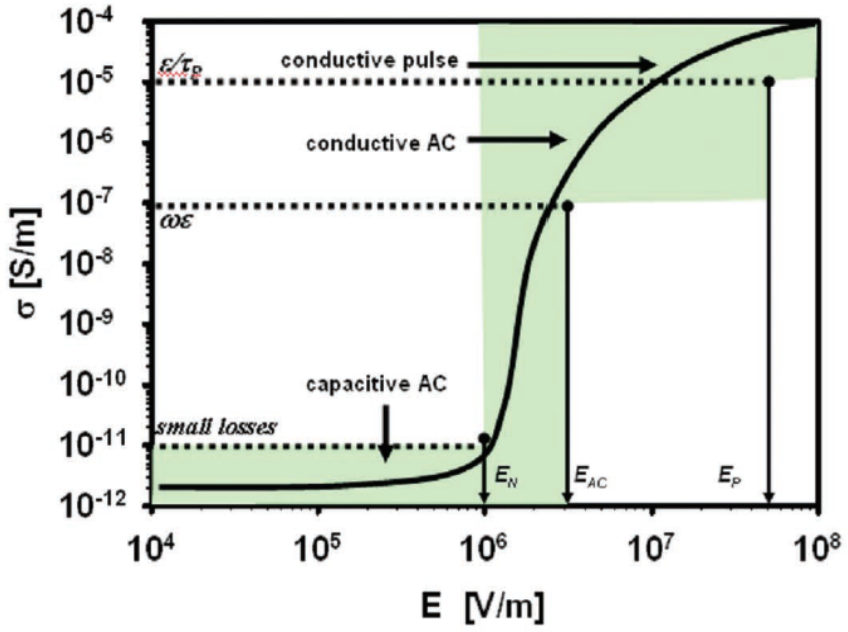

Figure 10: Illustration sketch of the $E-\sigma$ characteristic of an ideal non-linear resistive field grading material for ac applications [17]. As the field strength surpasses a critical value, the conductivity of the material increases strongly.

Both resistive field grading and conductor contact resistance can produce a considerable amount of heat, due to resistive losses. If heating occurs during prolonged periods, this might cause thermal ageing. The losses from maximum electrical stresses are considered negligible as they generally happen over short amounts of time.

2.3.3 Effect of External Factors on the Field Grading Material

The dependence of the field grading tube on temperature, humidity, electrical stress and thermal ageing was investigated in [1]. The stress tube investigated in [1] is comparable to the stress field grading material of the test objects in this thesis work. The conductivity of a dry virgin sample of the field control tube in room temperature was determined to be 4×10^{-12} S/m. Its dependence on external factors is summarised below.

Electric Field Strength No significant field dependence was observed up to 0.2 kV/mm, [1].

Temperature The conductivity of the stress tube was found be highly temperature dependent. The conductivity of a virgin sample was found to increase by a factor of 10^4 as the temperature was changed from $30°C$ to $150°C$ The tube was slightly less temperature dependent when aged, [1].

Humidity It was found that the conductivity of an unaged sample of the stress control tube increased by two decades when subjected to water absorption. This was observed as the relative humidity of the test object was increased from 0 to 95 %, [1].

Thermal Ageing Generally, ageing is irreversible degradation of the properties of the material. The conductivity of the stress control tube increases as a result of ageing caused by heat. The rate of ageing was found to be strongly dependent of the temperature the material was exposed to. The samples aged at 150°C had a conductivity increase rate that was more than 3 times higher than the samples aged at 98°C, [1].

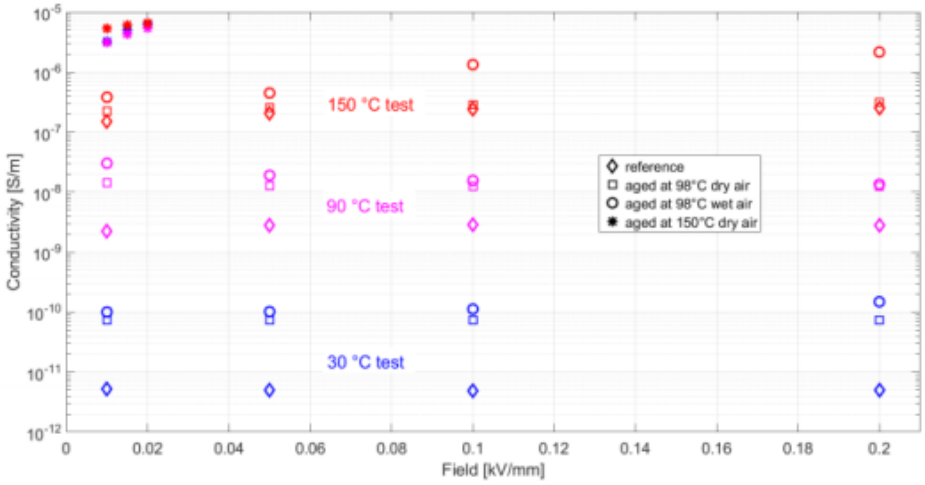

Figure 11: The conductivity of the field control tube plotted as a function of test temperature, electric field stress and ageing, [1]

2.4 Previous Work on PD in Loaded Cable

2.4.1 PDIV as a Function of Temperature in a Field Aged Joint

In the specialisation project leading up to this master thesis, [3], the temperature dependence of the PD in a field aged, medium voltage, heat shrink XLPE-XLPE cable joint was investigated. The joint had undergone considerable thermoelectric and mechanical stress. It was heated to different temperatures by load cycling and resultant resistive losses. Once at a stable temperature, PDIV and PDEV were measured. The results can be seen in figure 12

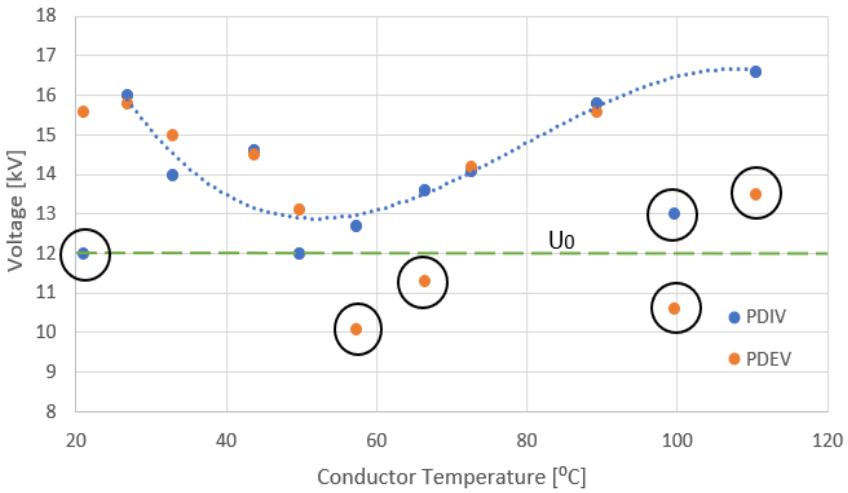

Figure 12: PDIV and PDEV of a field aged cable joint as a function of estimated conductor temperature, [3]. The stippled blue line shows the overall trend of the PDIV of the joint and the stapled green line shows the nominal voltage of the equipment. The encircled data points are not included in any trend lines.

It can be observed that the PDIV trend decreases from room temperature until the area between 50 and 70 °C. In this area, PDIV is around U_0.This is critically low as it means that if the joint was in service, it would experience continuous discharges and a potential fast failure. When the temperature is increased past this critical area, the PDIV trend increases again.

2.4.2 PD during Overheating of Paper Insulated Lead Covered (PILC) Belt Cables

Partial discharges in PILC cables were investigated in [2]. Parts of the Ph. D. thesis examined the effect of overheating on a three-phased cable sample under mechanical pressure.

By applying 500 A per phase to the sample, external testing temperatures of 55, 65, 75 and 80 °C were reached. Persistent plots of PD at 6 KV were made at each temperature, an example of such can be seen in figure 13. Based on these results, it was concluded that temperatures greater than the rated values don't initiate new PD sources.

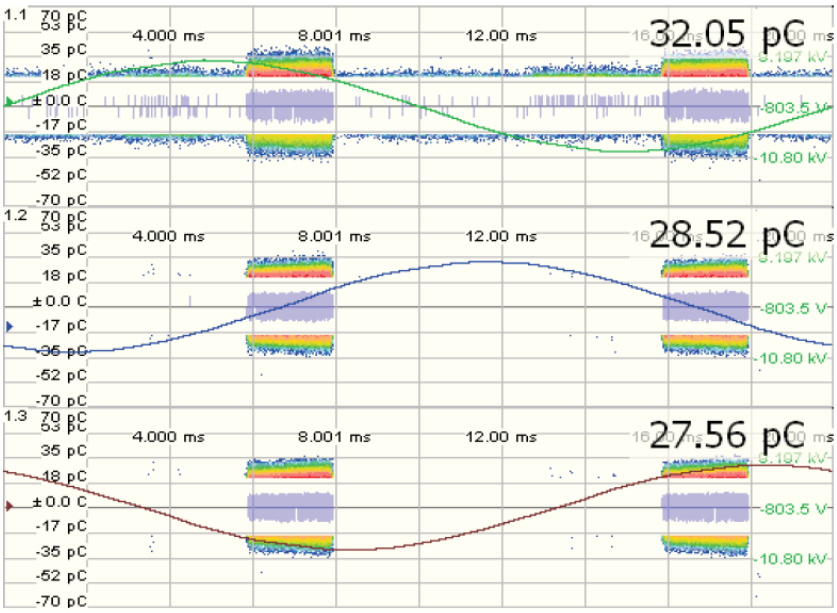

Figure 13: 20 s persistent PRDP plot of the sample at the over-temperature 75 °C, [2].

An overall reduction in PD activity was observed as the temperature increased. This was argued to be due to the increase in internal pressure that the cable experiences when overheated. When the pressure in any remaining voids increases, so will their break-down voltages. It was also mentioned that the mechanical pressure acting on the cable might force the cable impregnate into the voids- and thus extinguish them.

After this, the sample was left at 80 °C for 16 hours- and then cooled again. The PRPD pattern that was measured at 15 °C revealed that the cooling process had activated a significant amount of PD sources. This pattern can be seen in figure 14.

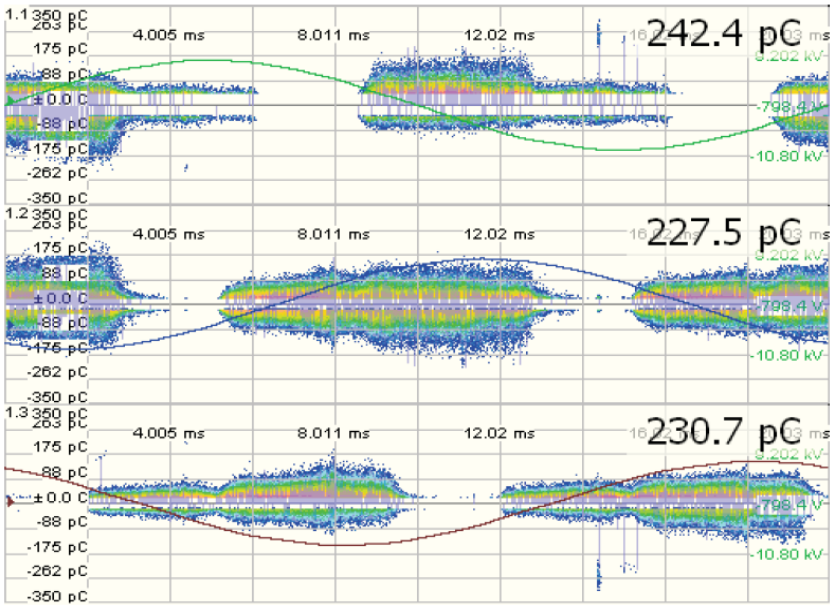

Figure 14: 20 s persistent PRDP plot of the sample at 15 °C after 16 hours at 80 °, [2].

The change of PD behaviour was explained by three conditions affected by cooling:

1. The viscosity of the impregnate is reduced, which results in a lesser ability to fill voids.

2. The cable's internal pressure is reduced, making creation of new voids likely.

3. The overheating of the cable might have stretched the lead sheath beyond its elastic limit, creating even more voids.

2.5 PD Testing of Medium Voltage Cable Joints in the Field

2.5.1 On-line and Off-line PD Measurements

The motivation for development of PD measurements as a tool is for it to be a reliable way to locate defects in cable systems. When PD is tested on cables in the field, this can be done either on-line or off-line. on-line testing is done without taking the cable out of service. There are several off-line testing methods who are all carried out by use of an external voltage source,[18]. Voltage sources with several different frequencies are used. These include 0.1 and 50 Hz sine voltages, as well as damped oscillatory voltages, so-called OWTS, at 300-500 Hz frequency. Both on-line and off-line methods have their advantages and drawbacks.

When a cable is taken out of service, the removal of voltage extinguishes any PD activity. PDIV is often 1.3-1.5 times that of PDEV. This means that during off-line PD testing, the voltage must be increased above normal operating voltage to activate PD that might have been active before the cable was taken out of service. If the cable is tested on-line without removing the voltage before testing, the PD sources that are usually active during normal operation are likely to still be active [18].

During on-line testing, discharges that are only active above operating voltage remain undetected. It is however possible to detect PD at different loading conditions. The size of some defects varies with cable loading, meaning that PD magnitude also varies with the cable loading. Thus, on-line testing can potentially detect different kinds of defects. The fact that no power outages are necessary is a significant advantage [19]. A considerable drawback is that the price of the testing is high, and therefore it is not usually prioritised for condition assessment of medium voltage cables.

Taking the cable out of service for off-line measurements is expensive, and in some cases not even possible. Also, the time available for testing is often limited. There is is a risk that defects that are prevalent at operating temperatures will not be discovered. The time limitations and stochastic nature of PD means that defects might not be activated at all. A benefit of off-line testing that should be considered is that it allows PD characterisation at multiple voltage levels, including determination of PDIV and PDEV [18].

2.5.2 PD Measurements at 50 and 0.1 Hz

A central issue with using external voltage sources for PD is that when the test object has a large capacitance, the source needs to supply a lot of reactive power at AC. One way to reduce the need for reactive power, is to lower the voltage frequency. Therefore, power cables in the field are often tested at 0.1 Hz, which is also referred to as very low frequency (VLF).

As discussed in section 2.2.6, the behaviour of partial discharges is dependent on the frequency of the applied voltage. This leads to a distortion of both the phase of the PDs, and the voltage which is necessary for them to occur. In other words, the PDIV of an apparatus might vary depending on the frequency of the voltage that is used to measure it.

Considerable efforts have been put into identifying the relationship between the PDIV's in cables measured at different voltage frequencies, two examples are included here. [11] found the PDIV at VLF to be ~ 5% larger than PDIV at power frequency. [20] did on the other hand measure cable joint

PDIV's at VLF that were a little more than half the PDIV that was measured at power frequency. Both works concluded that the matter needs further investigation.

2.6 Sources of Noise

Background noise is signals detected during PD measurements that come from other sources than the test object, [7]. Typical sources of noise are illustrated in figure 15.

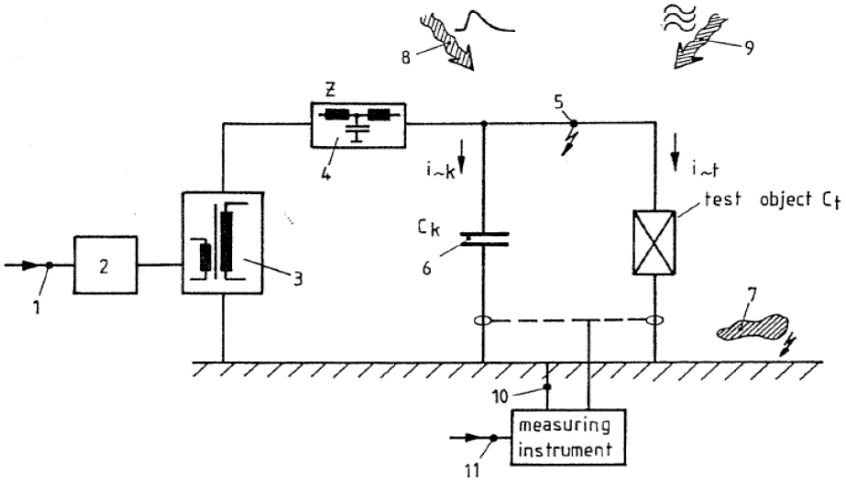

Figure 15: Typical sources of noise during PD measurements: 1. Power supply, 2. Variac, 3. High voltage source, 4. Filtering of High Voltage source, 5. Feeder line, 6. Coupling capacitor, 7. Loose conductive objects near the setup, 8. Pulse-shaped interference, 9. Radio Interference, 10. Interference in the grounding system[21]

2.7 Insulation Resistance Measurements

The resistance of the insulation of a joint can be found by applying a DC voltage and measuring the resultant leakage current. The insulation resistance is given by Ohm's law; $R = \frac{V}{I}$, and is used to characterise the condition of equipment.

For insulation to be well-functioning, it needs to have a high resistance. Otherwise, there would be large leakage currents. This means that if the insulation resistance is high(TΩ range), it is in a satisfactory condition, and vice versa. Moisture content, increased temperature and thermal ageing will reduce the detected resistance [22][23].

2.8 Acoustic localisation of PD

Partial Discharges can be measured in more ways than by its electrical properties. An alternative approach is to use the acoustic properties of PD, so-called acoustic PD detection. This method is known to be the most accurate way to localize PD sources.

There are several situations where acoustic PD detection is much more practical than electrical detection. These include test objects with large capacitances, and field measurements where there are lots of electromagnetic interference. In equipment such as transformers and switch-gear, it is critical to be able to locate the discharge source, as this is where the defect is. This is done more

accurately by acoustic than electrical methods. Furthermore, acoustic methods can be used in combination with on-line electrical methods. This can help confirm serious defects, or avoid false alarms, [24].

When a PD occurs, the energy released from it causes different phenomena. There are chemical and structural changes in the material and emission of electromagnetic waves. If the energy from the discharge evaporates the material close to it, this will behave as a small explosion. The explosion creates a mechanical wave which travels trough the structure. The waves can be detected by the right type of sensor and analysed by help of a data acquisition system, [24]. This mechanism is illustrated in figure 16.

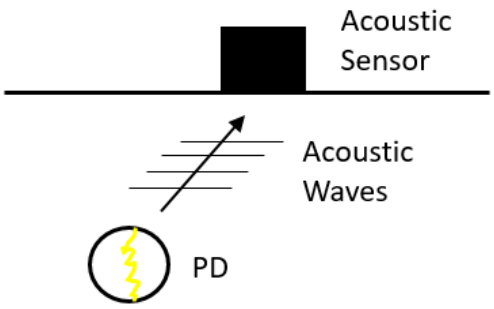

Figure 16: Illustration of the release, and detection of, mechanical waves from partial discharges in a material

The intensity of the acoustic wave is proportional to the energy, and conversely the apparent charge of the discharge that it was released by. As a wave propagates through a structure, it will gradually lose its intensity. This is a result of absorption (conversion of the wave's energy to heat), scattering of the wavefront and geometrical spreading of the wave, [24].

2.9 Data Analysis

2.9.1 Phase Resolved Partial Discharge Analysis

Phase resolved partial discharge(PRPD or PRPDA) plots is a graphical technique used to distinguish different types of PD. The phase position and discharge magnitude of PD is plotted on top of one voltage cycle. This allows the detected discharges to be compared to the applied voltage.

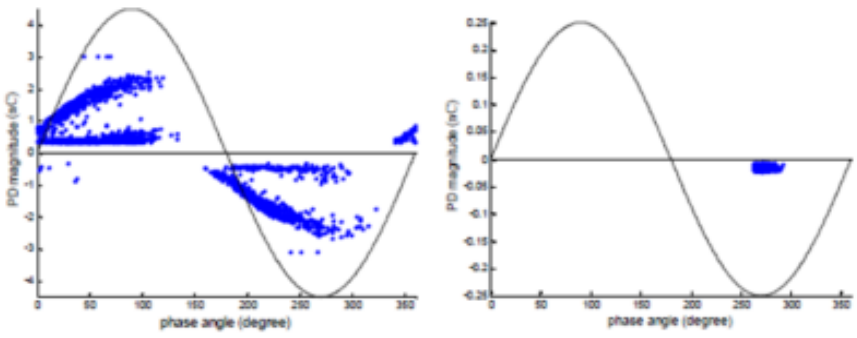

Figure 17: PRPD plots of void discharges(left) and corona discharges(right), [25].

As can be seen in figure 17, PD in cavities follow the positive growth of the sinusoidal voltage curve. In the cases where several layers or groupings of discharges are observed, this can be interpreted as a result of several defects. Discharges of near constant amplitude located at the maximum value of the voltage curve are, as seen in figure 17, identified as corona, [25].

2.9.2 Weibull Analysis

Weibull analysis is a statistical method which can be used to separate different defects that are experiencing PDs at the same time.

If one has a large number of discharge data, the probability of a PD having apparent magnitude q or lower is as given in equation 5, [10]

$$P(q) = \lim_{n\to\infty} \frac{n_0(q)}{n} \tag{5}$$

where n is the number of discharges, and n_0 is the number of discharges with an apparent magnitude of q or lower.

Due to the fact that the number of discharges is never infinite, the approximation given in equation 6 is used to plot the data, [10].

$$P(q) = \frac{n_0(q) - 0.3}{n + 0.4} \tag{6}$$

The probability distribution can also be approximated by 2-parameter and 5-parameter weibull functions, which models the case of one and two PD sources respectively, [26].

Plotting the cumulative probability as a function of apparent charge in a Weibull diagram makes it possible to see if there are one, or more PD sources. If the plot only has one slope, this is an indication of there only being one source. If there are several different slopes, it means that there likely are as many defects, [26]. This is illustrated in figure 18.

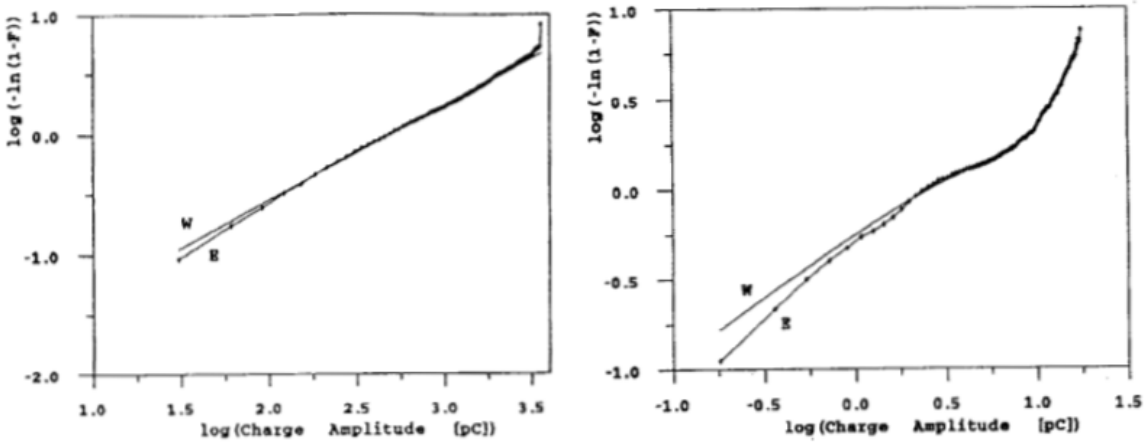

Figure 18: Left: Weibull plot of the PD in a flat cavity. With the exception of an outlier, the plot only has one slope, [26]. Right: Weibull plot of the PD from multiple flat cavity, several different slopes can be observed in the plot,[26].

3 Test Object

The test object used in this experiment is a three phased cable joint. It is a $1 \times 3 \times 240$ mm^2 stranded aluminium, XLPE-XLPE heat-shrink joint. Its insulation is EPR rubber. The cable which is joined is TXSE(T- XLPE insulation, X- no sheathing, S- concentric conductor, E- exterior sheathing, corrosion protection: PE or PP) The cable is dimensioned for 12 kV(phase to phase), and was used at a voltage of 11 kV. The phase to ground voltage applied has been 6 kV, this will be referred to as U_0. It was installed in 1987 and removed from service in 2017. The test object had not undergone any failures. A picture of the test object before the phases of the joint were separated can be seen in figure 19.

Figure 19: The three-phased cable joint that is used as the test object in the experimental work. The joint is covered in dirt from the trench it was laid in.

Being from 1987 the test object is likely to have a strippable outer semiconductor. The test object does most likely not have a water tight aluminium foil layer in its sheath. This makes the cable susceptible to water ingress, [27].

3.1 The Condition of the Test Object

3.1.1 Measurements on Test Object while still in Service

The cable system that the test object has been removed from was followed closely by the utility before it was removed from service. Insulation resistance and tanδ measurements were performed before the joint was removed. The insulation resistance that were measured are presented in table 1. This is very low, considering that a healthy insulation system has a resistance of several TΩ.

The phases were dubbed line 1, line 2 and line 3 during these measurements. Unfortunately, these specifications were not marked on the test object as it was sent to NTNU. Therefore, the relation between line 1, 2 and 3 and joint 1, 2 and 3 are not known.

Table 1: Insulation resistances of the cable system where the test object was connected, while it was still in service.

Measurement Specification	Line 1 Resistance [GΩ]	Line 2 Resistance [GΩ]	Line 3 Resistance [GΩ]
1 kV, 5 min	2.5	34.5	31.8
5 kV, 5 min	0.5	0.5	1.2

3.1.2 Observations of Deformation and Water Ingress

Deformation was observed on all three phases when they were separated. This is likely a result of the overheating the joints must have experienced while in service. The maximum temperature EPR can operate under is 90 °C, [31], so the joint must have experienced temperatures higher than

this. The overheating could either be due to overloading, or due to a high contact resistance in the metallic connector. The fact that only the joint, and not the cable was deformed suggests the latter. A picture of the deformation that was observed is included in figure 20.

A layer of green verdigris indicates that the copper of the grounding screen has been corroded. This can be interpreted as a confirmation that water has been present within the outer jacket, which means that the joints themselves are likely to have absorbed water. The joints are therefore believed to still be containing water and treated thereafter. A picture of the corrosion byproducts can be seen in figure 20.

Figure 20: Left: The flat line that can be seen on the joint is deformation caused by overheating in service. Right: There were green byproducts of corrosion of the screen inside the outer jacket of the joint.

3.2 Preparing the Test Objects

The test object arrived with all three phases in one body. Therefore, the natural first step was to remove the outer jacket and separate the phases as carefully as possible.

3.2.1 Application of Aluminium Tape

The joints were covered in a layer of aluminium tape with conducting glue, so as to keep all moisture inside the joint. Each piece of tape is fastened so it has a 1 cm overlap with the pieces next to it. After this, a layer of grounding wire is wound around the joint and fastened with PVC tape. A second layer of aluminium tape covers this as an added security. These steps are illustrated in figure 21.

Conducting glue on the aluminium tape ensures that the entire area covered by tape is at ground potential. To rule out this as a source of error, the conductivity of the aluminium tape was measured and found to be satisfactory. This is described in appendix B.

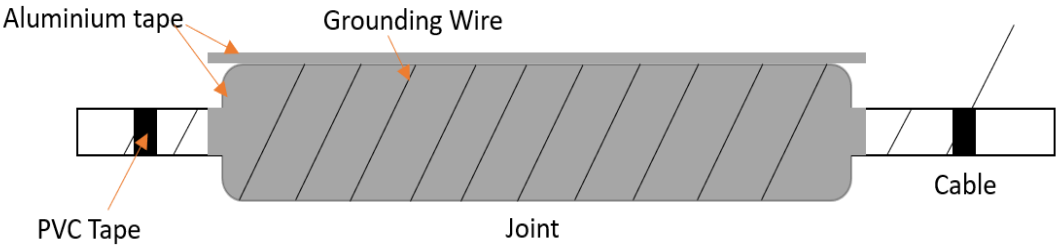

Figure 21: Illustration of the two layers of aluminium tape that are applied to the joints, with a grounding wire wound in between.

.

3.2.2 Re-sizing and Lugs

All three phases were cut into 1.9 meter long pieces, with the joint at the centre. This is a practical length as it matches that of the cycling dummy that will be used, and goes well with the size of the test cell.

The strippable outer semiconductor was peeled back 40 cm on each side. The insulator and inner semiconductor was removed down to the conductor for approximately 7 cm on each side. Cable lugs are pressured onto the conductor. Finally, the gaps between the insulator and lugs are covered in a double layer of aluminium tape to avoid any humidity diffusing out of the test object this way. This is illustrated in figure 22.

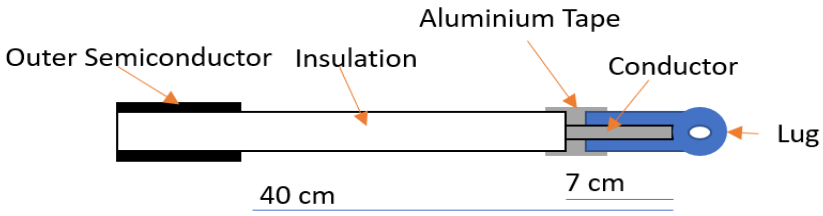

Figure 22: Illustration of the outer semiconductor being peeled back, and the conductor bared. Lugs are pressured onto the conductors, and the gap between it and the insulation is filled with aluminium tape.

After these steps, the reference resistance measurements described in section 4.6 were performed.

3.2.3 End Terminations

End terminations controlling the field between high voltage and ground are applied at the edge of the outer semiconductor.

A 12 cm long layer of field grading material is applied, so that it overlaps the semiconductor by 1 cm, and also itself by 1 cm. It is made sure that both edges are even and the field grading material is tightened. Self-vulcanising insulating tape is wound back and forth over the field grading material three times, overlapping by half its width. The innermost layer is wound especially tightly to remove any air. The construction of the terminations is illustrated in figure 23.

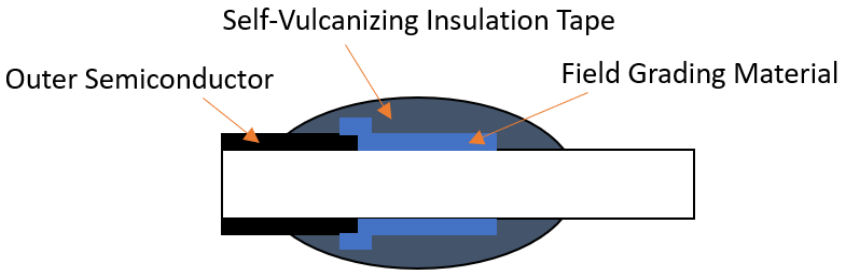

Figure 23: Illustration of the construction of end terminations.

After these steps, the reference partial discharge tests whose procedure is described in section 4.6 could be performed.

3.2.4 Thermocouples and Armaflex

Two thermocouples were applied to each test object, one on the joint's centre, and one on the cable, just on the side of the joint. Armoured duct tape is used to attach the sensors; one layer below to insulate it electrically from the test object, and one layer above to keep it in place.

A double layer of 1 cm thick Armaflex thermal insulation, affixed by self-vulcanising tape, completes the test object preparation. The thermal insulation reduces the cooling and thus helps the test object reach a stable temperature faster than it would otherwise. It is 65 cm long, meaning that it covers the joints and approximately 10 cm of cable on both sides.

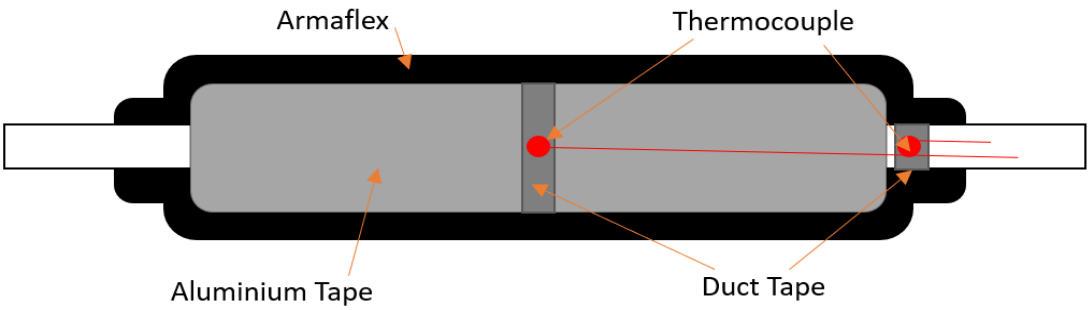

Figure 24: Illustration of the application of thermocouples and thermal insulation to the joints.

.

After these preparations, the test objects were ready for the current cycling that is performed according to section 4.7.

3.2.5 Preparations for Acoustic PD localisation

For the waves emitted by the discharge to be detected, it is necessary to have direct contact between the acoustic sensor and the test object. Therefore, the Armaflex and thermocouples applied before stage 2, were removed.

The measuring points, whose distribution will be discussed in section 4.8.1 were drawn onto the aluminium foil with a green marker. Having the measuring points marked up in advance saves

time and increases the accuracy of the localisation. A picture of a readily prepared joint can be seen in figure 25.

Figure 25: Picture of joint 3, readily prepared for acoustic PD localisation.

After this was done, the test objects were ready for the acoustic localisation whose procedure is detailed in section 4.8.1

3.2.6 Preparations for Break-down Voltage Testing

When a large voltage is applied to the test objects, the currents flowing through the insulation will make it very hot, and it might experience a thermal break-down. As a way to limit this effect, it was decided to use water terminations on the test objects.

For the water terminations to be applied correctly, the outer semiconductor was stripped off an additional ~ 15 cm on each cable. The terminations were applied to the test objects in turn, right before the break-down voltage measurements whose procedure is found in section 4.8.2. An illustration of the cable joint with water terminations applied can be seen in figure 26.

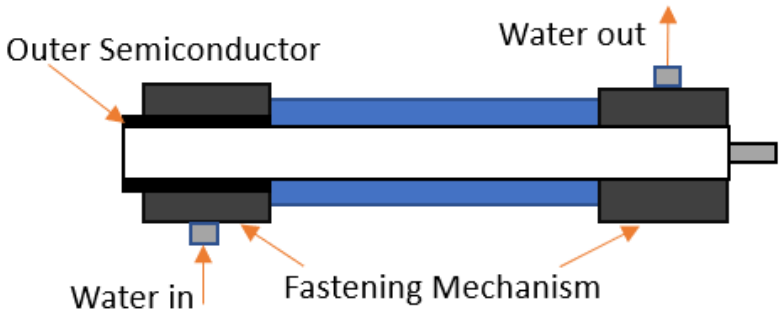

Figure 26: Figure of the cable on one side of the cable joints, with a water termination applied.

4 Method

4.1 Introduction

This chapter describes the practical work that was done for the thesis. The aim of the experimental work was measure PD, and specifically the PDIVs of the test objects during simulations of on-line and off-line conditions. Parts of the laboratory work is designed to investigate whether the defects acting as PD sources are temperature dependent. The laboratory work is divided into three stages. The measurements performed and the reasons for including them are detailed below.

Stage 1 In this stage, reference insulation resistance measurements, and "off-line" PD measurements were performed.

- The resistance measurements performed in this stage serve as a basis for comparison for the insulation resistances measured through test stage 2.
- PDIV and PDEV of the test objects were measured in room temperature under excitation from 0.1 and 50 Hz sources.
- These measurements were done with and without voltage conditioning, to see if this has any effect.
- The 50 Hz measurements were done with two different voltage time steps to see if this has any effect.

Stage 2 In this stage, PD measurements were performed during simulation of on-line conditions.

- The insulation resistance of the test objects was followed closely to ensure that their humidity stayed at similar levels.
- PDIV and PDEV are measured as the test objects were at stable temperature to investigate whether PD characteristics are load dependent.
- PDs were recorded at service voltage during the cooling of the test objects so that any changes in PD activity could be examined.

Stage 3 In stage 3, the PD sources were attempted identified and the PD measurements from the previous test stages were verified.

- Acoustic PD localisation was performed to see where in the joints the defects where PDs are placed.
- The break-down voltages of the test objects were measured as an additional way to assess their condition.
- Finally, the joints were dissected and the traces of PDs analysed,

The section begins by introducing the PD acquisition system that was used, OMICRON. A second subsection details the different setups that were used through the experimental work. After this, the dummy cable which was used to perform load cycling is presented. Four subsections describing the measuring procedures that have been followed succeeds this, first a section of general procedures, and then one section on procedures that are specific to each test stage. The final subsections of the chapter describe the estimation of conductor temperatures and processing of recorded data.

4.2 Partial Discharge Detection Method

The measuring system that is used to detect partial discharges is called OMICRON. The assembly of the system is illustrated in figure 27. The functions of the different components are explained briefly below, [28].

- **CPL542**is a RLC measuring impedance. Here, the current is transformed into a voltage form.
- **MPD600** is a signal measuring unit which is used to detect the partial discharges. It converts the acoustic signal to digital signals, and these are sent to the MCU502 unit through a fibre optic cable. This transportation method reduces the noise in the signal significantly.
- **MPP** is a battery pack that energises the MPD unit. This is used because it reduces the amount of noise in the measurements.
- **MCU502** is a media converter. It receives the signals from the MPD, converts it to a PC compatible format. The data then is transferred to the PC by USB.

A charge calibrator is used to calibrate the system when a new test object is introduced. It applies a known charge quantity, which by comparison to the detected charge magnitude, ensures that it is correct. Similarly, the test system must be calibrated by respect to voltage if a new voltage source is introduced. This is done by use of a voltage probe.

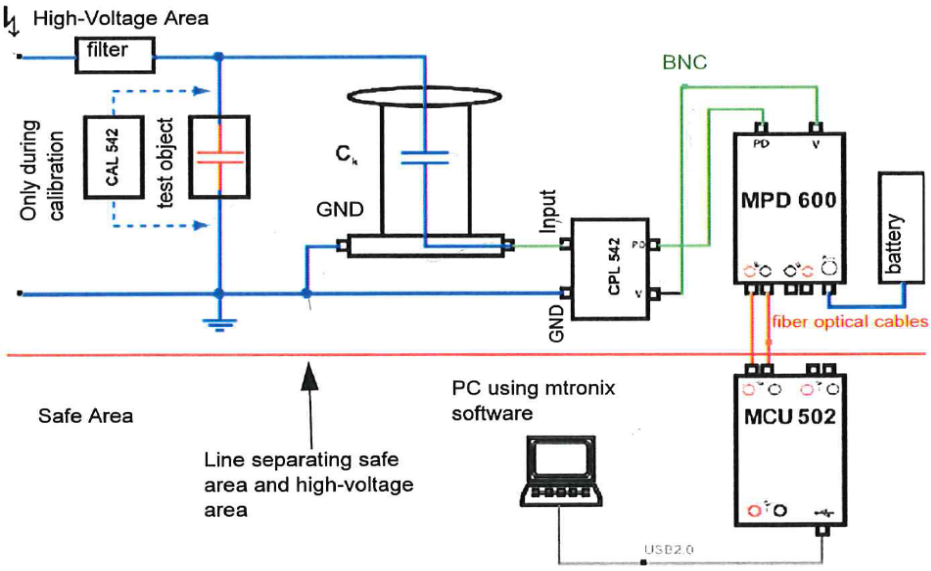

Figure 27: Illustration of the assembly of the OMICRON system, applied to a standard PD measuring circuit, [28]

.

The apparent charge magnitude is found by integration of the signal. This can be done in either the frequency or the time domain. Frequency domain integration was chosen for use in the thesis work, as this is in accordance with [7].

OMICRON is used to record two different types of files. It records PRPDA plots of the discharges, also referred to as histograms, in a PNG format. Streams are the second type of file that is recorded. A stream records every PD that is detected in terms of apparent charge magnitude, time and phase position, as well as the applied voltage. The streams can be converted to a MATLAB compatible format, which allows for further analysis.

In order to make the PRPDA plots, OMICRON measures the voltage applied to the test object. This does not work well when the voltage has a 0.1 Hz frequency. For the waveform to be identified, the voltage detection threshold has to be manually set to a low value. The trigger frequency of voltage detection is adjusted to 0.1 Hz.

4.3 Experimental Setups

In this section, the setups that were used in the experimental work are shown and explained.

4.3.1 PD Measurements at 50 and 0.1 Hz Test Voltage

This setup is a conventional PD measurement circuit where two voltage sources are used in turns. The result is essentially two setup varieties that can be seen in figures 28 and 29

A portable 0.1 Hz source with a maximum voltage of 28 kV, is used in the first case. The source contains frequency converters that change the voltage from the grid to a 0.1 Hz sine form. As this creates noise, a filter is connected in a series with the source. There are losses in the filter, so a low frequency, high voltage probe is used along with an oscilloscope to measure the potential over the test object. In the second variation of the setup, a grid connected variac and 230 V /100 kV high voltage transformer are used as a 50 Hz voltage source. Due to some instability in the OMICRON software, a voltage probe and multimeter are included.

Where the 50 Hz control desk has a built-in interlock, an external interlock is used with the VLF source. This means that when the sources are connected or disconnected to the setup, so are their interlocks. This includes re-coupling of wire to the door lock, warning light bulb and "earth knife". Because the VLF source is not made to be used along with an interlock, it is important that the source is turned off before the interlock.

The test object is held in place by two wooden supporters. They are placed upon a wooden pallet to keep a satisfactory distance between the high-voltage cable ends and the floor. Corona on sharp, metallic edges are avoided by use of metal corona rings.

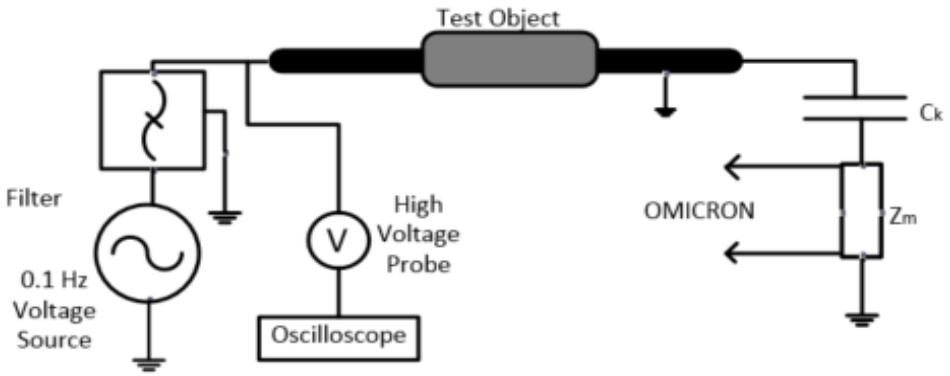

Figure 28: PD measurement setup with a VLF Source. The VLF source is coupled to the test object through a noise removing filter. Due to filter losses, a high voltage probe and oscilloscope is used to measure the test object voltage. The test object is coupled to a coupling capacitor and measuring impedance, which is used to detect PDs.

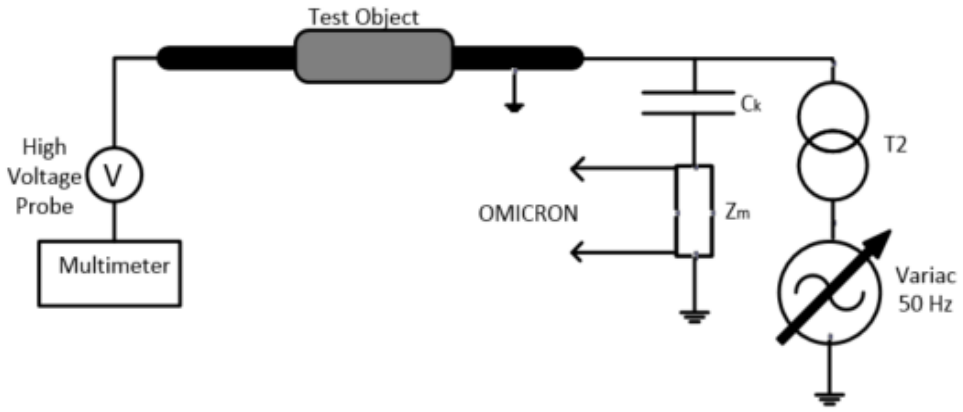

Figure 29: PD measurement setup with a 50 Hz voltage source. A voltage probe and multimeter is used to double check the voltage applied to the test object. The test object is coupled to a coupling capacitor and measuring impedance, which is used to detect PDs.

4.3.2 PD Measurements During Current Cycling

This test uses a hybrid of a PD measurement and heat cycling circuit that is illustrated in figure 30.

Voltage is supplied to the test object by the same variac and 230 V/ 100 kV transformer that was used in the previous setup.

The test object is parallel coupled to a dummy cable, and the heating current flows in this loop. Aluminium bus bars connects the test object to the dummy. This method is chosen to minimise the mechanical strain put on the test object. It was established that no critical heating occurs in the bus bars in [3].

The load current supplied to the dummy cable by a grid-connected variac and a ring transformer. A metallic tube that is connected to the dummy's screen and grounded ensures a potential of zero. The ring transformer is stabilised mechanically by help of a wooden box-like construction. A clamp-on ammeter connected to the data logger is used to track and adjust the current load.

The dummy cable is kept off the ground by the ring transformer, and two wooden supporters do the same for the test object. This is again lifted off the ground by a wooden pallet, to avoid any flash-overs between high voltage and the ground. The thermocouples mounted on the test object are drawn to the data logger by the cell walls, avoiding them being stepped on. All the edges in the setup are rounded off by corona rings in order to avoid sparking. A picture of the completed setup can be seen in figure 31.

It should be noted that the placement of the measuring impedance causes the polarity of the recorded discharges to be opposite of the discharges that are actually occurring.

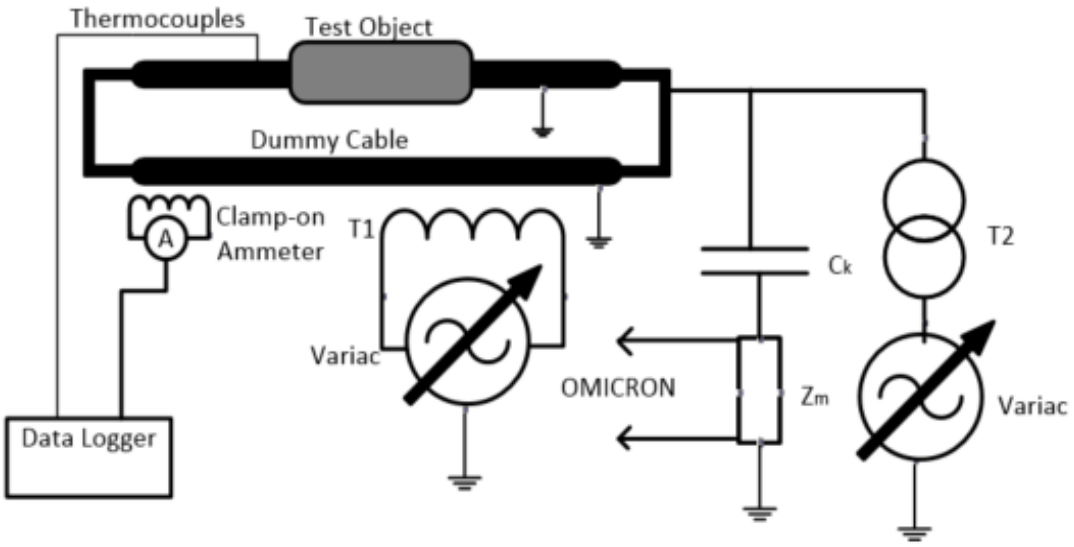

Figure 30: Circuit diagram of the setup used to measure PD in the test objects during temperature cycling. Current is induced in the test object and circulated through a dummy cable. Voltage is applied to the test object by a variac and transformer. PD is detected by help of the coupling capacitor C_k and OMICRON. A data logger records the temperature on the outside of the test object by the thermocouples that are applied to it.

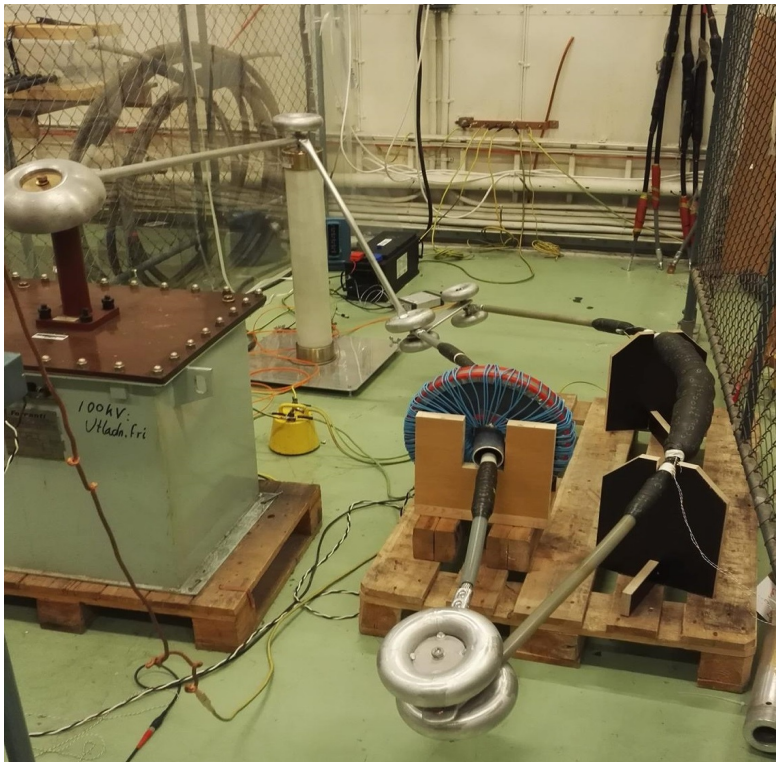

Figure 31: Picture of the completed experimental setup used test stage 2.

4.3.3 Acoustic localisation of PD

The setup that is used for acoustic PD location is a combination of a conventional electrical PD measurement circuit and an acoustic sensor, and can be seen in figure 32.

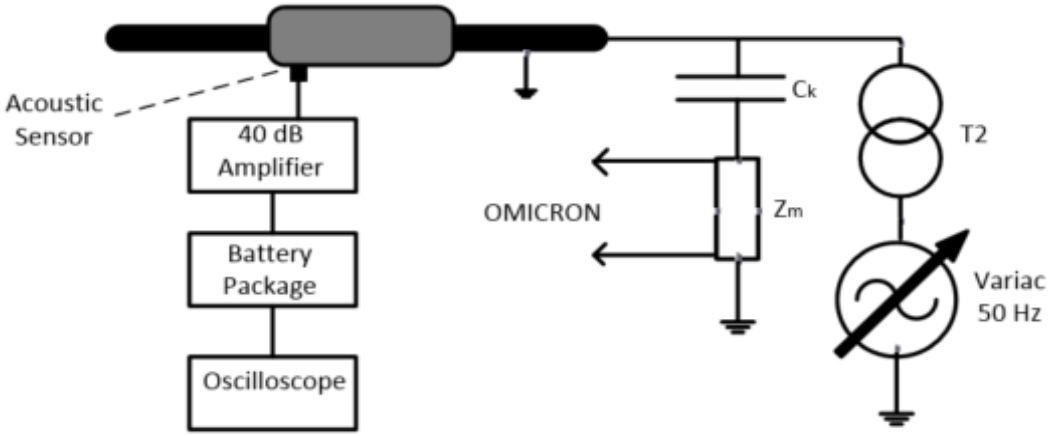

Figure 32: Circuit diagram of the setup used to perform acoustic localisation on the test objects. Voltage excitation and electrical PD detection is done by a conventional test circuit. PD is measured acoustically by acoustic sensor, amplifier, battery package and oscilloscope, all coupled in a series.

As previously, the test object is connected to a coupling capacitor and voltage transformer. The test object is held by two wooden supporters on top of a pallet, and all sharp edges are rounded off by corona rings. The OMICRON system is used as a tool to keep the discharges in the test object constant through the localisation process.

The acoustic sensor is fastened to the test object by help of a slice of wood and a rubber band, this is illustrated in figure 33. Vaseline is used to improve the contact between the sensor and test object. The acoustic sensor is coupled to a 40 dB amplifier and a battery pack before it reaches the oscilloscope where signals are processed.

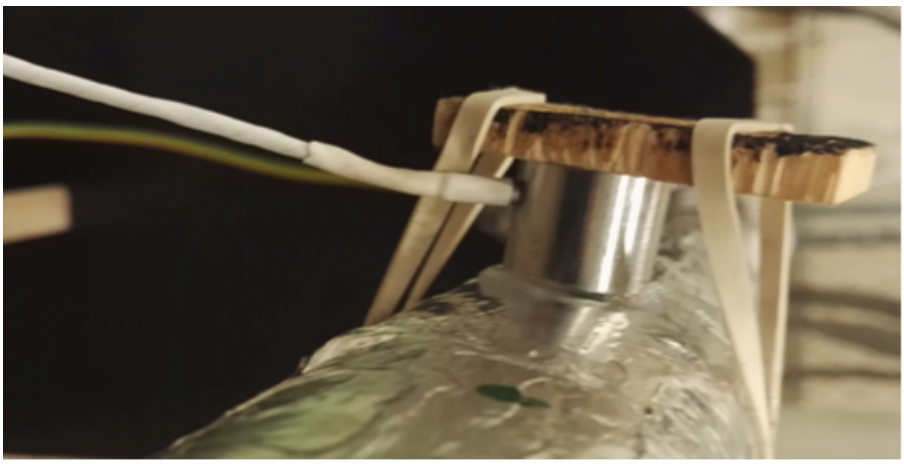

Figure 33: Picture of how the acoustic sensor is fastened to the test object, by help of a piece of wood and an elastic band. Vaseline ensures good contact between the test object and sensor.

4.3.4 Break-down Voltage Testing

A diagram of the setup that was used to measure the break-down voltages of the test objects can be seen in figure 34.

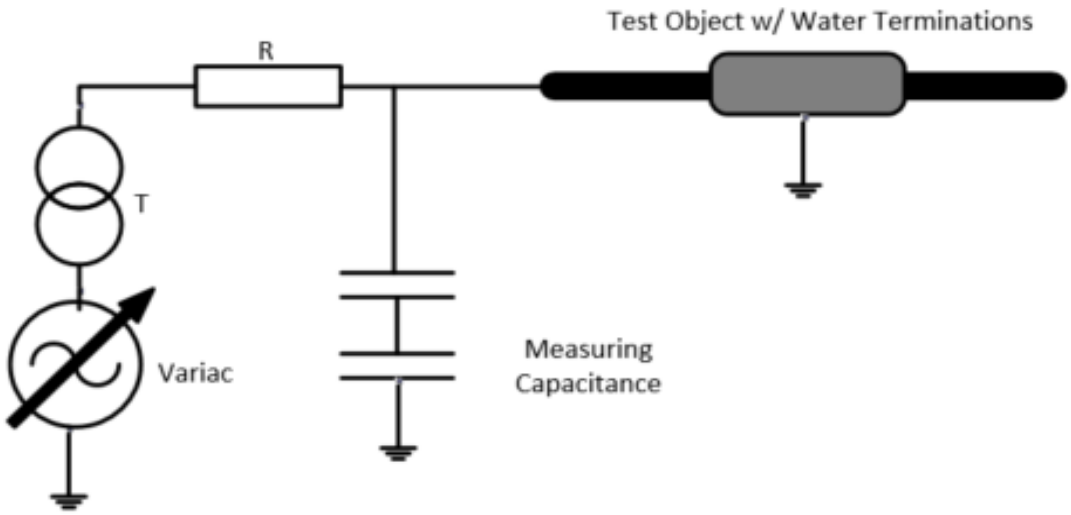

Figure 34: Circuit diagram of the setup used to measure the break-down voltages of the cable joints. A variac controls the voltage supplied to the 500 kV transformer. The transformer is coupled in series with a resistor which limits the current inrush after a break-down. A capacitive voltage divider and measuring capacitance is parallel coupled to the test object.

Because it is not known if the 100 kV transformer would be able to provoke any break-downs, it was decided to use a 500 kV transformer instead.

As mentioned in section 3.2.6, water terminations were used in an attempt to prevent thermal break-downs of the joints. Two water hoses were connected to each termination with the supplying hose placed the highest up, ensuring the best possible cooling effect. The test object is held in place at a satisfactory distance from the ground by a large wooden supporter.

As the current inrush to the transformer from the break-down can be damaging, a resistor is included in the circuit as a damper. A capacitive voltage divider is used to measure the voltage across the test object. A picture of the complete setup can be seen in figure 35.

Figure 35: Picture of the setup used to measure the test objects' break-down voltages. The transformer can be seen on the left, and the coupling capacitor is on the right. The test object with water terminations can be seen in the middle.

4.4 Preparation and Reference Testing of the Dummy Cable

During the current cycling measurements, the test object is parallel coupled to a dummy cable which can be seen in figure 36.

Figure 36: Picture of the dummy cable used.

During PD measurements, it is important to know that the discharges are coming from the test object and not from the dummy cable. This is achieved if the PDIV of the dummy cable is higher than the testing voltage range. The temperature dependence of the PDIV of the same dummy cable was tested thoroughly in [3]. Here, it was found that PDIV of the dummy only increased by 2 kV as temperature was increased from 20 to 90 °C. It is assumed that this relationship still holds.

The dummy had previously been used in not only [3], but also in [29] and [12], meaning it had been subjected to considerable thermal stress. As the end terminations were growing brittle as a consequence of this, it was decided to change them. The old end terminations were removed as carefully as possible, and new ones wound as described in section 3.2.3. With the new end terminations in place, the PDIV of the dummy cable was measured, and found to be 29 kV. As no higher testing voltages than 12 kV would be applied to the test object, it was concluded that the dummy cable will not disturb any PD measurements.

The insulation resistance of the dummy cable was also measured, and found to be larger than 3 TΩ at both 1 and 5 kV.

4.5 General Experimental Procedures

4.5.1 Conditioning of the Test Object

Each discharge influences the condition of the cavity in the sense that they create starting electrons. This does again affect the discharge behaviour that this observed. Therefore, applying a given voltage to the test object for a certain amount of time before PD measurements will improve the reproducibility of the testing. This procedure is called conditioning. In this work, conditioning will be performed by applying U_0 of 6 kV for 1 hour.

4.5.2 Partial Discharge Inception and Extinction Voltages

In this work, partial discharge inception- and extinction voltages(PDIV and PDEV) are determined for voltages with frequencies of 0.1 and 50 Hz.

The voltage is increased in steps of 0.5 kV every 4 minutes. The step size is chosen based on [20], where the frequency dependence of PD in medium voltage cable joints was investigated. An initial voltage of 0.5 kV is used so that if the inception voltage found is very low, it can still be found with satisfactory accuracy.

Once PDIV is believed found, the voltage is turned up one more step, to make sure that PDIV was measured correctly. This method has been chosen to limit the stress on the test object. After this, the voltage is decreased with the same step size until the PDs are extinguished and PDEV is identified. Then, the voltage is turned off and the test object grounded. A PRPDA plot and stream is made at each voltage step, so that the data can be re-examined. The testing procedure is plotted in figure 37.

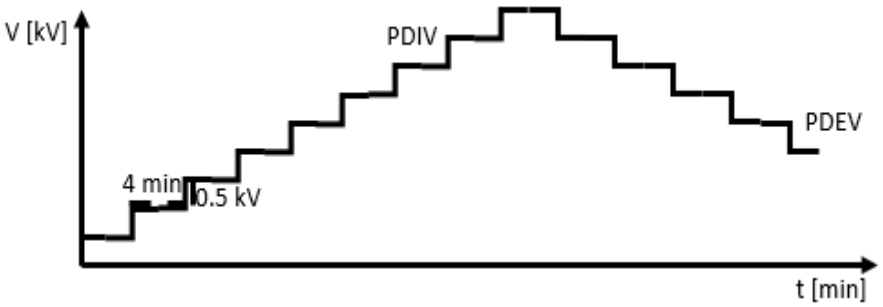

Figure 37: Illustration of the procedure for measuring PDIV and PDEV.

PDIV Criterion A criterion for how many discharges constitute PDIV must be established. Some works define PDIV as the voltage amplitude that is applied when the first PD is detected, [14]. Others use the voltage that yields minimum one pd per cycle to define PDIV, [30].

To be sure that the discharges are PDs, and not noise, a minimum requirement of 10 discharges is set for PDIV to be considered found during 0.1 Hz measurements. These discharges must be in the expected phase areas and larger than the band of noise.

4 minutes at 0.1 Hz contains 24 voltage cycles. During 4 minutes at 50 Hz frequency, 12 000 cycles occur. Thus, the 10 discharge requirement at 0.1 Hz translates to 5000 discharges during 4 minutes

at 50 Hz. This means that if PD is only recorded for one minute, 1250 discharges are required observed. Correspondingly, PDEV is defined as the last voltage step where 10 and 5000 discharges are observed, respectively.

4.5.3 Insulation Resistance Measurements

The insulation resistance is found by use of a Megger, which applies a DC voltage and measures the resultant current. Moisture content, increased temperature and thermal aging will reduce the detected resistance [22][23].

The resistance of the cable system, was measured at 0.5, 1, 2.5, 5 and 2.5 kV once more in the field. This was done while the test objects were still in service, and after they were removed. The polarisation and depolarisation currents were recorded for five minutes each. The experimental work uses a simplified version of this, as testing voltages of 1 and 5 kV are chosen. This reduces the amount of data and required time, while still giving an indication of the test object's condition. The polarisation and depolarisation currents are recorded for five minutes each, as in the field.

The voltage source and coupling capacitor are disconnected to avoid the results being distorted. The Megger is coupled to the test object as illustrated in figure 38. During the current cycling measurements, the joint and dummy cable are parallel coupled. However, as the insulation resistance of the dummy cable is in the TΩ range and the test object in the GΩ range, the dummy cable resistance becomes negligible. The resistance tester is connected to a PC with PowerDB software, which records the data continuously. The joint that is being tested is grounded between each measurement, to avoid any memory effects.

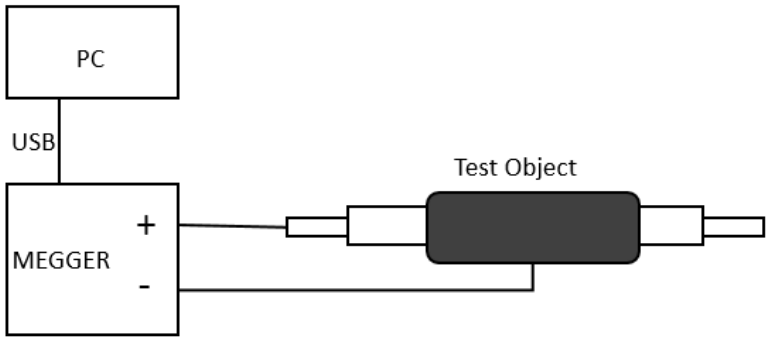

Figure 38: Circuit diagram of how the resistance tester/Megger is coupled to the test object.

4.6 Stage 1 Measuring Procedures

The measurements described in this subsection were performed on each test object in turn. The test objects are grounded for approximately 24 hours between every PD testing to avoid any memory effects. The measuring procedures are described in the sections below, in the order they were performed in.

4.6.1 Resistance Measurements

This measurement is performed as described in section 4.5.3.

4.6.2 VLF PDIV and PDEV

PDIV and PDEV for 0.1 Hz voltage were measured in accordance with section 4.5.2. A little break is included before each new voltage step is considered begun as the source takes some time to stabilise. This measurement is first done without any conditioning, to give an indication of what can be expected. The procedure is then done after the test object has been conditioned. The measurements are illustrated in figure 39.

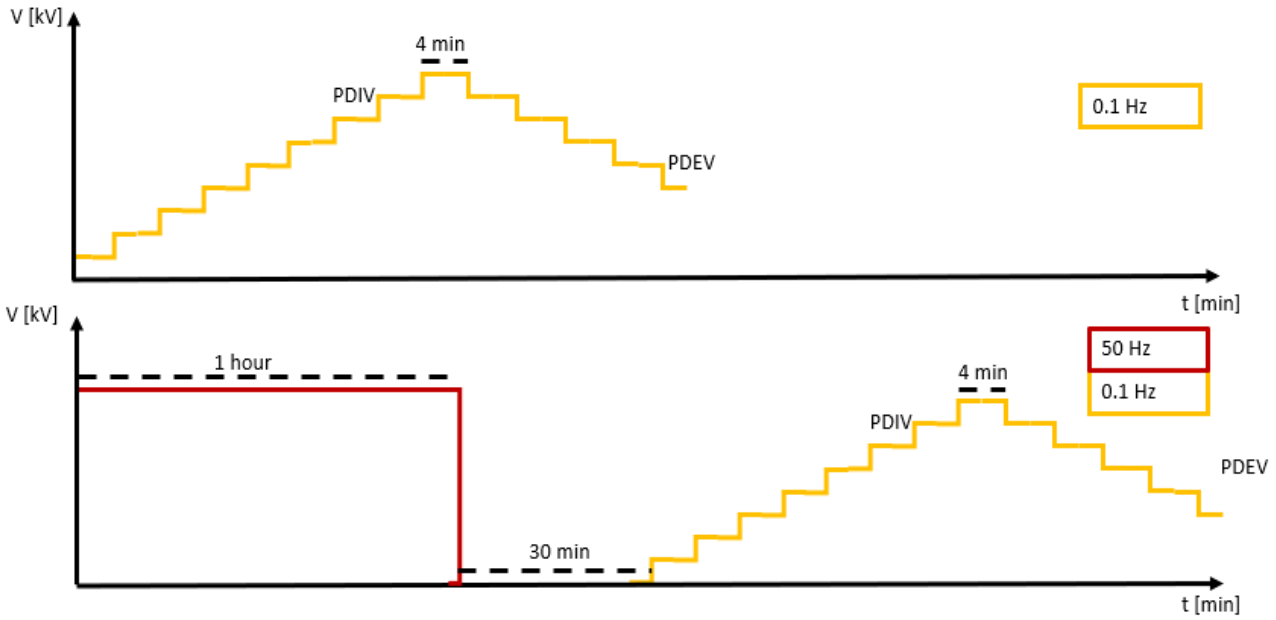

Figure 39: Illustration of the voltage applied during the 0.1 Hz PDIV and PDEV measurement. PDIV and PDEV are found both with and without U_0,50 Hz conditioning.

The test object is conditioned for 1 hour with the nominal voltage 6 kV, at 50 Hz. This simulates the joint being in service. Before PDIV and PDEV is measured, the test object is grounded for 30 minutes. This represents the transition where the test object is taken out of service and connected it to an external voltage source. During this pause, the 50 Hz voltage source is interchanged with the 0.1 Hz voltage source, and their interlocks are re-coupled.

4.6.3 50 Hz, 4 Minute Step Intervals

This test was performed in precisely the same way as the 0.1 PDIV/ PDEV Hz test described in section 4.6.2, only with 50 Hz voltage applied through the test instead.

4.6.4 50 Hz, 1 Minute Step Intervals

In this test, PDIV and PDEV were measured by the exact same procedure as the 50 Hz, 0.5 kV/4 min test, but with 0.5 kV/1 min voltage steps instead.

4.7 Stage 2 Measuring Procedures

In this test, the test objects were temperature cycled in turn. One current magnitude was applied on the test object and parallel dummy cycling loop, and the temperature was allowed to stabilize.

Then partial discharge properties were measured at stable temperature and during the cooling of the joint. PD was measured under temperature conditions ranging from room temperature to approximately 60°C. The full testing cycle can be seen in figure 40.

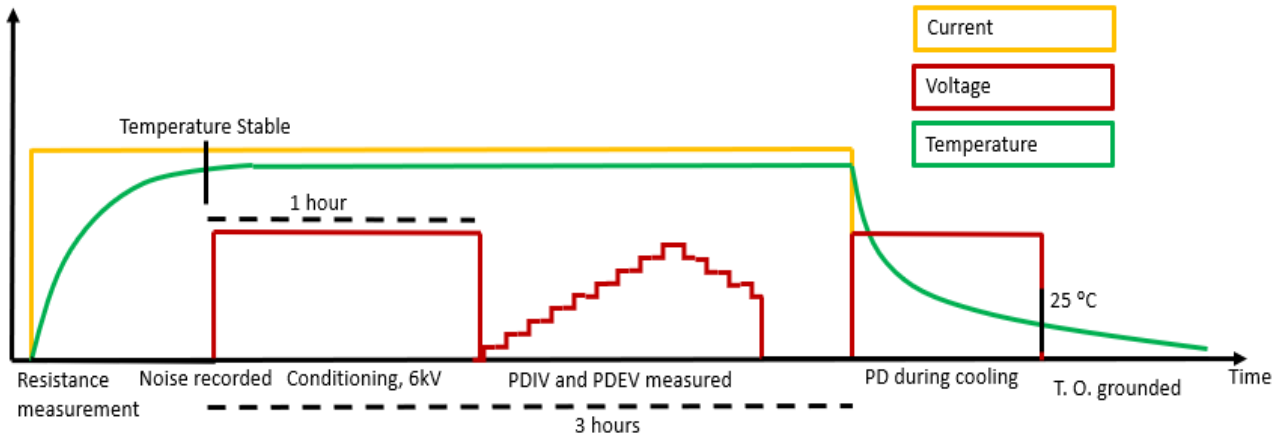

Figure 40: Illustration of applied voltage, load current and the resultant test object temperature through the main test. All the measurements that are done through the test day are labeled, in their order, on the figure.

The procedures that the cycling tests are made up of are elaborated in the order they were performed below.

4.7.1 Insulation Resistance Measurements

The insulation resistance and polarisation/depolarisation currents are measured in accordance with section 4.5.3.

The results are evaluated quickly. If the test object is believed to have a moisture content comparable to previously, the cycling test is begun.

4.7.2 Heating of the Joint by Resistive Losses

The joint is heated by resistive losses in its conductor and metallic connector. Thermocouples on the outside of the test object and a data logger are used to scan the test object temperature.

The highest permissible operating temperature of XLPE is 90°C [31]. If the material is heated past it, it will begin to melt. This changes the mechanical properties of the material and deteriorates it.

50-70 °C is the area where the largest temperature effect on PD behaviour was observed, in [3]. Therefore, this is chosen as a maximum conductor temperature for the joints to reach in the test. By heating the test object past this, one could have further ageing of the test object and a reduction in humidity, which would reduce the reproducibility of the results.

Defining Temperature Stability When choosing the definition of what a stable temperature is, a compromise between accuracy and time efficiency was attempted found. Furthermore, one would want to reduce the time the joints are heated as this could affect the humidity content of the test object.

A stability criterion of a temperature increase of less than 0.5 $°C$ over the past 0.5 hour was set. A result of this is that during the three hours of PD testing, the test object temperature might increase by 1.5 $°C$. The average temperature over this time is used to represent the temperature level.

The data logger was turned off before the PD measurements were performed as its scanning causes noise.

4.7.3 Current Magnitudes for Temperature Cycling

As previously discussed, the effect on PD behaviour, of conductor temperatures from 20 to 50-70$°C$ were to be investigated. The testing range should be evenly divided across the distribution. Considering that three joints are being tested and large amounts of data are accumulated each day, the number of testing temperatures should be limited.

The PD measurements should be performed in room temperature so that any effects of increased temperature can be identified.

Initial Current Magnitudes The initial cycling loads were chosen based on the first draft of the COMSOL simulation model. This testing range was 100, 150, 175, 200 and 225 A, this was believed to result in temperatures up to 50 °C. These were all applied to joint 2, and found to give a maximum temperature of 35 °C. A plot of all the stable temperatures can be seen in appendix C. Any temperatures below 35 are too far below the 50-70 °C range, and should therefore not be spent time on.

Final Current Magnitudes The 225 A load yielding 35 °C on the outside of the cable is kept to see if there is any change of PD behaviour between room temperature and 50-70 °C.By interpolating the first set of temperatures and a test day in the lab, it was found that a load of 350 A gives 55 °C on the outside of the cable.

PD measurements at room temperature, and during load cycling of 225 and 350 A, is believed to give a satisfactory level of detail. The current magnitudes and their expected temperatures are summarised in table 2.

Table 2: Chosen cycling loads and their expected resultant temperatures

Cycling Load [A]	Expected Temperature on Cable Outside [°C]
0	21
225	≈ 35
350	≈ 55

Each current was adjusted with help of a clamp-on ammeter which is connected to the data logger. After the temperature was found to be stable, the current was kept on for 3 more hours, while PD measurements were performed. Then it was turned off.

4.7.4 Partial Discharge Measurements at Stable Temperature

1. 1 minute of noise is recorded at a low voltage, this is used to decide the level of noise that will be removed when the results are processed.

2. The joint is conditioned as described in section 4.5.1. 1 minute streams and histograms are accumulated every 5 minutes.

3. The inception and extinction voltage of the joint is measured, as described in section 4.5.2.

4. 6 kV is applied for the last 5 minutes the current is turned on. During this time, a 1 minute stream is recorded. This stream is used as a basis of comparison for the PD that is recorded during the cooling of the joint.

4.7.5 Partial Discharge Measurements During Cooling of the Joint

Once the PD measurements have been performed, the data logger is turned back on. The current is turned off 3 hours after the temperature was found to be stable. This time includes a margin in case the PDIV increases with temperature and thus takes longer to measure. In the cases where the stable temperature on the outside of the joint is over 25 $°C$, PD is recorded at U_0 of 6 kV kV until test object has reached this temperature. PD streams are recorded for 1 minute, with 1 minute breaks between. The data logger scans temperatures during this break. This arrangement ensures that the noise produced by the temperature scans doesn't impact the PD streams. Having detailed information about both PD and temperature makes it possible connect any PD traits to specific stages in the cooling process.

After 25 $°C$ in the thermocouples has been reached, the voltage is turned off and the test object grounded. It is made sure that the joint has reached room temperature before the next temperature cycle is begun.

4.8 Stage 3 Measuring Procedures

4.8.1 Acoustic PD localisation

There are two different ways to localise PD by acoustic sensors. The first option is to triangulate by the time different between the signals detected by different sensors, giving perhaps the most accurate indication. The less complicated alternative is to find where the highest signal amplitudes are detected, as this is likely close to the source. This requires only one sensor, [32]. As there was only one sensor available, the signal magnitude approach was chosen in this work.

Measuring Points The more measuring points, the more accurate, but also time consuming, will the localisation of the discharge source be. The aim for of the testing if to get an indication of placement rather than exact location. Therefore, the measuring points are placed with 5 cm separation along the length of the joint. The acoustic sensors detect waves in only one spatial direction, [32]. This is compensated for by placing the measuring points with 90 ° around the axis of the joint. The resultant testing mesh consists of approximately 40 points. The measuring points were drawn onto the test objects, and this was described in section 3.2.5.

Discharge Magnitude during Detection For the measurements to be as comparable as possible, it is desirable to do the measurements with a constant discharge magnitude in the test object. The discharges should be relatively large. After some trial and error, it was found that the apparent charge of the PD was stable around 100, 200 and 150 pC in joints 1, 2 and 3, respectively. These discharge magnitudes were reached with voltages around 30 kV. Thus, the acoustic localisation was performed with voltages that caused these PD levels applied.

Testing Procedure PD was localised in each measuring point by the following procedure;

1. The sensor is attached to the test object in a given measuring point.
2. The voltage is turned up until the desired apparent charge level is reached.
3. The discharges are left on for a minute.
4. If any wave forms are detected, the scope view is frozen. The peak-to-peak magnitude of the signals are measured by cursors and a picture of the waveform is saved. A typical scope view can be seen in figure 41.
5. The voltage is turned off, test object is grounded and the acoustic sensor is moved to the next testing point.

Figure 41: The view of the oscilloscope as PD is found in a measuring point. As can be seen in the figure, cursors are used to measure the peak-to-peak magnitude of the signal.

4.8.2 Break-Down Voltage Testing

When the break-down voltages were measured, the voltage applied to the cable joints was increased by 5 kV every minute until a break-down occurred.

These time steps were chosen based on [20]. The fast increase of voltage is due to the low insulation resistances of the joints which result in large currents and resultant heating when excited with high voltages. It is desirable to have an electrical breakdown rather than a thermal, as it gives a better measure of the joint's dielectric strength.

4.9 Estimation of Conductor Temperature

It is desirable to know the conductor temperature of the joint as this is the temperature the insulation system is exposed to. The easiest way to find this out would be to place a thermocouple on the conductor, if it weren't for the fact that one could no longer apply a high voltage. Therefore, a simulation model was built in the multiphysics software COMSOL. The exact composition of the joints is not known, therefore the cable on the side of the joints was simulated instead. The development of the model, as well as how it was adapted to the measurements in the lab, is described

thoroughly in appendix D. The thermocouple and conductor temperatures that were computed by the simulation model at 225 and 350 A can be seen in figure 42.

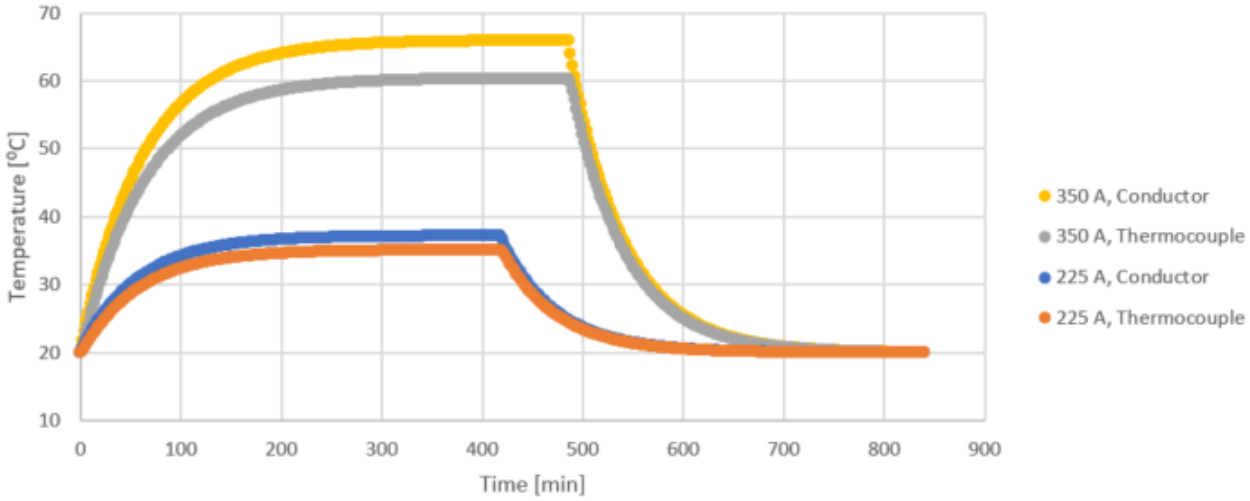

Figure 42: Plot of the simulated temperatures in the cable conductor and thermocouple when the cable is loaded with 225 and 350 A. The 225 A load is turned off after 7 hours and the 350 A load is turned off after 8 hours.

When the conductor temperature was read out of the simulation results, it was found out when the when the measured and simulated temperature on the outside of the cable are the same. Then, the conductor temperature at this time was read out.

4.10 Data Processing

The stream recordings of PD were used to identify PDIV/PDEV, and to make PRPD and Weibull plots. When this was done, the recorded streams were opened in the OMICRON software, and filtered with regards to noise. How this was done is described in detail in appendix E.

Identification of PDIV and PDEV When PDIV was determined, the filtered streams were examined. The first stream to show the required number of discharges in the right phase position (see section 2.9.1), represents PDIV. PDEV was found the same way.

PRPD Plots PRPD plots were made in the OMICRON software interface. Here, the axes could be adjusted, and the scope view saved as a png file.

Weibull Plots In order to make Weibull plots, the filtered streams were exported to a MATLAB compatible format by the OMICRON software. The files were then run through the MATLAB scripts that can be seen in appendix F).

5 Results and Discussion

In this section, the results from the experimental work are presented and discussed. The first three subsections treat one test stage each. Two subsections where the results are gathered and discussed follow.

5.1 Stage 1: "Off-line" and Reference Testing

5.1.1 Resistance Measurements

The insulation resistance of the test objects were measured at voltage stresses of 1 and 5 kV, for 5 minutes while voltage was applied and 5 minutes after it had been removed. As the insulation resistances had been allowed to stabilise after 5 minutes, these are the values which have been chosen for examination. They are presented in table3.

Table 3: Reference Measurements of Insulation Resistance

Measurement Specification	Joint 1 Resistance [GΩ]	Joint 2 Resistance [GΩ]	Joint 3 Resistance [GΩ]
1 kV, 5 min	103.4	19.1	3.4
5 kV, 5 min	4.5	1.0	0.5

As mentioned in section 2.7, healthy apparatus have insulation resistances in the TΩ range. The resistances in table 3 are all well below these, and some of the values can be considered extremely low. These results indicate high contents of moisture and can be interpreted as a confirmation of significant ageing.

5.1.2 Partial Discharge Measurements

The PDIV and PDEV of the test objects were measured using different measurement procedures which are described in section 4.6. The cable joints were tested in room temperature, by voltage sources with frequencies of 0.1 and 50 Hz. The 50 Hz measurements were done with two different voltage steps, to see if this made any difference.

Two versions of these procedures were performed, one with and one without voltage conditioning. Here, the measurements with conditioning simulate the case where the joint is taken out of service right before it is tested. When conditioning was not done, this simulated when the joint have been taken out of service and left grounded over a longer period of time.

The results are presented in tables 4, 5 and 6, which are sorted by the voltage frequency and time steps used during the measurements.

Table 4: PDIV and PDEV of the test objects, measured with steps of 0.5 kV/4 min and 0.1 Hz voltage, with and without conditioning.

	Joint 1		Joint 2		Joint 3	
Test	PDIV [kV]	PDEV [kV]	PDIV [kV]	PDEV [kV]	PDIV [kV]	PDEV [kV]
No conditioning	1.0	1.0	1.5	1.5	1.5	1.5
Conditioning	3.0	3.0	6.0	5.0	3.5	3.0

Table 5: PDIV and PDEV of the test objects, measured with steps of 0.5 kV/4 min and 50 Hz voltage, with and without conditioning.

	Joint 1		Joint 2		Joint 3	
Test	PDIV [kV]	PDEV [kV]	PDIV [kV]	PDEV [kV]	PDIV [kV]	PDEV [kV]
No conditioning	7.1	6.7	5.9	5.8	6.6	5.9
Conditioning	7.6	6.7	6.5	6.1	7.1	7.3

Table 6: PDIV and PDEV of the test objects, measured with steps of 0.5 kV/1 min and 50 Hz voltage, with and without conditioning.

	Joint 1		Joint 2		Joint 3	
Test	PDIV [kV]	PDEV [kV]	PDIV [kV]	PDEV [kV]	PDIV [kV]	PDEV [kV]
No conditioning	7.0	6.7	5.7	5.6	6.5	6.7
Conditioning	7.1	6.0	6.6	6.7	6.1	6.1

PDIV and PDEV at VLF In the VLF tests without conditioning, the PDIVs of the test objects were found to be either 1 or 1.5 kV, these are extremely low values. Inception voltages this far under the service voltage causes continuous discharges in the equipment, which again can lead to severe ageing. When conditioning was done, an increase of PDIV to values between 3 and 6 kV could be observed.

The extinction voltages were all measured to be 5 kV or lower at this frequency, meaning that PDs at service voltage are unlikely to be extinguished.

Effect of Conditioning at VLF Whether or not voltage conditioning is done appears to have a significant effect on the PDIV that was measured. This behaviour can mean that the recent history of the test objects has an impact on what is discovered by VLF voltage testing. An implication of this is that it can be necessary to have control of the time from the cable section is taken out of service, until it is tested. Otherwise, the measuring results might become more inconsistent than desired.

PDIV and PDEV at 50 Hz The PDIVs that were measured with 50 Hz voltage were between 5.7 and 7.1 kV, and 6.1 and 7.6 when conditioning was applied and not, respectively.

The PDIVs of joint 2 were 5.9 and 5.7 when the joint was not conditioned, in all other cases the inception voltages were higher than 6 kV. In the same two measurement series, there were also extinction voltages below 6 kV. One measurement of joint 3 also showed an equally low extinction voltage.

One interpretation of this, is that joint 2 is likely to experience PDs during service while the other two joints are not. It could also mean that discharges initiated during a fault might not necessarily extinguish as the joints return to service voltage.

Effect of Conditioning at 50 Hz In the 50 Hz voltage measurements, whether the test object is conditioned or not, appears to have little effect on the measured PDIV.

Effect of Voltage Time Steps at 50 Hz When comparing the PDIVs measured with 0.5 kV/ 4 min and 0.5 kV/1 min steps (tables 5 and 6), changes of PDIV are only seen in 2/12 tests. The PDIV of a conditioned joint 1 decreases by 0.5 kV, whereas the PDIV of a conditioned joint 3 decreases by 1 kV. Neither of these changes result in any dramatically different condition assessments of the test objects.

Further Improvements of the Experimental Work There is one important aspect of off-line testing that this experiment fails to include. This is the fact that when the cable section has just been disconnected, it might still be heated from the current it has conducted. If there is in fact a dependence on temperature, these measurements would be more representative of the conditions in the field, than what has been done in the thesis work.

This cooling during off-line measurements could have been included in the experiment by a third test series. The cable joints could have been load cycled until they reached a steady state temperature. Then, voltage conditioning would have been applied, and the current turned off. PDIV and PDEV would have been measured after the joint had been allowed to cool for 0.5 hour.

By the time this was thought of, there was not enough time to perform the measurements. They would, be interesting to examine in another work.

5.2 Stage 2: Simulation of Service Conditions

5.2.1 Insulation Resistance Measurements

Before any current loading was applied to the test objects, their insulation resistances were measured. The polarisation and depolarisation currents were recorded for 5 minutes each, at a voltage of 1 and 5 kV. The resistances recorded after 5 minutes are plotted against the estimated test object conductor temperature from the previous testing day in figure 43. This is done to evaluate if the insulation resistance of the test objects is affected by the thermal stresses they are exposed to.

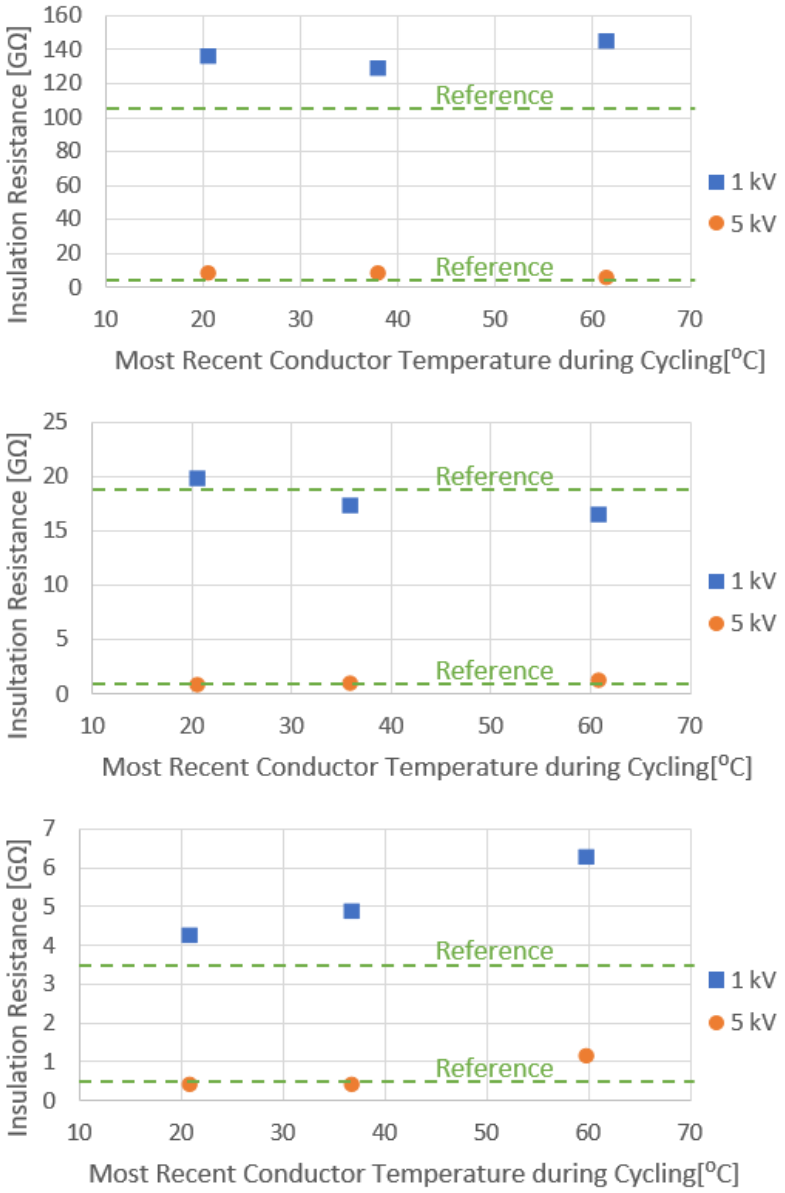

Figure 43: The insulation resistances of the test objects, plotted against the stable conductor temperature that was reached on the previous testing day. The green, stippled lines indicate the reference insulation resistances that have been measured. Top: Joint 1, middle: Joint 2, bottom: Joint 3.

When comparing the changes of the insulation resistances in figure 43 with the reference values that are indicated with stippled green lines, it can be seen that they are relatively small.

The highest increase of resistance can be observed in joint 3, at 5 kV. Here, the resistance increases from 0.5(reference) to 1.2 GΩ, growing to 2.4 times its initial value. Still, this change is much smaller than the decade range increase of field grading material conductivity which was identified at increased humidity, which was discussed in section 2.3.3. On this background, it can be concluded that the humidity level in the test objects is consistent enough trough the temperature cycling for the results to be comparable. This means that the aluminium tape used to prepare the test objects served its purpose well.

5.2.2 Stable Temperatures During Load Cycling

The test object temperatures were measured through the load cycles by thermocouples placed on the outer semiconductor of the cable and joint. The average of the temperatures measured before and after the PD measurements is referred to as the stable temperature.

The temperature in the conductor was estimated based on the temperature on the outside of the cable by help of a COMSOL model. The details on how this was done can be seen in section 4.9. The temperatures on the outside of the cable and joint, as well as the estimated conductor temperature are plotted as a function of loading for all three test objects in figure 44.

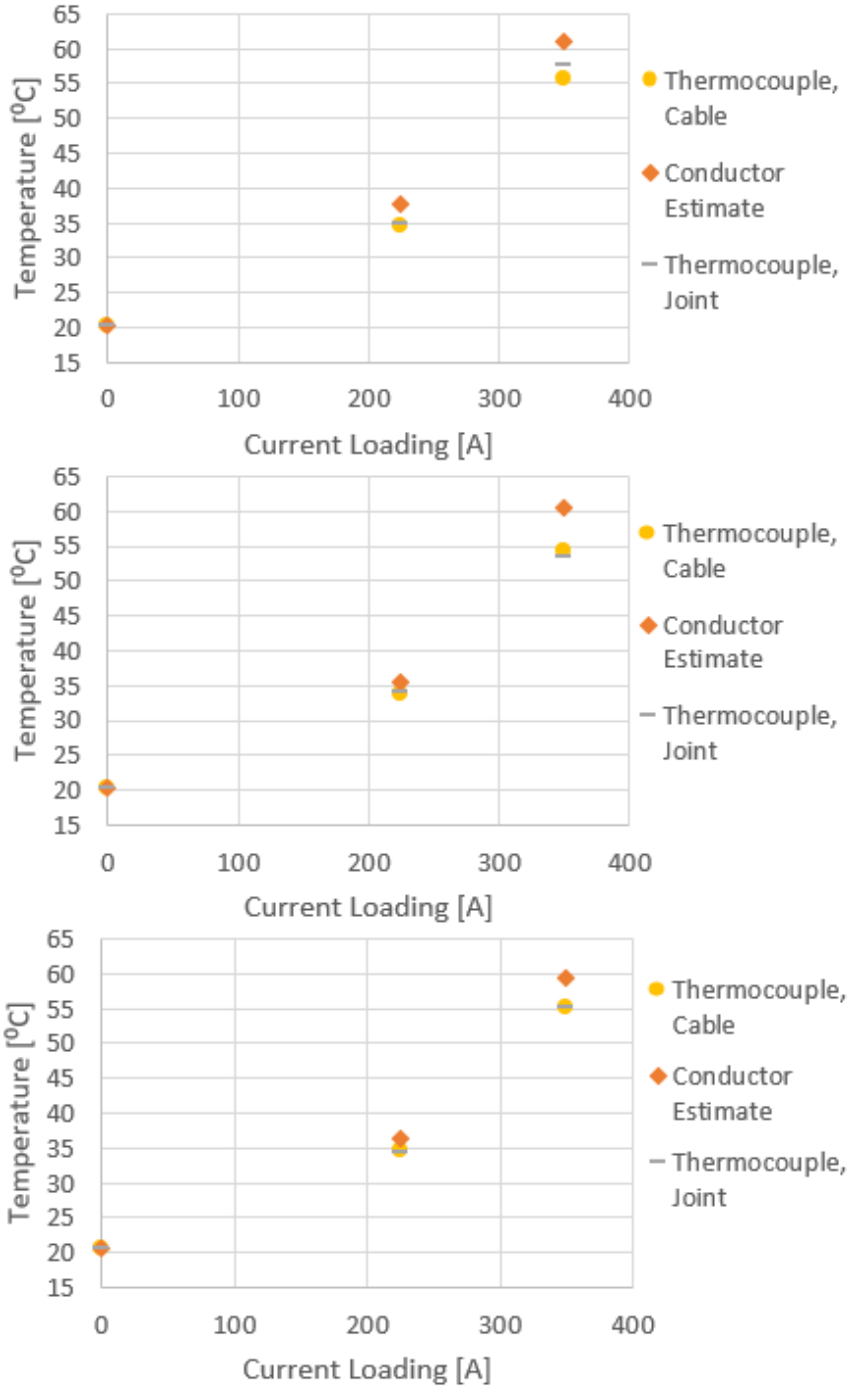

Figure 44: Plots of the stable temperatures measured in thermocouples on the outside of the cable and joint body, as well as the estimated conductor temperatures. Top: Joint 1. Middle: Joint 2. Bottom: Joint 3.

Figure 44 shows that the cycling currents reached the temperatures the thesis aims to investigate.

The average temperature on the outside of the cable and joint are close to each other. The only exception to this is the temperature on the outside of joint 1, which is slightly higher than at the cable. The difference between the estimated conductor temperature and the thermocouples is larger during cycling of 350 A than 225 A, this is as expected.

Comment on the Sensitivity of Temperature Estimation Due to the joint being thicker than the cable, the physical distance between conductor and thermocouple is bigger in the joint than in the cable. The heat thus has to travel longer from conductor to thermocouple in the joint that in the cable. When the thermocouples measure the same temperatures, the metallic connector in the joint is likely to be a few degrees warmer than the cable conductor. Considering that the simulation model used for temperature estimation is based on the cable's topology and not the joint's, it is possible that the estimated conductor temperatures are a couple off degrees off.

There are also error sources in the COMSOL model itself which affect the estimation of the conductor temperatures. These are discussed in further detail in appendix D.3.9

Alternative Method An alternative, much more accurate way to determine the conductor temperatures would be to install thermocouples in the conductor and metallic connector of a cable joint. Because thermocouples can't be used in high-voltage areas, this would require that a test object is reserved for this purpose. It would also be necessary to ensure that all test objects experience the same thermal conditions.

5.2.3 PDIV and PDEV

The inception and extinction voltages of the PD in the joints were measured while the joints were at stable temperature. After one hour of conditioning at the nominal voltage of 6 kV, the voltage was increased by 0.5 kV every 4 minutes until 5000 discharges could be observed in 4 minutes. When PDIV had been identified, the voltage was turned up an extra step, before it was turned down and PDEV was measured. PDIV and PDEV in all three joints is plotted as a function of estimated conductor temperature in figures 45 and 46, respectively.

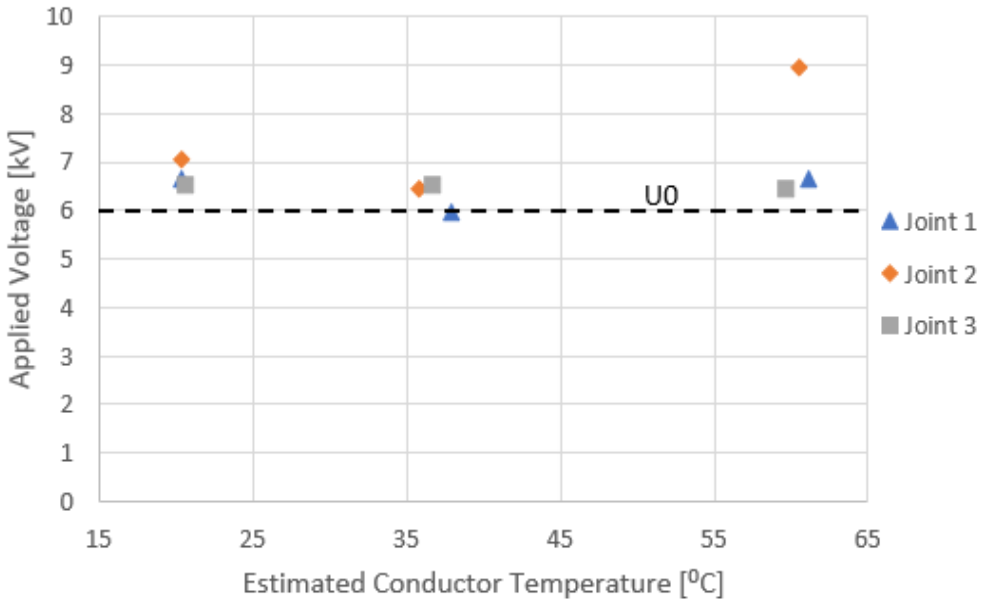

Figure 45: Partial discharge inception voltage is plotted as a function of estimated conductor temperature for all three cable joints. The service voltage of 6 kV is marked by a black, stippled line.

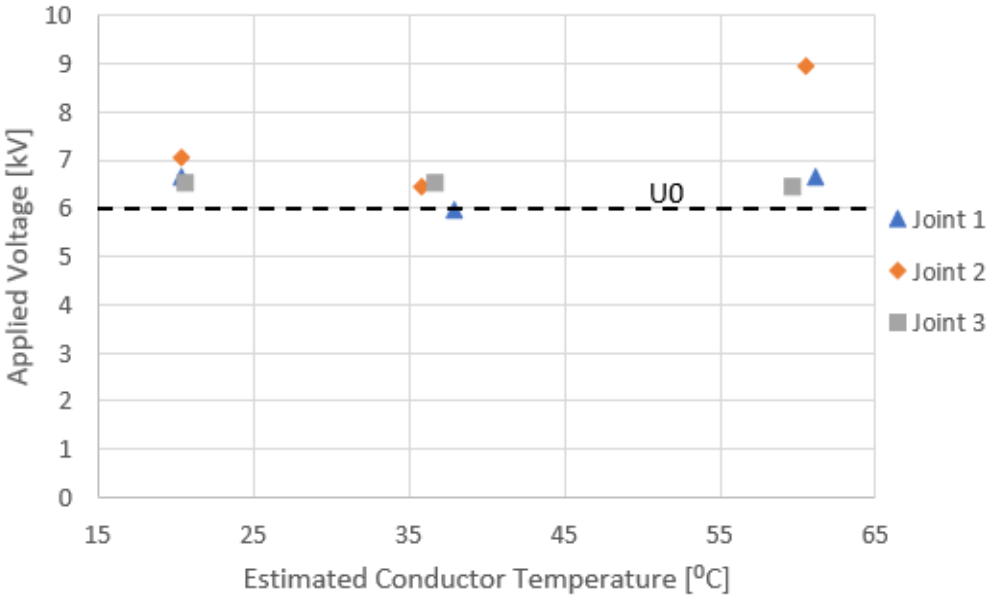

Figure 46: Partial discharge extinction voltage is plotted as a function of estimated conductor temperature for all three cable joints. The service voltage of 6 kV is marked by a black, stippled line.

As can be seen in figure 45, there is no clear trend in the PDIVs that were measured. The PDIVs measured at ~35 °C are slightly lower than those measured at room temperature. When measured at ~ 60 °C, 2 of the PDIVs showed similar values to the room temperature results. Joint 2 diverged from this by having a PDIV of 9 kV. With the exception of this measurement, all the PDIVs are in the relatively small range of 6 to 7.1 kV. The PDIVs measured in joint 3 can be said to be more or less constant across the different temperatures.

Similar traits are observed in the PDEVs in figure 46. The PDEVs show a small decrease at ~ 35 °C with respect to the measurements at room temperature. The ~ 60 °C PDEVs show an increase from the ~ 35 °C measurements. There are two outliers, both measured in joint 2(4.6 kV at ~ 35 °C and 8.7 kV at ~ 60 °C). Other than this, all the PDEV are in the range of 6.1 to 7.2 kV.

There are a couple of measurements where PDEV is found to be higher than PDIV, which should not be physically possible. During the measurements, the voltage is turned up an extra step after PDIV is believed found, as a way to ensure that the inception voltage was identified correctly. This, and the stochasticity of the PD mechanism is what makes the result possible.

Only one of the PDIV that were measured suggests that there could be discharges as the joint is in service. There is also only one PDEV which means that PDs don't necessarily extinguish during service.

Comparison with Specialisation Project Results These results are different from the changes of PDIV that were observed as the joint temperature was increased in the specialisation project work prior to this thesis, [3]. The PDIVs that were measured in the project work are plotted against the estimated conductor temperatures in figure 12. Here, it can be seen that the PDIV of the test joint was 16 kV in room temperature, and close to the service voltage of 12 kV in the temperature area 50-70 °C. [3] suggested that the temperature dependence observed in the joint might be due to the large mechanical stresses it had been subjected to previously.

The test objects used in this thesis work have not been exposed to similar mechanical stresses, and don't exhibit the same temperature dependence of PDIV. This supports the suggestion made in the specialisation project.

Comparison with Literature [2] examined the partial discharges in mass impregnated medium voltage cables at temperatures ranging from 55 to 80 °C. In the PhD thesis, an overall reduction in PD activity was observed as the temperature was increased. Hunter explained the decrease by the fact that the internal pressure of the cable increased along with its temperature. The increase of internal pressure means that the pressure in the voids is increased. The Paschen curve(figure 2) shows how this increases the void's break-down voltage.

This reasoning can also be used to explain why there is no particular decrease of PDIV in this work. The cavities in the XLPE joints will also experience an increase of pressure as temperatures are raised. Thus, their break-down voltages might also be increased.

Other Explanations If any temporary defects were developed during load cycling due to delaminations or changes in the properties of the field grading material, they do not appear to have any lower inception voltages than the other defects in the test objects.

Comment on Sensitivity It should be noted that the noise in the PD recordings in some cases make it hard to judge whether the 5000 discharge criterion is reached or not. One consequence of this, is that the actual PDIV might be 0.5 kV higher than what is recorded. This also applies to the "off-line" PD measurements. If these issues were to be avoided, the measurements would have to be performed in a smaller lab with less background noise.

5.2.4 PD During Cooling of the Joint

The service voltage of 6 kV was applied to every test joint from right before the cycling current was turned off until it had reached 25 °C. PD streams were recorded for 1 minute every second minute. The temperature on the outside of the test object was scanned between every recording.

PRPD and Weibull plots were made, and used as a tool to analyse the data. This required some data processing. Firstly, the noise in the streams were removed, the details of how this was done can be found in appendix 4.10. Logarithmic PRPD plots were made in the OMICRON software. Weibull plots were made by exporting the streams to MATLAB and running them through the scripts that can be seen in appendix F.

Small versions of the PRPD plots of the PD that was recorded just before the cooling of the test objects had begun can be seen in figure 47. The full-size versions of the PRPD plots can be seen in appendix G.

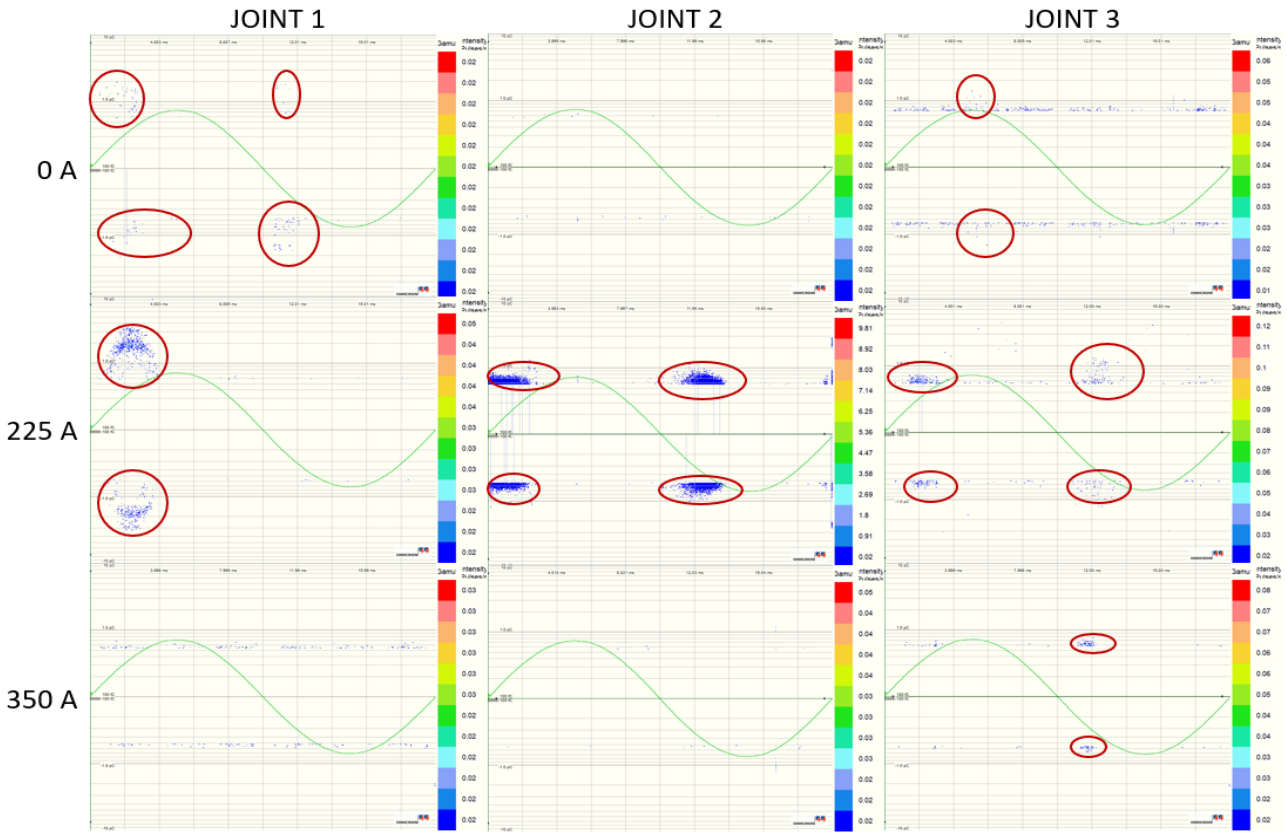

Figure 47: PD recorded for 1 minute at 6kV at each stable temperature, for every joint. The events where PDs were observed are marked in red circles. The full size versions of the PRPD plots can be seen in appendix G.

PD during Cooling from ~ 60 °C As can be seen in figure 47, there is little or no PD measured at 6 kV in room temperature and after load cycling of 350 A. PDs were identified in joint 3 for the first 5 minutes after the 350 A cycling load had been turned off. Other than this, no PDs were measured during the cooling of any joints from ~ 60 °C. The fact that no PDs were observed at 6 kV as the joints were cooled from ~ 60 °C means that during this cooling process, there were no defects with inception voltages of 6 kV or below. This neither confirms nor denies any changes of PD sources. What the results show, is that if there are any temporary defects created by delaminations or the stress control tube, they are not serious enough to cause PDs at service voltage.

If it had been necessary to examine the PD activity during the cooling of the joints from ~ 60 °C, a higher voltage could have been applied. However, this would no longer be representative of the joints' service conditions.

PD during Cooling from ~ 35 °C. Figure 47 shows that there was a significant amount of PDs measured in all three joints as 225 A was about to be turned off. There were also continuous PDs through the cooling of the joints. These are analysed by use of Weibull plots, in order to identify how many PD sources are active during the cooling process.

It was decided to examine the PD recorded every 8th minute as a measure to reduce the amount of plots. The positive and negative discharges are plotted independently, in the same diagram. The PD streams were coordinated with the temperature recordings, and the conductor temperature during the different PD recordings were estimated, as described in section 4.9. All the plots that were produced can be found in appendix H. The trends that were observed in the plots is illustrated by small versions in the paragraphs below.

Section 2.9.2 introduced that each separate slope in a Weibull plot represents a separate PD source. Therefore, the number of slopes through the cooling process are observed.

Joint 1 Weibull plots representing the key developments of PD during the cooling of joint 1 are presented in figure 48

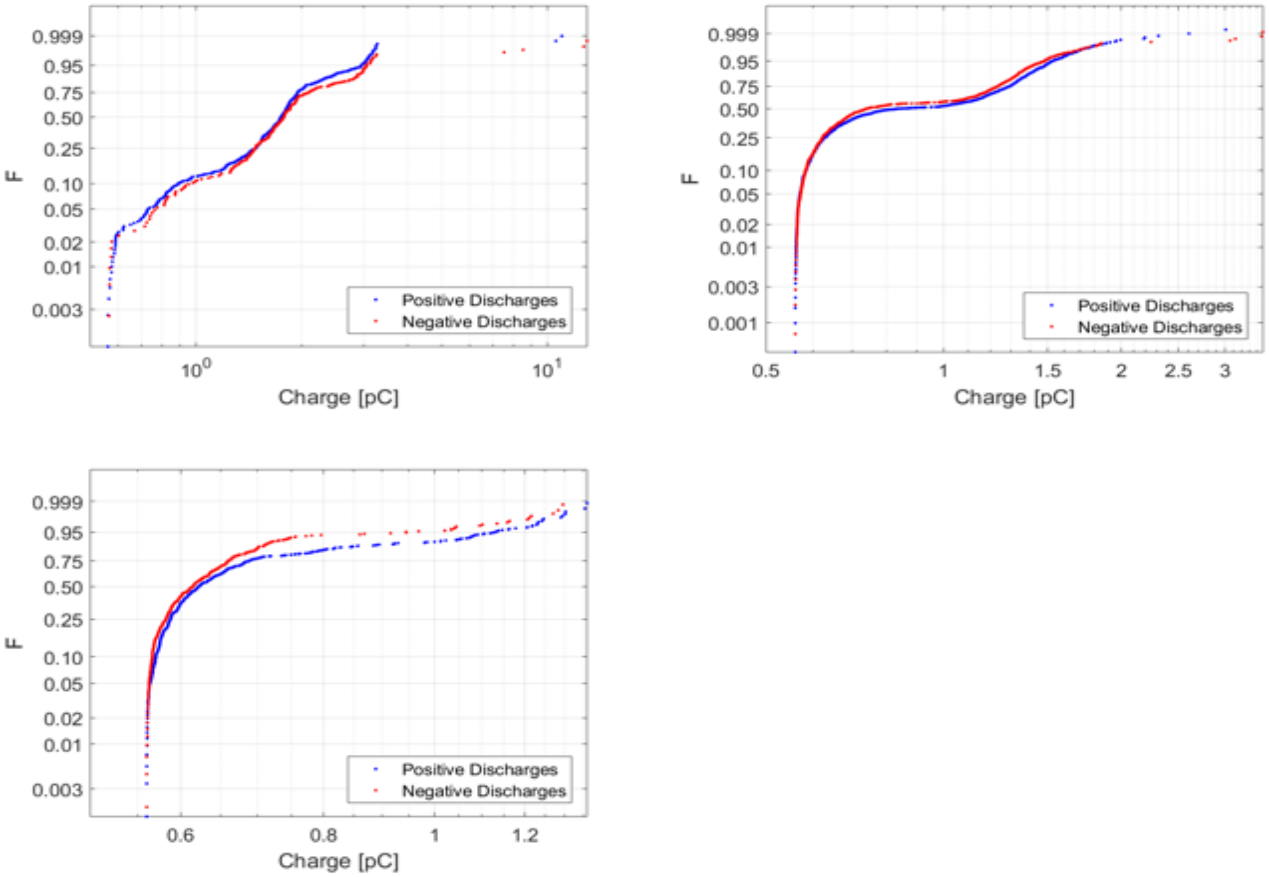

Figure 48: PD recorded in joint 1 at 6 kV during cooling. Upper left: 0 minutes after current turned off, estimated conductor temperature: 36.7 °C. Upper right: 24 minutes after current turned off, estimated conductor temperature: 32.7 °C. Lower left: 1 hour and 52 minutes after current turned off, estimated conductor temperature: 26.6 °C.

6 different slopes can be observed in the plot from right after the current was turned off. The estimated conductor temperature at this time was 36.7 °C. 24 minutes after the current was turned off, the number of observable slopes was reduced to 4. At this time, the estimated conductor temperature is 32.7 °C. After 1 hour and 52 minutes, 2 different slopes remain. Now, the conductor temperature is estimated to be 26.6 °C.

Thus, a decrease in active PD sources through the cooling process- from 6, by 4, to 2 is observed in joint 1.

Joint 2 The Weibull plots that were made trough the cooling of joint 2 all had 2 clear slopes. Two plots illustrating this can be seen in figure 49.

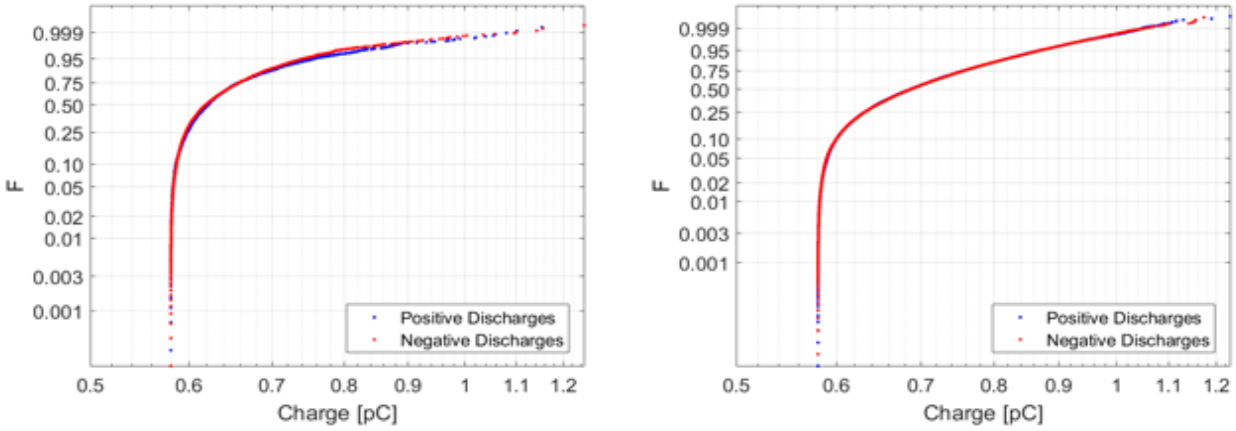

Figure 49: PD recorded in joint 2 at 6 kV during cooling. Left: just before current turned off, estimated conductor temperature: 36.7 °C. Right: 2 hours and 8 minutes after current turned off, estimated conductor temperature: 25.4 °C.

Based on this, it was concluded that there were 2 active PD sources throughout the cooling process of joint 2.

Joint 3 The development of PDs that were measured during the cooling of joint 3 can be seen in figure 50.

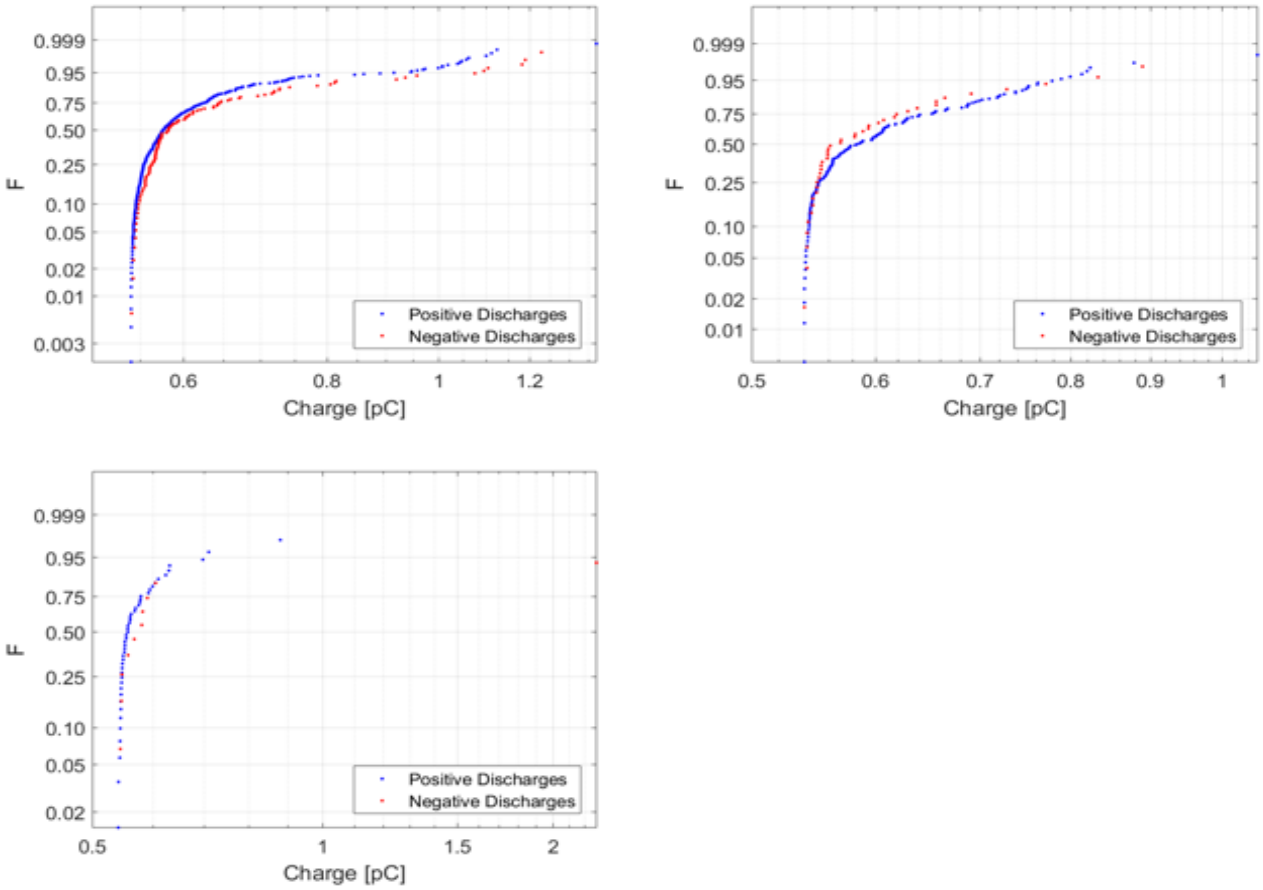

Figure 50: PD recorded in joint 3 at 6 kV during cooling. Upper left: 0 minutes after current turned off, estimated conductor temperature: 36.7 °C. Upper right: 1 hour and 4 minutes after current turned off, estimated conductor temperature: 29 °C. Lower left: 2 hours and 8 minutes after current turned off, estimated conductor temperature: 25.5 °C.

The Weibull plot that was made right after current was turned off can be said to have either 3 or 2 slopes, depending on how conservative the interpretation is. At this time, the estimated conductor temperature is 36.7 °C. 1 hour and 4 minutes, as the conductor temperature is estimated at 29 °C, 2 slopes are seen. In the final plot that is presented, there is only one slope in the plotted data.

So the number of active PD sources in joint 3 is also seen to decrease through the cooling process.

Analysis of the Findings In 2/3 of the cooling processes from ~ 35 °C, a varying number of PD sources was observed.

This could be a result of uneven contraction of the materials in the joints, or due to the temperature dependence of the stress control tube. It could also be due to a reduction in internal pressure, and hence increase of break-down strength of cavities. But it is should also be kept in mind that this reduction of active PD sources could be entirely random. Partial discharges are after all a highly stochastic phenomenon, and this would not be the first time the PD in a defect was extinguished for no apparent reason.

Comparison with Literature These findings are a contrast to the results in [2], where the number of PD sources was found to have increased considerably after the mass cable had cooled down from 80 °C. The change of PD characteristics was explained by a decrease of impregnate viscosity and reduction of internal pressure- both increasing the likelihood of creation of new voids. In

addition to this, the overheating might have stretched the cable's lead sheath further than its elastic limit.

The test objects in this work were not exposed to overheating, and do, of course not, contain any mass impregnate that can fill voids. This might justify the different results.

5.3 Stage 3: PD localisation, Break-Down Voltage and Dissection

5.3.1 Acoustic Localisation of PD

Acoustic localisation done in an attempt to to identify the PD sources of the cable joints. This was done by moving an acoustic sensor to predetermined measuring points around the test objects. PDs were initiated and any detected signals were recorded. The applied voltage was increased to approximately 30 kV, where electrical measurements showed stable apparent charge magnitudes. These were 100, 200 and 150 pC for joints 1, 2 and 3.

As explained in section 2.8, the energy of the acoustic signals emitted by PDs is absorbed by the material it travels through, and so the signal is damped. This can be interpreted to mean that PD sources are likely to be located close to the measuring points where acoustic signals were identified.

The signals that were measured are presented and discussed for each joint below.

Joint 1 The peak-to-peak magnitudes of the PD signals that were measured acoustically on joint 1 are displayed in table 7.

Table 7: Peak-to-peak magnitudes of acoustically detected PD signals in joint 1, given in [mV]. If no signal was detected in the point, this is marked by a "-".

	Detection Point								
Row	1	2	3	4	5	6	7	8	9
1	-	-	-	-	-	-	-	-	-
2	55	41	-	-	-	-	11	-	-
3	-	-	-	-	30	23	-	19	-
4	-	-	32	-	-	-	-	-	-

These results indicate that there are several discharge sources in the test object. They are spread along the joint and vary in size.

Joint 2 The peak-to-peak magnitudes of the PD signals that were measured acoustically in joint 2 are displayed in table 8.

Table 8: Peak-to-peak magnitudes of acoustically detected PD signals in joint 2, given in [mV]. If no signal was detected in the point, this is marked by a "-".

	Detection Point								
Row	1	2	3	4	5	6	7	8	9
1	-	-	-	-	-	-	-	-	-
2	-	-	52	-	-	-	-	-	-
3	-	-	37	-	-	-	-	-	-
4	-	-	-	-	-	-	-	-	-

These measurements indicate one or two discharge sources located by measuring point 3, in two adjacent rows. This location is indicated on the test object in figure 51.

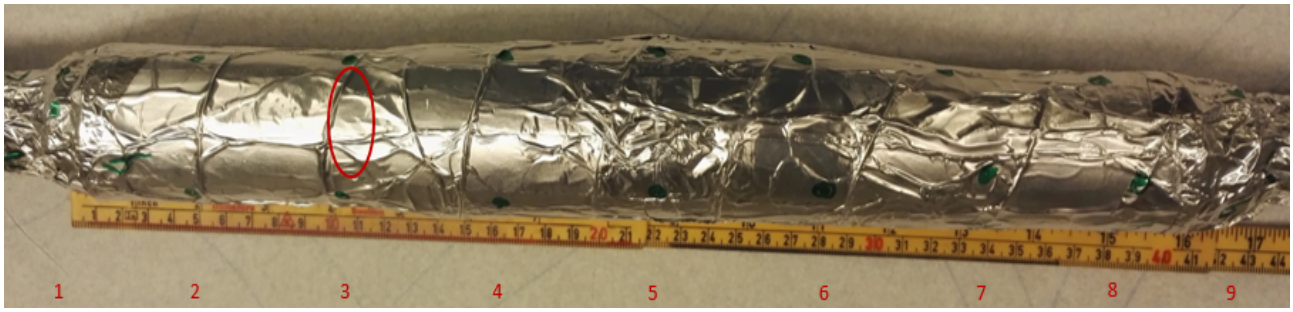

Figure 51: Illustration of where the PD sources are detected in joint 2.

As can be seen in figure 51, the measuring points where PD is detected are located by the cut-off of the cables' outer semiconductor. This means that the defect might be associated with the field grading material in the joint.

Coincidentally, the Weibull plots of PD during the cooling of joint 2 in section 5.2.4 indicates two sources.

Joint 3 The peak-to-peak magnitudes of the PD signals that were measured acoustically in joint 3 are displayed in table 9.

Table 9: Peak-to-peak magnitudes of acoustically detected PD signals in joint 3, given in [mV]. If no signal was detected in the point, this is marked by a "-".

	Detection Point								
Row	1	2	3	4	5	6	7	8	9
1	-	75	-	-	25	37	-	27	-
2	-	25	-	-	25	34	-	-	-
3	-	30	-	-	-	-	-	-	-
4	30	23	30	19	100	67	-	-	-

Similarly to joint 1, these results also indicate several PD sources spread along the joint. PDs were detected in the majority of the measuring points on row 4, this is also where the largest signals were measured.

Remarks on the PD Located in Joints 1 and 3 The results in both joints 1 and 3 show many sources, along all of the joint. In both cases, more sources are located acoustically, than what was identified during the cooling of the joints. This is a result of the high voltages of ~ 30 kV that were applied during acoustic localisation. There is no way of saying which of the acoustically located PD sources are active when 6 kV is applied during the joint's cooling.

It would have been very interesting to be able to measure PDs during cooling, and perform acoustic localisation, under excitation of the same voltage. This would give more information about some of the sources that are active during the cooling process. However, this would have to be at a higher voltage than 6 kV, as the PDs that were measured at this voltage are too small to be detected by acoustic sensors.

5.3.2 Break-Down Voltages

The break-down voltages of the test objects were measured by use of a 500 kV voltage transformer. Water terminations were applied to the joints in order to avoid overheating and subsequent thermal break-down. For this reason, voltage steps of 5 kV/ 1 minute was chosen. The break-down voltages that were measured are presented in table 10.

Table 10: Measured break-down voltages, given in RMS.

	Break-down Voltage [kV]
Joint 1	65
Joint 2	65
Joint 3	50

As can be seen in table 10, all break-down voltages are around 8-11 times the service voltage. This means that if a fault were to happen in the distribution grid, it would take a large over-voltage for break-downs to occur in the joints. This is an indication of the test objects being in a relatively good condition. condition.

5.3.3 Observations from Dissection

After the break-down voltage tests had been performed, all three test joints were dissected. This was done by removing all the heat shrink tubes the joints were built up of. The findings were documented by pictures taken by a cell phone and a digital microscope. The findings will be presented joint by joint, before some common traits are analysed in the end of the section.

Joint 1 Joint 1 showed signs of having undergone a thermal break-down. Pictures of these can be seen in figures 52 and 53.

Figure 52: Above: signs of punctuation and tracking on the stress control tube. Below: signs of punctuation and tracking by semiconductor cut-off and on joint body.

Figure 53: Tracking observed on the outer semiconductor.

As can be seen in the pictures, there are signs of a large current on the surfaces of the joint's components. The puncture from the break-down appears to be located by the cut-off of the outer semiconductor, just a few mm from where the conductive varnish stopped.

The joint mastic was originally yellow, and can be seen to have aged.

Joint 2 Pictures of the damages observed on joint 2 can be seen in figure 54

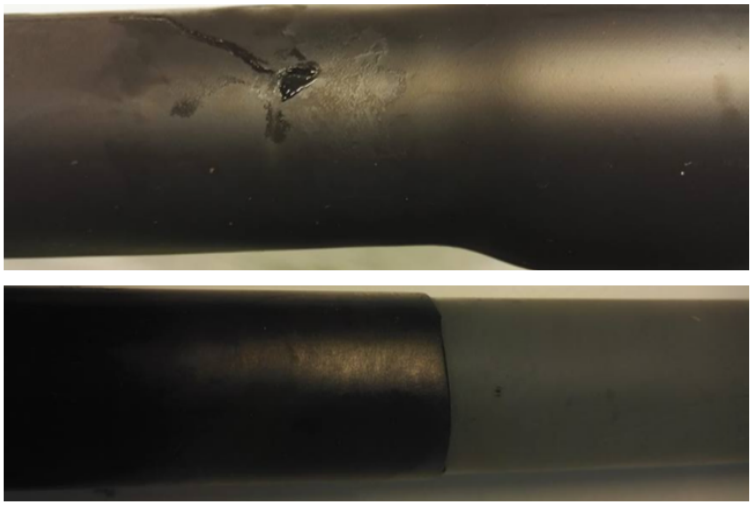

Figure 54: Above: puncture on the stress control tube. A liquid byproduct comes out of it. Below: Puncture on the XLPE

Here, there are less traces of tracking and a much smaller puncture. This joint also has its puncture close to the outer semiconductor cut-off. Microscopy of the puncture shows that an electric break-down has occurred, this can be seen in figure 55.

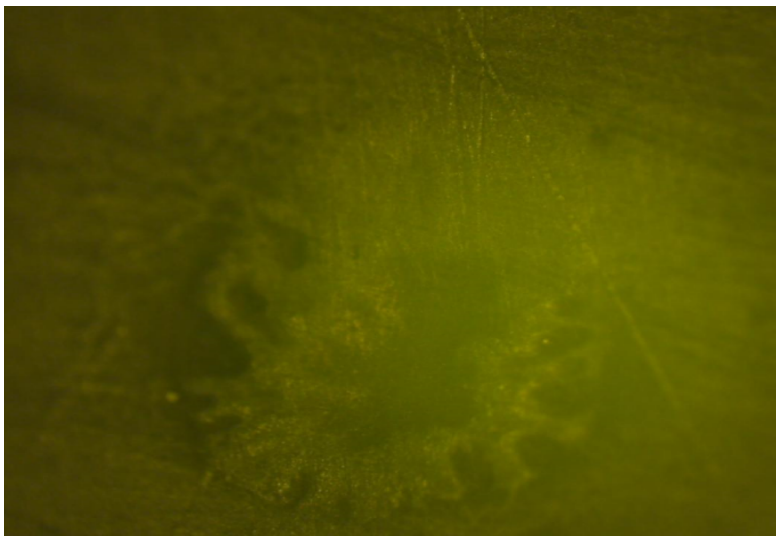

Figure 55: Picture taken of the puncture of joint 2, by help of a digital microscope.

Joint 3 The damages that were identified on joint 3 can be seen in figure 56.

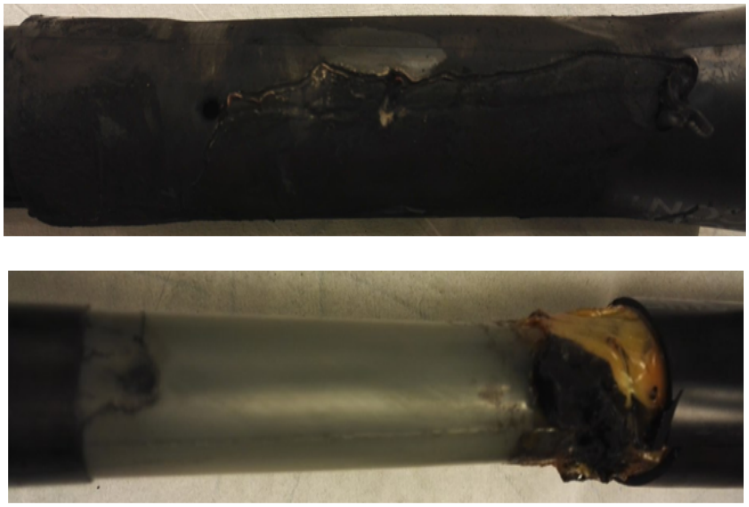

Figure 56: Above: signs of punctuation and tracking on the stress control tube. Below: signs of punctuation and tracking by semiconductor cut-off and on joint body.

Similarly to joint 1, joint 3 show signs of having undergone a thermal breakdown. There is tracking, and parts of the joint body appears to be burnt. The puncture is also here located close to the outer semiconductor cutoff.

Analysis of Findings The tracking that has been observed on the test objects could be a result of PDs prior to the break-down, or a result of the break-down test itself. This could be investigated in future work by dissecting before any break-down testing is performed. By doing this, one would also lose valuable information, so the trade-off would have to be considered carefully.

A combination of black and white marks were found in the interface between the outer and middle heat shrink tubes of all three joints. These can be seen in figure 57

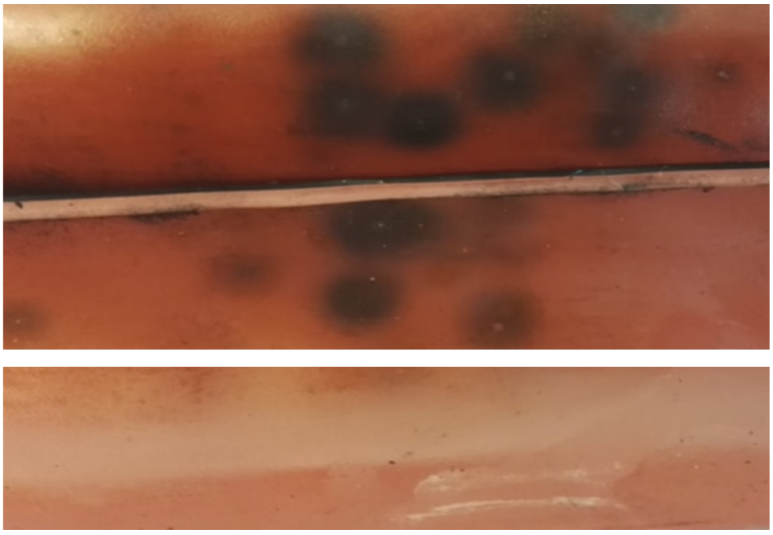

Figure 57: Above: black marks in the interface between the middle and outer heat shrink tubes

These were studied closer by help of a digital microscope. Close-up pictures of the black areas can be seen in figure 58.

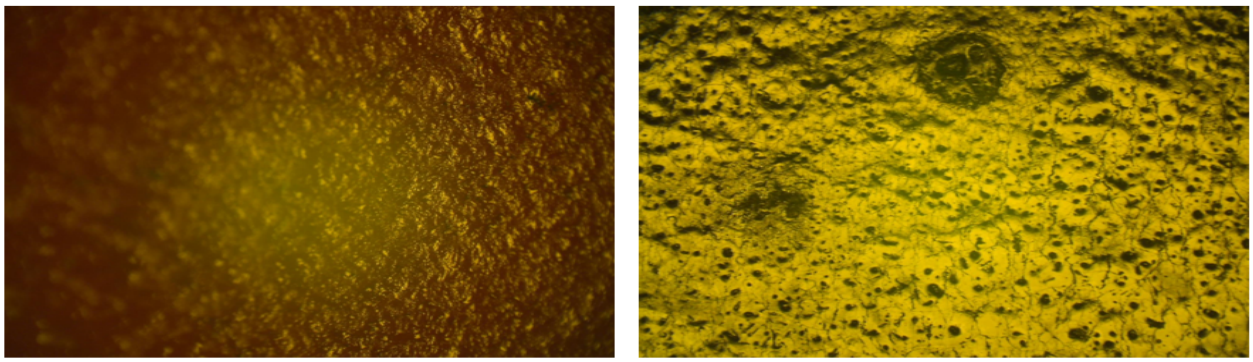

Figure 58: Left: Insulation without any marks. Right: The yellow part of the picture is one of the black circles that are seen on the insulation, the black circle in the picture, is one of the white points inside the black circle on the insulation.

Microscopy of the black circles on the insulation shows signs of erosion, as seen in figure 58. The pits are particularly deep in the black circle on the picture- which is the white points inside on of the black circles in figure 57. The erosion is likely to be the result of partial discharges, and the white points could be pits that are in a process of developing to electrical trees,

A picture of the white areas in figure 57 taken by help of a digital microscope can be seen in figure 59.

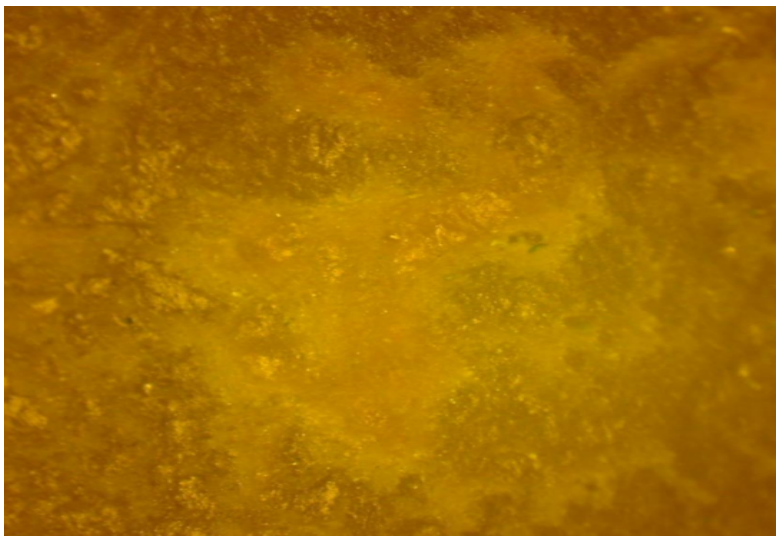

Figure 59: Picture of parts of the white areas on the insulation, taken by digital microscope.

The picture in figure 59 shows degradation of the insulation surface. This ageing is very likely a result of the water which is known to have penetrated into the cable joints.

5.4 Analysis of PDIV Measured "On-line" and "Off-line"

The key objective of this master thesis was to analyse how well off-line PD testing with 0.1 and 50 Hz voltages describe the condition of a three-phased service aged, medium voltage cable joint. This was mainly characterised by the PDIV measured during simulation of on-line and off-line conditions.

The PDIVs that were measured are summarised below:

- "Off-line", 0.1 Hz: PDIV is 3-6 kV or 1-1.5 kV depending on whether or not conditioning was performed.
- "Off-line", 50 Hz: PDIV is 5.7-7.1 kV when the joints are conditioned and 6.1-7.6 kV when they are not.
- "On-line", 50 Hz: With the exception of one (higher) outlier, the PDIV measured when the joints were at typical service temperatures were all between 6 and 7.1 kV

The PDIV measured with a VLF source were very low(1-1.5 kV) when conditioning was not performed and mostly low (3-6 kV) when it was. The majority of these PDIV are far under the service voltage, indicating that the equipment is in a critical condition. The scattering of the results makes it hard for the utility to decide which PDIV represents the condition of the equipment.

As a contrast to this, the PDIVs that were measured "off-line" at power frequency are much more consistent. They indicate that there might be discharges in one of the joints depending on its voltage history, meaning that they show a much better condition than the VLF measurements.

The "off-line" PDIVs measured with 50 Hz voltage are much closer to the findings during "on-line" PDIV measurements than what the PDIVs at 0.1 Hz voltage were. Hence, they might be the best representation of the joint's condition during service, and of its condition in general. This is supported by the relatively high break-down voltages that were measured in all joints. They show that although the joints may be aged, they are not in such a critical condition as the VLF PDIVs indicate.

The "off-line" 50 Hz measurements were also showed to yield reliable results with relatively short voltage steps. This can be utilised to reduce the time the equipment is taken out of service.

If the 0.1 Hz results are interpreted too literally by the utility, it risks misdiagnosing the cable system, which could result in substantial economic losses.

5.5 Analysis of Findings About PD Sources

The second aim of this thesis was to investigate whether the PD sources in the cable joints are temperature dependent. This is interesting due to the finding of temperature dependence of resistive field grading tubes' conductivity ([1]), which could cause critical field enhancements near the outer semiconductor cut-offs on the cables. In addition to this, there is a possibility of temporary delaminations during the joints' load variations.

Three activities in the experimental work targeted this topic specifically. These were the recording of PDs during cooling of the joints with subsequent Weibull analysis, acoustic PD localisation, and the dissection of the joints after their break-down voltages had been measured.

In the cases where PDs were detected at 6kV during cooling, Weibull analysis showed a decreasing number of PD sources in 2 out of 3 cases. In the third case, joint 2 showed 2 clear PD sources throughout the cooling process. When acoustic localisation was performed on joint 2, 1-2 sources were located, by the cut-off of the outer semiconductor.

Acoustic localisation showed many sources that were spread along the joints, in joints 1 and 3. These are hard to relate to the findings during cooling, as the acoustic localisation had to be performed at a higher voltage excitation.

Dissection of the joints after break-down testing showed punctures by the outer semiconductor cut-offs on all three joints. Hence, this was the location that reached the break-down field strength first on all three joints. In 2 of the joints, these were thermal break-downs, where current had heated the field grading material, degrading their ability to redistribute the electric field. Analysis by microscope showed signs of water degradation and PDs occurring between the insulating heat-shrink tubes in all three joints.

These findings can be interpreted to point in the direction of there being temperature dependence in the active PD sources. Being able to confirm anything would, however, require further investigation.

One way of doing this would be to find a way to perform acoustic localisation on the cable joints while they are at different temperatures. This would be hard to do securely if the heating was done by current cycling. Another way in which it could be done is to keep the test object inside a heated compartment, and perhaps use several acoustic sensors at the same time.

6 Conclusions

This master thesis has compared the condition assessment of service aged medium voltage cable joints by partial discharges when the joint is "on-line" and "off-line". Off-line conditions were simulated by performing PD measurements in room temperature with 0.1 and 50 Hz voltage sources, with and without voltage conditioning. On-line conditions were simulated by load cycling and voltage conditioning of the test objects.

A second aim of the thesis work has been to investigate whether there is any temperature dependence in the defects with PD activity. This was examined by Weibull analysis of the PDs recorded during cooling of the cable joints, acoustic PD localisation and dissection of the joints.

- With the exception of one higher outlier, the PDIV of the test objects was not found to vary significantly with the service temperature.
- The PDIVs measured "off-line" with a VLF voltage were very dependent of whether voltage had been applied recently or not. Some of the results showed a very critical condition while others didn't, this can make the measurements hard to interpret for the utility.
- The PDIVs measured "off-line" at power frequency were more consistent with regards to conditioning than those made at VLF. The PDIVs measured "off-line" and "on-line" at power frequency were in the same, fairly narrow range. This indicates that PDIV measurements made off-line at 50 Hz describe the joints' condition during service well.
- The break-down voltages that were measured confirm that the PDIVs measured "off-line" at 50 Hz described the joints' condition better than those measured at VLF.
- Investigations of the nature of the PD sources suggests that they might be caused by the temperature dependence of the field grading material, and that temporary delaminations might also have occurred. Further investigations will be necessary for any certain conclusions to be drawn.

7 Further Work

The following work could be done in continuation of this thesis:

- "Off-line" PD measurements should be performed also while the test objects are cooling down. This would simulate the situation where loading is removed right before PD is measured off-line.
- Estimation of the conductor temperature could be improved by installing thermocouples in the conductor of a test joint, provided there is an extra available.
- It would be interesting to perform electrical PD measurements during the cooling of the cable joints, and acoustic PD localisation, at the same voltage.
- If a method of how to perform acoustic PD localisation at different temperatures was developed, this would be a good way to investigate whether PD sources are temperature dependent.

References

[1] B. Abil,"Condition Assessment of Medium Voltage Cable Joints: Dielectric Spectroscopy of Field Grading Materials", M. S. Thesis, Dept. Elect. Power Eng., NTNU, Trondheim, Norway, 2017.

[2] J. Hunter, "An investigation into partial discharge activity within three-phase belted cables", Dept. Elect. Eng. and Comp. Sci., University of Southampton, Southampton, UK, 2013.

[3] I. Bjurholt, "The Effect of Temperature Cycling on Partial Discharges in a Field Aged Cable Joint", Specialization Project Report, Dept. Elect. Power Eng., NTNU, Trondheim, Norway, 2017.

[4] E. Ildstad, "Condition Assessment of Power Apparatus", *Internatonal Conference on Communication, Computer and Power*, Muscat, Oman, 1998, pp. XIX- XXIII.

[5] F. H. Kreuger, "Industrial High Voltage Volume II" Delft, Netherlands: Delft University Press, 1992.

[6] IEC Report, Publication 505, "Guide for Evaluation and Identification of Insulation Systems of Electrical Equipment", 1975.

[7] *High-voltage test techniques - Partial discharge measurements*, IEC Standard 60270 , 3rd ed., 2000.

[8] F. H. Kreuger, "Industrial High Voltage Volume I" Delft, Netherlands: Delft University Press, 1992.

[9] L. Niemeyer, "A Generalized Approach to Partial Discharge Modeling" *IEEE Trans. on Dielectr. Electr. Insul.*, vol. 2, no. 4, pp. 510-528, August 1995.

[10] E. Ildstad, *TET4160 Insulating Materials for High Voltage Applications*, Trondheim: NTNU 2015.

[11] T. Dao et al., "A Comparative Study of Partial Discharges Under Power and Very Low Frequency Voltage Excitation", *Annual Report Conference on Electrical Isulation and Dielectric Phenomena*, Des Moines, IA, USA, 2014.

[12] K. Skjelsvik, "Overoppheting av mellomspennings PEX kabelskjøter", M. S. thesis, Dept. Elect. Power Eng., NTNU, Trondheim, Norway 2017.

[13] El-Sayed M. El-Refaie, M. K. Abd Elrahman and O. Zidane, "Internal Discharge Properties for Different Solid Insulating Materials", 2016 ©IEEE. doi: 10.1109/MEPCON.2016.7837013.

[14] C. Forssen "Modelling of cavity partial discharges as variable applied frequency",Ph. D. Dissertation, Dept. Elect. Eng., KTH, Stockholm, Sweden 2008.

[15] E. Ildstad,*TET 4195 High Voltage Equipment, Cable Technology*Trondheim: NTNU, 2009.

[16] "Electrical test of a straight joint, Type SXSU 5131 for screened single core plastic insulated-cable 20 kV without armour", Raychem GmbH, Munich, Germany. Rep. PPR 763, 1986.

[17] T. Christen et al, "Nonlinear Resistive Electric Field Grading Part 1: Theory and Simulation, " IEEE Electr. Insul. Mag., vol. 26 (Volume: 26, Issue: 6, November-December 2010).

[18] *IEEE Guide for Partial Discharge Testing of Shielded Power Cable System in a Field Environment*, IEEE Standard 400.3, 2006

[19] J. Perkel and J. C. Hernandes-Mejia, "Chapter 7: Medium Voltage Cable System Partial Discharge" in *Cable Diagnostic Focused Initiative- CDFI Phase II*, GA: Georgia Tech Research Corporation, 2016.

[20] H. Tollefsen, "Tilstandskontroll av mellomspennings kabelskjøt", M. S. Thesis, Dept. Elect. Power Eng., NTNU, Trondheim, Norway, 2014.

[21] L. Lundgaard, "Partielle Utladninger: Begreper, måleteknikk og mulige anvendelser for tilstandskontroll", SINTEF Energi, Trondheim, Norway. Rep., 1996.

[22] *5 kV Digital Insulation Testers MEGGER BM11D MEGGER BM21*, 9th ed., MEGGER, England.

[23] J. C. Fothergill et al.,"The measurement of very low conductivity and dielectric loss in XLPE cables: a possible method to detect degradation due to thermal aging", IEEE Trans. Dielectr. Electr. Insul.,vol: 18, no: 5, October 2011, pp. 1544-1553.

[24] L. Lundgaard, "Partial Discharge- Part XIII: Acoustic Partial Discharge Detection- Fundamental Considerations", IEEE Electr. Insul. Magazine, vol. 8, no. 4, pp. 25-31, July/August 1992.

[25] H. Illias et al., "Partial Discharge Patterns in High Voltage Insulation", *IEEE International Conference on Power and Energy*, Kota Kinabalu Sabah, Malaysia, 2012, pp. 750-755.

[26] A. Contin et al., "Applications of the Weibull Function to Partial Discharge Data Coming from Different Sources Typologies", *Conference on Electric Insulation and Dielectric Phenomena*, Virginia Beach, VA, USA, 1995, ©IEEE. doi: 10.1109/CEIDP.1995.483732.

[27] H. Faremo et al. "Service Experience for XLPE Cables Installed in Norway- From Graphite Painted Insulation Screens to Axially and Radially Water Tight Cable Constructions" in *14th International Conference ad Exhibition on Electricity Distribution*, Birmingham, UK, 1997, pp. 3.2.1-3.2.5.

[28] *MPD 600 User Manual*, MPD600:AE.2 ed, OMICRON electronics GmbH, 2009.

[29] K. Skjelsvik, "PD-målinger på mellomspennings PEX-kabelskjøt ved lastsykling", Specialization Project, Dept. Elect. Power Eng., NTNU, Trondheim, Norway, 2016.

[30] S. Boggs, "The Case for Frequency Domain PD Testing in the Context of Distribution Cable", IEEE Electr. Insul. Mag., vol: 19, no: 4, pp. 13-19 Aug. 2003.

[31] *Draka Teknisk Håndbok*, 4th ed., Draka Norsk Kabel, Drammen, Norway, 2010.

[32] L. Lundgaard, "Partial Discharge- Part XVI: Acoustic Partial Discharge Detection- Practical Application", IEEE Electr. Insul. Magazine, vol. 8, no. 5, pp. 34-43, September/October 1992.

[33] *TSLF (3X1), twisted single phases*, Data Sheet, Nexans, Norway, Generated 2018.

[34] COMSOL 5.3a Software Documentation, COMSOL AS, 2017.

[35] *ABB Switchgear Manual*, 12th ed., ABB, Dusseldorf, 2006.

[36] M. R. Ward, *Electrical Engineering Science*, McGraw-Hill, 1971.

[37] *Electric cables - Calculation of the current rating - Part 1-1:Current rating equations (100% load factor) and calculation of losses - General*, IEC Standard 60287 , 2nd ed., 2014.

[38] K. Solheim, "Electric Heating of Subsea Pipelines: Design and Testing of an Applicable Ring Core Transformer", M. S. Thesis, Dept. Elect. Power Eng., NTNU, Trondheim, Norway, 2013.

Appendix A Equipment List

Registration Number	Type	Nominal Value	Producer
B01-0013	HV Transformer, 1 phase	220 V/100 kV	Ferranti
B01-0293	Transformer Control Unit, 1 phase	0/260V-8-A max, 1 phase	NTNU
B01-0791	Variac Transformer, 1 phase	230 V- 0-300V, 3-900 A	Noratel
G05-0150-02	Data Logger Module	300 V, 1 A, 50 W	Agilent
G05-0172	Data Logger	300 V, 100 $M\Omega$, 10 MHz	Agilent
H02-0172	OMICRON PD Detection System		Power Diagnostix
H01-0121	Insulation Resistance Tester	15 kV	Megger
P03-0193	IR camera		Thermo Tracer
P07-1569-07	PC		Dell
P07-2263	PC		Dell
G04-0258	Oscilloscope	100-120 V, 30 W	Tetronix
B02-0635	VLF Voltage Source	20 kV, 20 mA, 0.01-0.1 Hz	b2 High-Voltage
B02-0635-1	VLF Voltage Filter		b2 High-Voltage
I06-0413	Voltage Probe	40 kV, peak	Fluke
106-0140	Voltage Probe	12 kV, peak	Electronix
S03-0355	Multimeter	10 A, 600 V	Fluke
N07-0088	Filter	10 kHz-1.2 MHz, 20, 40, 60 dB	Physical Acoustics
N07-0088-01	DC Source	27 V DC	NTNU
	Acoustic Sensor, PAC 515D-389		

Appendix B Testing Aluminium Tape Glue Resistance

The resistance of the glue on the aluminium tape is tested to ensure that the glue conducts well. If the tape resistance is high, this can lead to an uneven potential distribution in the aluminium tape, which should all be at ground potential. Another undesirable effect is that the capacitive current which should be flowing in the grounding could be redirected to the semiconductor.

The glue resistance was measured in a simple way. Two approximately 2×12 cm large pieces of aluminium tape were applied evenly to a flat slab of copper. The copper was cleaned by an isopropanol solution in advance to remove any dirt. The test configuration can be seen in figure 60.

Figure 60: A flat copper slap with two pieces of aluminium ape

The resistance between the top of the tape and copper slab was measured by help of a fluke multimeter, at regular spacing of 1 cm along the pieces of tape. The goal in testing along the length of the piece was see that is had a consistently low resistance. The multimeter probes were applied with an even pressure, and the resistance value was allowed to stabilise before it was recorded. The measured resistances can be seen in figure 61.

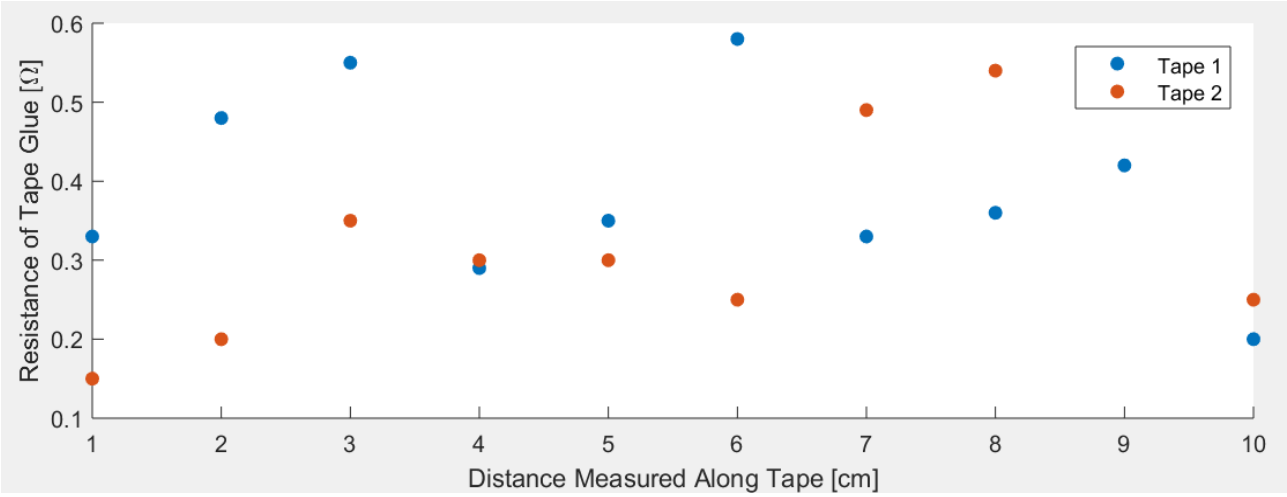

Figure 61: The resistances measured along two pieces of aluminium tape, mounted on a copper slab.

As can be seen in figure 61, the resistance measured along both pieces are well below 1Ω, which means that the glue conducts well. The error sources mentioned previously are thus unlikely to impact this work considerably.

Appendix C Initial Testing of Cycling Loads

A first range of cycling currents was set based on the initial draft of the COMSOL model. These were 100, 150, 175, 200 and 225A, and they were estimated to reach temperatures up to 50 °C. Joint 2 was temperature cycled with these loads at the beginning of test 2. The resultant stable temperatures are plotted in figure 62.

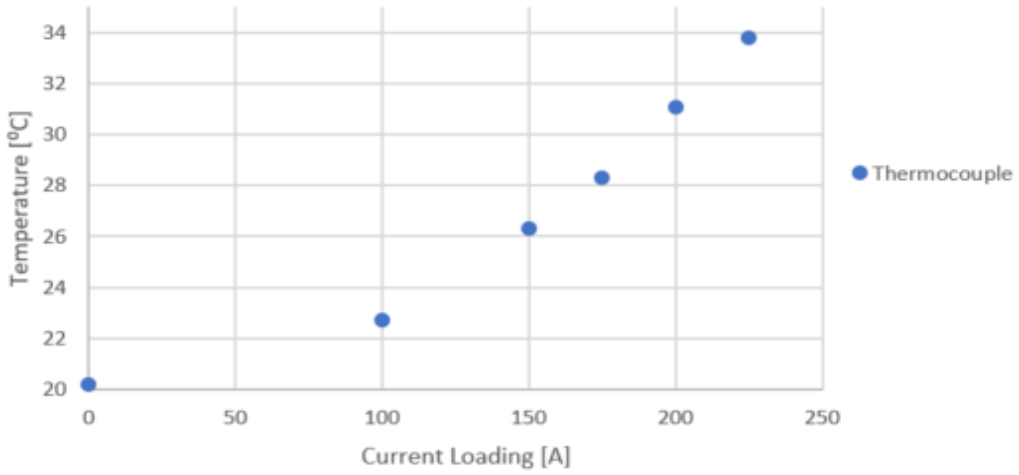

Figure 62: Plot of the stable temperatures measured in the thermocouple on joint 2 during the initial cycling tests.

As can be seen in the figure, the maximum temperature that was reached is 35 °, which is colder than anticipated.

Appendix D COMSOL Simulation

D.1 Introduction

Because the conductor temperature is best indication of the thermal stress the field grading material and insulation is exposed to, it is desirable to know. It is not possible to measure temperature with thermocouples in high voltage areas. This means that during PD measurements, the only information of temperatures available is that which is measured on the outside of the test object.

Finding the conductor temperature based on the outside measurements can be done either by calculations, or by simulating the system. As calculating the conductor temperature would be complex and most likely require over-simplifications, it was decided to build a simulation model.The exact composition of the test joints are not known, and therefore it is not possible to model their thermal conditions. What is known, is how the cable part of the test object is built up, and therefore, it is simulated in the joint's place.

The contact resistance in the joints' metallic connectors is most likely higher than the resistance in the cable conductors. This means that the conductor temperature found by help of the simulation model probably is lower than the conductor temperature experienced by the joint connector. By tracking the temperature on the outside of both the cable and joint parts of the test objects, it is possible to get an indication how good the temperature estimate is. If the outside temperatures are similar, the conductor temperatures might also be so, and vice versa.

A thermoelectric model of the test object cable is built using the multiphysics software COMSOL. It will be used as a tool to determine the cycling currents that will be used in the cycling part of the experimental work, and to calculate the cable conductor temperature at steady state and during cooling. At first, an initial model was made. Later on, it was adjusted to fit the lab measurements as well as possible.

The rest of this chapter details how the simulation model was built and the choices that were made underway. It starts by describing the physical system that is being modelled. Then basic features of the model and its geometrical structure are explained. Then the material properties are given, and the selection of electrical and thermal conditions are discussed. A subsection detailing how the model was adapted to fit the lab observations follows.

D.1.1 Description of the System being Modelled

The system that is modelled is a cable, covered in a layer of thermal insulation. The current flow and resistive losses in the conductor is the main heat source. The heat is conducted out through the cable's semiconductor and insulation, and slightly less so trough the thermal conductor. From the surface of the thermal insulation, the heat is transported into the air by convection and radiation [15]. An illustration of the physical system can be seen in figure 63.

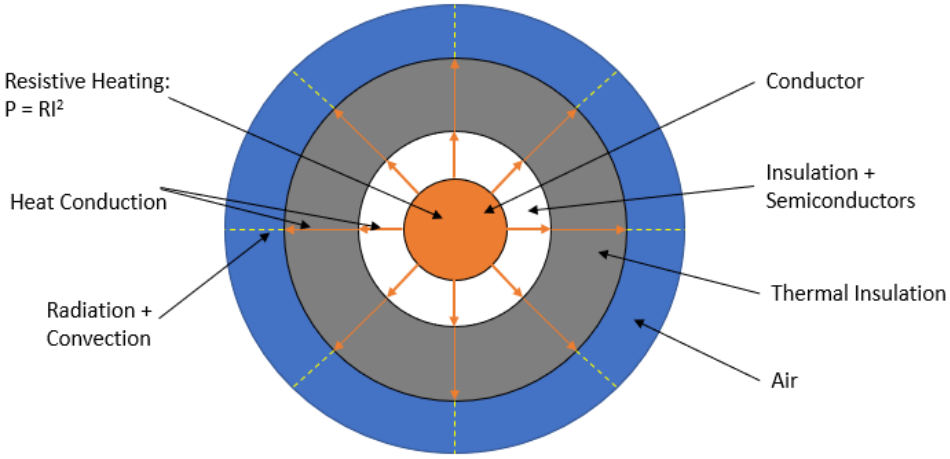

Figure 63: Figure of the test object cable with thermal insulation. The orange/ yellow details symbolize the heating and cooling of the cable. The arrows on the left side of the figure identify the heating and cooling mechanisms in action. The arrows on the right side of the figure identify the different components of the test object cable.

D.2 Building the Model: First Draft

The construction of the first draft of the model is described in this section. Some system parameters are assumed in this version of the model. These will be adjusted to fit the measurements made on the test object in a second draft.

D.2.1 Basic Features

Because the heat in the cable moves radially, a 2D space dimension was chosen for the model geometry. This makes the three-dimensional cable into a concentric circular configuration, a simplification that will reduce convergence time of model.

Two physics packages were chosen. Magnetic Fields(mf) is used to model the resistive losses in the conductor, and Heat Transfer in Solids (ht) the consecutive heating, and heat transportation through the test object. The packages are coupled by use of the Electromagnetic Heat Source (emh1) interface, which helps them communicate. In this way, the magnetic field package can adjust the conductor resistivity according to the temperature, and the heat transfer in solids package can convert the electrical losses to heat.

Frequency-stationary and frequency-transient studies were used in the simulations. The frequency component of the time studies account for the effects associated with the current being AC. The frequency-stationary study computes steady state temperatures, and is mostly used as a tool during the development of the model. The frequency-transient study is used to see how the conductor temperature stabilizes over time, during both heating and cooling.

D.2.2 Model Geometry

The key part of the geometry is the cable with its thermal insulation. It is placed in the center of the model's coordinate system, and consists of three circles that are elaborated below;

- The conductor is wound of strands with a total, cross-sectional area of 240 mm^2. The space taken up by the strands, and therefore the physical dimension of the conductor is larger than

this. Because the origin of the test object cable is unknown, an effective radius of 9.1 mm is read out of a data sheet for a similar cable with the same dimension [33], and used in the model.

- The thickness of the inner semiconductor, insulation and outer semiconductor was found to be 5 mm by a circumference measurement. These layers are assumed to be one, as they are all plastics with similar thermal properties, and it would reduce the model's convergence time. Thus, the insulation and semiconductors are represented by a circle with a 14.1 mm radius.
- A 20 mm thick layer of thermal insulation is added outside the cable, as a circle with radius 34.1 mm.

The thermal insulation is held in place by self-vulcanising insulation tape. The tape is made of polyethylene, and is thus similar to XLPE. The layer of tape is approximately 1 mm thick, and due to having a much higher thermal conductivity than the insulation, will not affect the distribution considerably. The layer is excluded because it will increase the model's computation time.

A 1 cm thick, circular return current conductor, whose necessity is discussed in section D.2.3 is defined. Had the layer been any thicker, it might have impacted the cooling of the test object more. And if it had been smaller, the mesh would have to be finer, and the computation time increased. It is placed as a coaxial layer, 1 m out from the cable.

A last domain of air is defined 10 m out from the return conductor. The cable, return conductor and air domain can all be seen in figure 64.

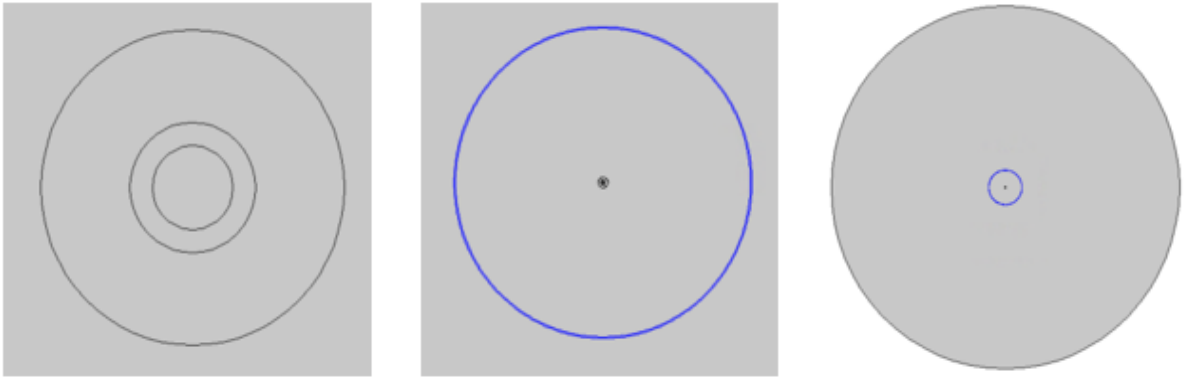

Figure 64: Figures of the features of the model geometry. Left: Cable with thermal insulation. Middle: Concentric, 1 cm thick return conductor. Right: The outer air domain.

D.2.3 Magnetic Fields Conditions and Properties

The default nodes associated with the physics package are;

- Ampere's Law: This node specifies the domains where the magnetic field is controlled by Ampere's Law; meaning all other domains than the conductors.
- Magnetic Insulation: A default boundary condition of the interface, which sets the tangential component of the magnetic potential to zero [34]. It is typically used for modelling lossless metallic surfaces, which is not relevant to the model. Therefore, it is not applied to any domains.

Coils The current flow in the cable's conductor is modelled by a Coil. Coils are AC current sources that models phenomena such as the skin effect. The current amplitude is specified by a parameter and is changed depending on the scenario.

For the simulations to converge, there must also be a return conductor of the same amplitude. This must have the same amplitude, but opposite polarity of the original current source. The coaxial, conducting layer described in section D.2.2 is included in the model for this purpose. It is placed 1 meter outside of the cable so that they don't affect each other's fields considerably.

Impedance Boundary Condition This boundary condition is useful when the electromagnetic field only penetrates a short distance outside the boundary. It approximates the penetration which means that one doesn't have to make another domain. The boundary conditions are defined around the edge of the outer air domain, and its parameters relative permittivity, relative permeability and electrical conductivity are set to 1, 1, and 1×10^{-5} [S/m].

D.2.4 Heat Transfer in Solids: Conditions and Properties

There are three default nodes in the Heat Transfer in Solids physics package, they are listed below;

- Solid: In this node, the solid parts of the model are specified, and their properties read in from the defined materials. Also, the model's absolute pressure is set to 1 atm in this node.
- Initial Values: This node defines an initial temperature of 293.15 K for the system, which is used as an initial condition for time dependent studies.
- Thermal Insulation: Defines a boundary across which there is no heat flux. This is placed on the return current conductor as the thermal conditions outside of it are not important.

Heat Flux This node adds convective heat flux at the boundary of the test object, and is defined on the edge of the thermal insulation. The external temperature of 293.15 K and the convective heat flux coefficient is defined. The conditions in the lab can be described as natural convection in a room with walls, ceiling and floor. According to [35], appropriate constants for these conditions are 5 and 7 [W/(m^{2}K] for air moving upwards and downwards, respectively. This was not known, so a coefficient of 7 [W/(m^{2}K] was assumed.

Diffuse Surface This condition adds radiation as a way of cooling to the test object boundary. It is defined around the outside of the thermal insulation. In the node, ambient temperature is set to 293.15 K, and the emissivity coefficient ϵ is set to 1 because the outermost layer of self-vulcanising tape is black [34].

D.2.5 Electromagnetic Heat Source

This node defines what domains the multiphysics package is active in. The test object and return current conductor are selected here.

D.2.6 Material and Their Properties

Four different materials are used in the simulation model. These are aluminium, cross-linked polyethylene (XLPE), Armaflex and air. The cable and return current conductors are made of aluminium. The cable insulation is XLPE, and the thermal insulation is Armaflex. The remaining domains are defined to be air.

Aluminium and air are built-in materials, while XLPE and Armaflex are user defined. Each material is defined by six properties; relative permeability μ, electrical conductivity σ[S/m], relative permittivity ϵ, thermal conductivity k [W/(mK)], density ρ [kg/m^3] and heat capacity C_p [J/(kgK)]. These values are defined for Aluminium, XLPE and Armaflex in table 11.

Table 11: Properties of the materials defined in the simulation model.

Material Property	Aluminium	XLPE	Armaflex
Relative Permeability, μ	1	1	1
Electrical Conductivity, σ[S/m]	$\sigma = F_f \frac{\sigma_{20°C}}{1+\alpha(T-20°C)}$	1×10^{-5}	1×10^{-5}
Relative Permittivity, ϵ	1	2.3	1.2
Thermal Conductivity, k [W/(mK)]	238	0.23	0.04
Density, [kg/m^3]	2703	1	60
Heat Capacity, C_p [J/(kgK)]	900	0.189×10^7	1200

Some of these properties require more elaboration, this is done in the paragraphs below.

Aluminium Electrical Conductivity The conductivity of aluminium is, as can be seen in table 11, temperature dependent. The correlation is approximated to a linear expression, [36]. The variables in the equation are;

- $\sigma_{20°C}$ is the room temperature conductivity of aluminium, which is 3.3×10^7 [S/m], [31].
- α is the temperature coefficient per unit K, and is given to be 0.004 [1/K], [37].
- F_f accounts for the stranding of the conductor by reducing its conductivity. It is given by equation 7.

$$F_f = \frac{A_{detailed}}{A_{solid}} \tag{7}$$

Where $A_{detailed}$ is the area of the conductor strands, 240 mm^2 in this case. A_{solid} is the total conductor area, which is calculated to 260.16 mm^2 for this model.

XLPE Density and Heat Capacity When calculating temperatures, COMSOL uses the formula that can be seen in equation 8, [34].

$$Q = V\rho C_p(T - T_0) \tag{8}$$

Where V is the volume of the body, ρ is the density of the material and C_p is the heat capacity of the material. Thus, the heating of the material is dependent on the product of the material density and heat capacity.

By setting density the density to 1, and the heat capacity to 0.189×10^7, a volumetric heat capacity is defined, as in [38].

Armaflex Heat Capacity The heat capacity of the Armaflex was assumed. Based on similar materials, it was set to 1200 [J/kg*K]. This could be altered if the stabilization of test object temperature diverges from the simulation model.

D.2.7 Meshing

A physics-controlled, fine meshing size was chosen. This is a compromise between accuracy and a manageable computation time.

D.2.8 Global Definitions

All the properties that will be optimized for the second draft of the model are defined as **parameters**. This allows for evaluation of the parameters in parametric sweeps. Properties that are functions of conditions such as temperatures, are defined as **variables**.

When calculating the temperature of the test object during cooling, it is desirable to have the current sources on until the temperature is stable, and then turn them off. This is solved by help of a **step function** and an **analytic function**. The step function goes from 1 to 0 after a predetermined amount of time. The analytic function multiplies the step function with the current magnitude parameter, and is defined as the current magnitudes in the coil definitions.

D.2.9 Solver Settings

A parametric sweep tab was defined. This will be used to investigate different parameter values as the second draft of the simulation model is developed.

A PARDISO solver was chosen under the direct, time-dependent solver settings. This reduced the computation time of the model drastically.

In the settings for the time-dependent solver, the time steps taken by the solver were set to "strict" instead of the default of "free". This was done as trial and error showed that it increased the accuracy of the temperature computations significantly.

D.2.10 Data Sets

The information one wants to achieve by the simulation, is the temperature of the conductor and its relation to the temperature on the outside of the outer semiconductor. The simplest way to read out the these two temperatures are to create to data points; One where the thermocouple is placed on the outer semiconductor, and one on the edge of the conductor.

When the simulation solution is fed into the data points, the values observed in the points can be organized in plots or tables. The tables can be exported into software such as Excel for further processing.

D.3 Second Draft: Adjusting the Model to Observations

In this section, the cable temperatures computed by the model are compared to the temperatures measured during load cycling of the joint 2 at 225 A. Some critical parameters are evaluated and changed to make the simulation model as close to the measured temperatures as possible. These parameters are:

- The convective heating flux coefficient
- The thickness of the layer of thermal insulation
- The density of the thermal insulation
- The heat capacity of the thermal insulation
- The thermal conductivity of the thermal insulation

All of these properties are defined as "parameters" in the COMSOL model. Parametric sweeps are used to run several parallel simulations, with different values of the properties. The results of the improved model are compared to the temperatures measured during the cycling of 350 A, to ensure that is is good enough. When this is a place, the simulation model is used to estimate conductor temperatures.

D.3.1 Evaluation of the first draft

The thermocouple temperature found by measurements and simulation is plotted as a function of time after the current is applied, in figure 65.

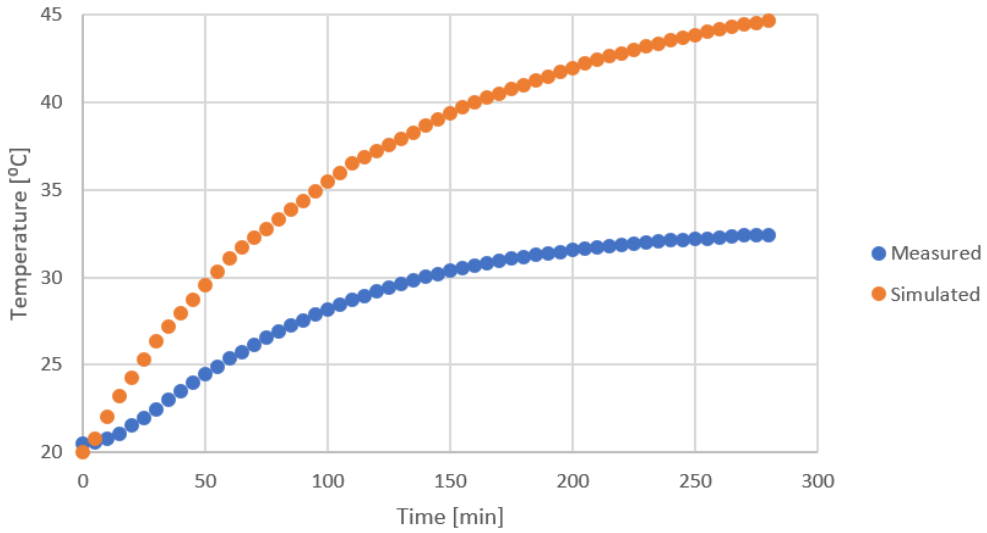

Figure 65: Comparison of the outer semiconductor temperatures found by measurements in the lab and simulation at a load of 225 A.

Figure 65 reveals that the temperatures that are measured in the lab, are much lower than those found by simulation. This indicates that the cooling of the model should be increased.

D.3.2 Parametric Sweep of the Convective Heat Flux Coefficient

Convective flux coefficients ranging from 5(free convection) to 20 $\frac{W}{m^2 * K}$, (forced convection) were tested in a parametric sweep. This was done at a 20 mm thickness of thermal insulation, 0.04 $\frac{W}{m * K}$ thermal conductivity, 1200 $\frac{J}{kg * K}$ and a density of 60 $\frac{kg}{m^3}$. The measured and computed temperatures are plotted as a function of time in figure 66

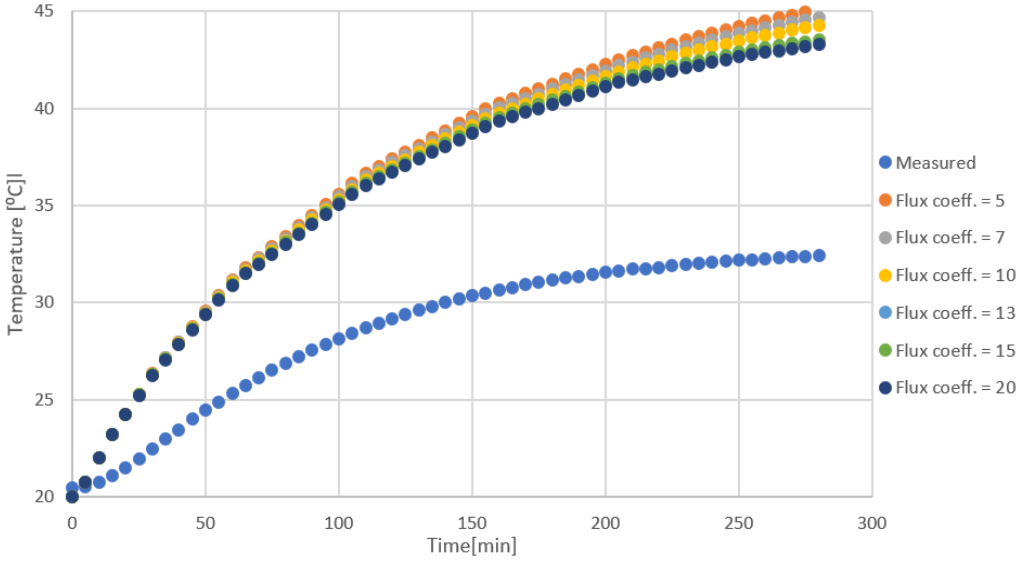

Figure 66: Comparison of the outer semiconductor temperatures found by measurements in the lab and simulation with different flux coefficients, at a load of 225 A.

As can be seen in figure 66, the flux coefficient doesn't appear to have a big effect on the temperature development in the cable. As it represents the free convection that is experienced in the lab, the previously chosen value of 7 will be kept.

D.3.3 Parametric Sweep of the Thermal Insulation Thickness

In order to make the self-vulcanising tape that the thermal insulation is fastened with stick, it needs to be tightened. This compresses the thermal insulation, meaning that its actual thickness is less than 20 mm. The effect of the thermal insulation thickness on the development of the thermocouple temperature was investigated by a parametric sweep from 15 to 20 mm. This was done with a flux coefficient of 7 $\frac{W}{m^2 * K}$, 0.04 $\frac{W}{m * K}$ thermal conductivity, 1200 $\frac{J}{kg * K}$ in heat capacity and a density of 60 $\frac{kg}{m^3}$. The measured and computed temperatures are plotted as a function of time in figure 67

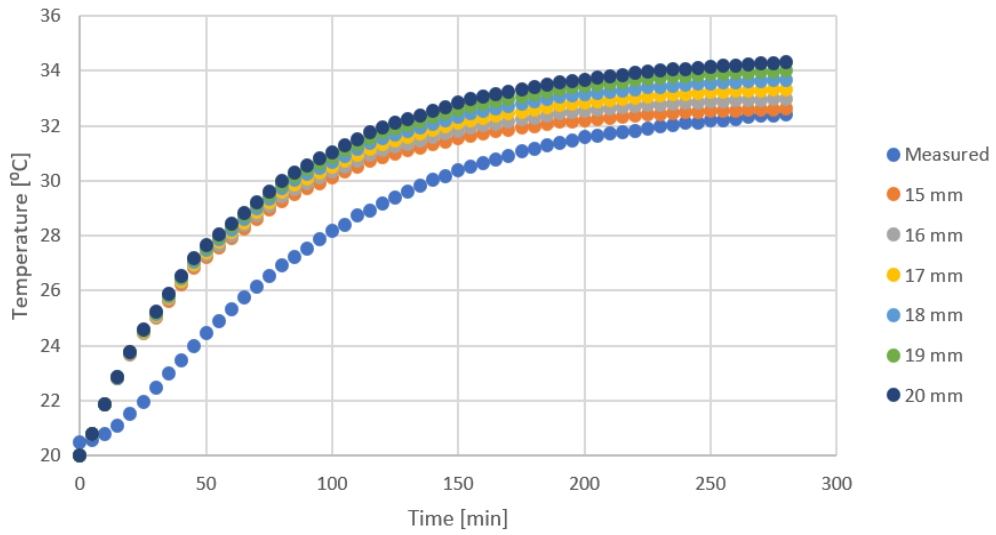

Figure 67: Comparison of the outer semiconductor temperatures found by measurements in the lab and simulation with different thermal insulation thicknesses, at a load of 225 A.

Figure 67 reveals that the temperature increases with the thickness of the thermal insulation. Based on measurements of the test objects, a thickness of 17 mm is selected.

D.3.4 Parametric Sweep of the Thermal Insulation Density

The compression of the thermal insulation causes an increase in its density, from 60 to 70 $\frac{kg}{m^3}$. A parametric sweep is done to see whether this has a large impact on the development of the thermocouple temperature. The resultant temperatures can be seen in figure 68.

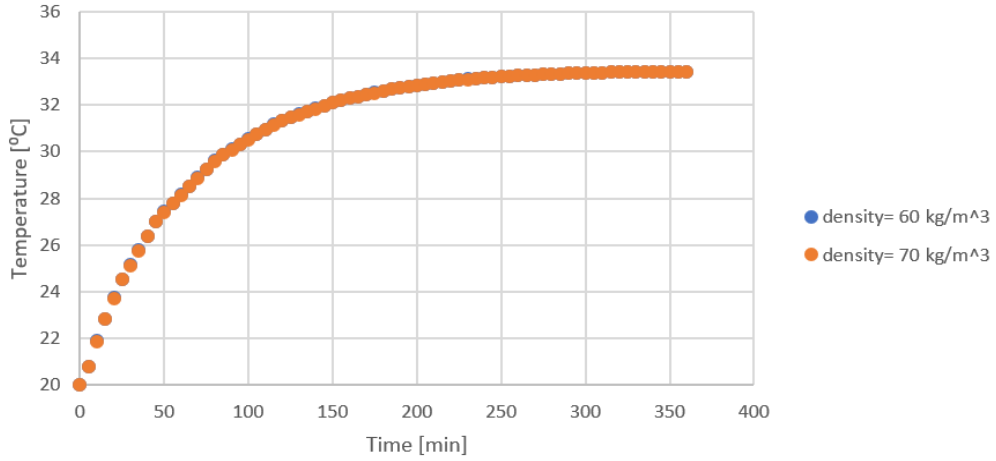

Figure 68: Comparison of the outer semiconductor temperatures found by simulation at two different thermal insulation densities, at a load of 225 A.

Figure 68 shows that the thermal insulation density has very little effect on the development of the thermocouple temperature. Thus, the parameter is changed to 70 $\frac{kg}{m^3}$.

D.3.5 Parametric Sweep of the Heat Capacity of the Thermal Insulation

The heat capacity of the thermal insulation was tested by sweeping it from 1000 to 1800 $\frac{J}{kg*K}$. During the simulation, a thermal insulation thickness of 17 mm was used. The thermal conductivity was kept at 0.04 $\frac{W}{m*K}$, the density at 70 $\frac{kg}{m^3}$ and the convective flux coefficient at 7 $\frac{W}{m^2*K}$.

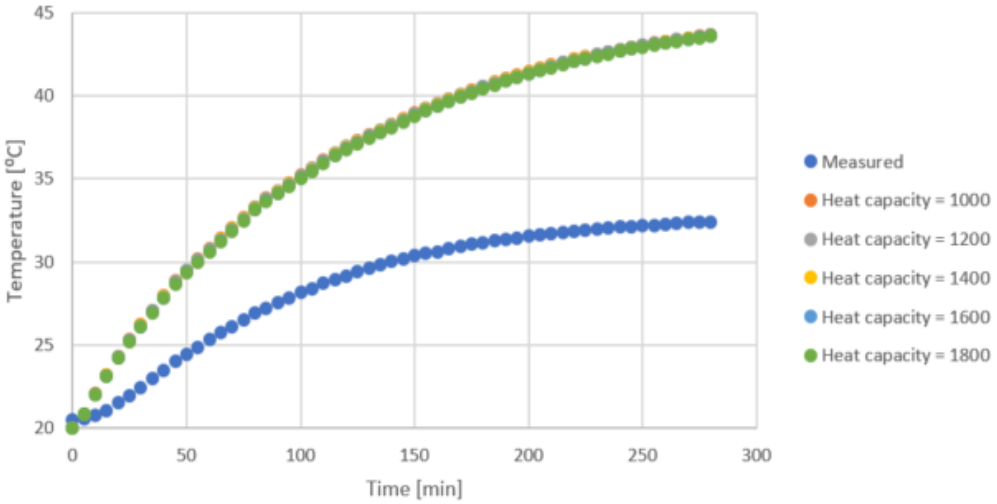

Figure 69: Comparison of the outer semiconductor temperatures found by simulation at different thermal insulation heat capacities, at a load of 225 A.

As can be seen in figure 69, the temperature in the thermocouple is more or less exactly the same for all heat capacity magnitudes. The initial value of 1200 $\frac{J}{kg*K}$ is therefore kept.

D.3.6 Parametric Sweep of the Thermal Insulation Thermal Conductivity

When compressed, the air bubbles that otherwise keeps a low thermal conductivity in the thermal insulation will lose their effect. Therefore, this property must be adjusted.

After some preliminary testing, a range of thermal conductivity from 0.06 to 0.08 $\frac{W}{m*K}$ was tested. This was done with a thickness of 17 mm, heat capacity of 1200 $\frac{J}{kg*K}$, density of 70 $\frac{kg}{m^3}$ and flux coefficient of 7 $\frac{W}{m^2*K}$. The resultant temperatures are plotted as a function of time, 70. Because this is the final property to be determined, the temperatures of the two other joints are also considered, along with the temperatures measured after 3 hours as the current is turned off.

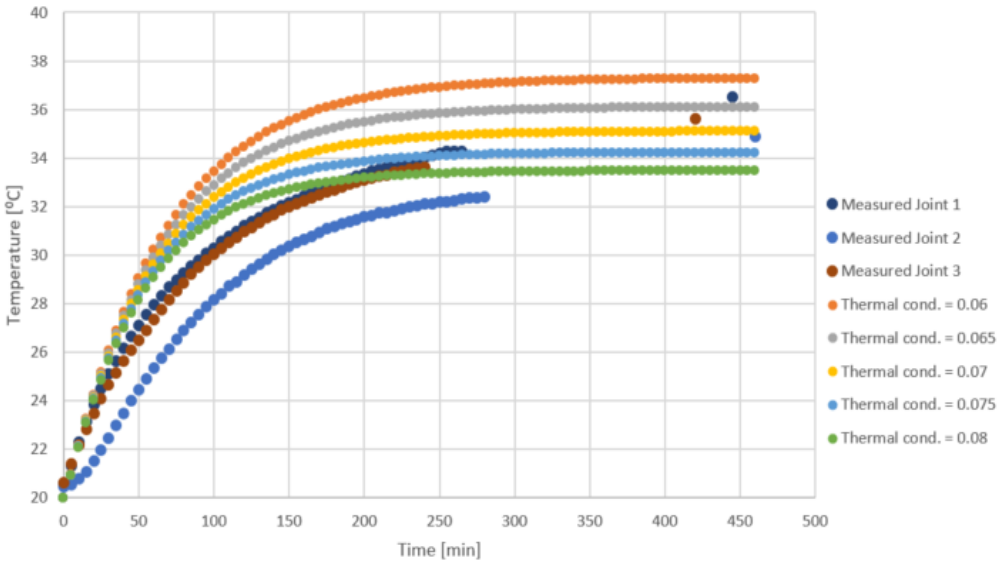

Figure 70: Comparison of the outer semiconductor temperatures found by measurements in the lab and simulation with different thermal conductivities, at a load of 225 A.

In figure 70, it can be seen that neither of the thermal conductivities give perfect fits. A thermal conductivity of 0.07 $\frac{W}{m*K}$ might however give the best compromise, and therefore it is chosen. The fact that the simulated temperatures have a much steeper growth than the measured means that the model is still far from exact. However, the simulations will mostly be used to read out momentary temperatures, and are still believed to give a reasonably good indication of conductor temperatures.

D.3.7 Chosen Parameters

The parameters that have been chosen are summarised in table 12

Table 12: Parameters chosen in the second draft of the simulation model.

Parameter	Value
Convective Cooling Flux Coefficient $[\frac{W}{m^2*K}]$	7
Thickness of Thermal Insulation [mm]	17
Thermal Insulation Density $[\frac{kg}{m^3}]$	70
Thermal Insulation Heat Capacity $[\frac{J}{kg*K}]$	1200
Thermal Insulation Thermal Conductivity $[\frac{W}{m*K}]$	0.07

D.3.8 Comparison of Simulated and Measured Temperatures at 350 A Load Cycling

To test the second draft of the simulation model, it is run at a load of 350 A, and plotted against the temperatures measured on the test objects. The resultant plot can be seen in figure 71.

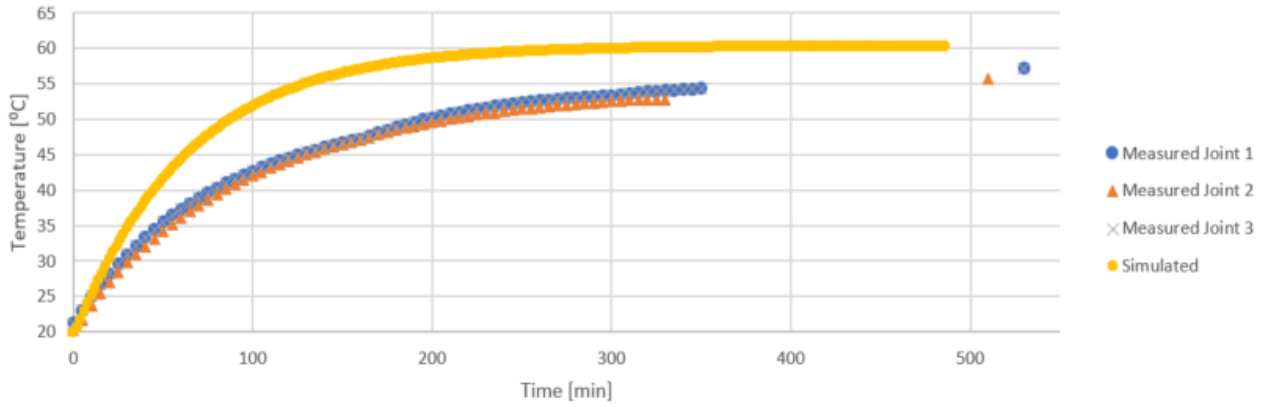

Figure 71: Comparison of the outer semiconductor temperatures found by measurements in the lab and simulation with the chosen parameters, at a load of 350 A.

In figure 71, it can be seen that the simulated temperature initially has a larger slope than the measured in the beginning. The simulated temperature stabilizes at a slightly higher value than what is measured. The temperatures measured right before the cycling currents were turned off are, however, only a few degrees below the simulation. This is about as close as the simulations can be expected to get as a result of all the error sources that occur in the lab during the measurements. These will be discussed further in section D.3.9.

D.3.9 Error Sources

The room temperature in the lab where the experiments are conducted varies between 18 and 21 °C. This is a result of the opening and closing of the lab door, which leads to a cold hallway. The intensity of the air conditioning system in the laboratory varies strongly. The convective cooling of the test object varies along with it.

The resistance in the conductor of the test object is temperature dependent. This means that the load as seen from the transformer and current source is so too. Hence, the current that is drawn into the circuit will vary as the test object is heated. This again will impact the heating of the test object.

It should also be mentioned that the test objects have undergone countless cycles of heating and cooling, which is likely to have affected its thermal properties.

All of these factors are affecting the heating of the test object, but are impossible to include in the simulation model. Hence, it is not possible to construct a simulation model that replicates the heating and cooling of the test object perfectly.

Appendix E Noise Filtering of PD Streams

The noise bands in the streams are removed based findings in the noise recordings made after the test objects reached stable temperature. The PRPDA plot of one such recording can be seen in figure 72.

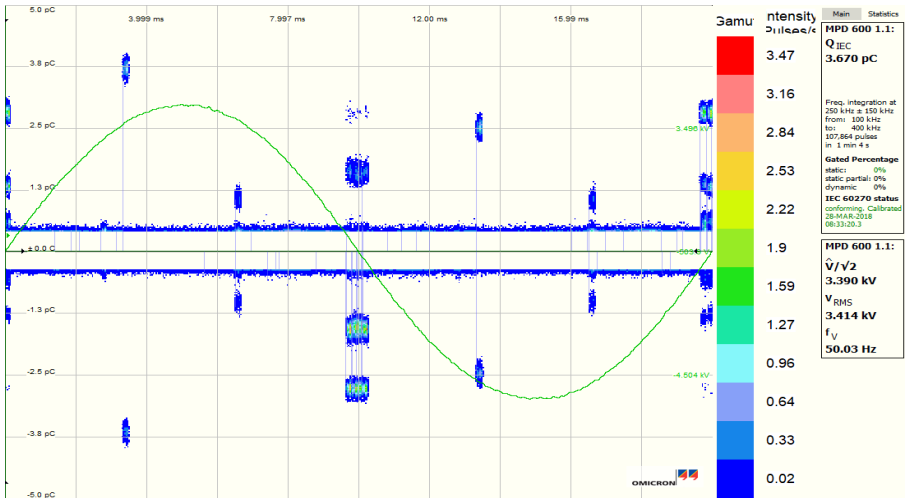

Figure 72: PRPDA-plot of a typical noise recording

All the noise streams were studied, and PD detection thresholds that would remove the noise band were identified. The noise band magnitudes that were found during the PD measurements in stage 2 can be seen in table 13.

Table 13: PD detection thresholds identified during the PD measurements in stage 2.

	Joint 1 [fC]	Joint 2[fC]	Joint 3[fC]
0 A Cycle	560	550	600
225 A Cycle	560	550	540
350 A Cycle	520	560	560

The noise at the voltage zero crossing and downwards slope are removed by use of gating. These are areas where PD is not expected to appear. If groupings of noise are observed in the phase area where PD usually occurs, and has a higher intensity than the PD, these are also gated away. This method allows almost all of the noise to be removed. The area of the PRPDA plot where PD is filtered out is illustrated in figure 73.

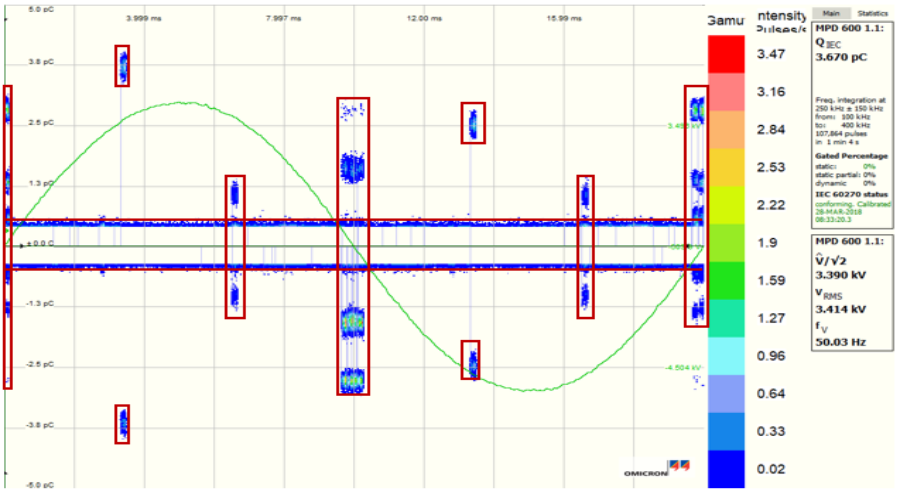

Figure 73: Illustration of the noise that is removed from the PD recordings. All the red squares indicate noise that is filtered out.

The two cleaning operations are performed as the streams are processed in the OMICRON software. A PRPDA plot of the filtered stream can be seen in figure 74. Here, the majority of the noise is gone.

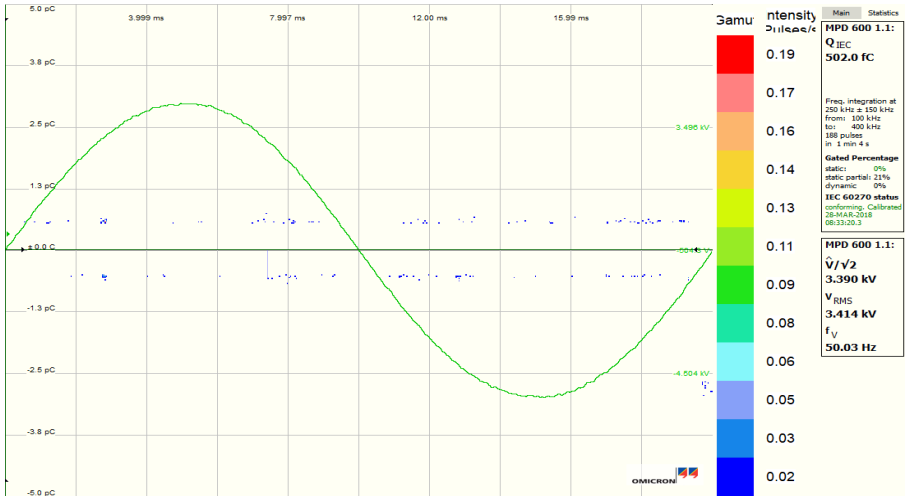

Figure 74: PRPDA-plot of the stream, after all the noise has been filtered away.

Appendix F MATLAB Scripts

statistisk_analyse_2_param_weibull_ingz.m | masterMappeAnalyse.m | importAllDataFunc.m

```
% THIS SCRIPT TAKES IN A PATH- MINUS THE TWO FINAL NUMBERS, IN ADDITION TO
% THE AMOUNT OF FOLDERS TO ITERATE TROUGH. IT THEN IMPORTS DATA, AND
% WEIBULL PLOTS THEM.
%ONLY WRITTEN FOR UP TO 99, CONSECUTIVE FOLDERS

% DEFINE VARIABLES
pathbase = 'C'; % Path minus the 2 final numbers
firstnum = 1; % first file number
lastnum = 17; % last file number


for i = firstnum : lastnum % iterate through folders
    % GENERATE PATH TO FILE
    if i < 10 % need to add an extra 0 in the path
        newpathbase = strcat(pathbase, '0'); % add 0
        num = num2str(i); % make iterator a string
        path = strcat(newpathbase, num); % complete path
    else % don't need extra 0 in path
        num = num2str(i); % make iterator a string
        path = strcat(pathbase, num); % complete path
    end

    %READ OUT DATA FROM STREAMS
    [PH, phase_deg, Q, t_q, t_v, V] = importAllDataFunc( path );
    Q = -Q; % reverse sign of Q

    % GENERATE WEIBULL PLOT
    statistisk_analyse_2_param_weibull_ingz( Q, i )
end

```

statistisk_analyse_2_param_weibull_ingz.m | masterMappeAnalyse.m | importAllDataFunc.m

```
function [PH, phase_deg, Q, t_q, t_v, V] = importAllDataFunc( path )
% clc
% clear all

%Uncomment the following line if trendplot.m is needed:
%trendplot
%Digitized, pre-processed PD parameters

file = path;
%Voltage sampled every 48 microsecond
[t_v, V] = importVdata(file, 'unit1.1');

%The apparent charge of every PD event and the time of occurance
[t_q, Q] = importQdata(file, 'unit1.1');

%Phase position for every PD event [0,1] where the number represent the
%percentage of the voltage cycle.
PH = importPHdata(file, 'unit1.1');

%Phase of each PD event in degrees
phase_deg = PH*360;
%Importing data from text file
%See the trendplot script to change the file being read from

clearvars file

end
```

The functions importVdata, importQdata and importPHdata are the same as those used in [29].

statistisk_analyse_2_param_weibull_ingz.m | masterMappeAnalyse.m | importAllDataFunc.m

```
function [ ] = statistisk_analyse_2_param_weibull_ingz( Q, plotNum )

Q= -Q;
%ITERATE THROUGH Q AND ASSIGN VALUES TO QPOS AND QNEG
Qneg = zeros(3,1);
Qpos = zeros(3,1);
posCount = 1;
negCount = 1;
for i = 1: length(Q)
    if ( Q(i) < 0) %Discharge negative
        Qneg(negCount, 1) = Q(i);
        negCount = negCount + 1;
    elseif( Q(i) > 0 ) %Discharge positive
        Qpos(posCount, 1) = Q(i);
        posCount = posCount + 1;
    end
end
%Q neg given positive sign
Qneg = -Qneg;
%%
%Sorting the data:
Q1data = sort(abs(Qpos))*1e12;
Q2data = sort(abs(Qneg))*1e12;
%%
%Median rank approximation:
n1Data = length(Q1data);
prob1 = ((1:n1Data)-0.3)./(n1Data+0.4);
y1Data = log(log(1./(1-prob1)));

n2Data = length(Q2data);
prob2 = ((1:n2Data)-0.3)./(n2Data+0.4);
y2Data = log(log(1./(1-prob2)));

```

```
%% Two-parameter Weibull Distribution Plot
figure(plotNum), ...
    semilogx(Q1data, y1Data,'b.');
    hold on
    semilogx(Q2data, y2Data, 'r.');
    hold off

    ylabel('F')
    xlabel('Charge [pC]')

    %DEFINE AXES
    p = [0.001 0.003 0.01 0.02 0.05 0.10 0.25 0.5...
         0.75 0.95 0.999];
    label = {'0.001','0.003', '0.01','0.02','0.05','0.10','0.25','0.50', ...
         '0.75','0.95', '0.999'};
    tick  = log(log(1./(1-p)));
    set(gca, 'YTick', tick);
    set(gca, 'YTickLabel', label, 'Fontsize',13);
    ylim([log(log(1./(1-0))) log(log(1./(1-.9999999)))])
    xlim([0.5 inf])
    set(gca,'xscale','log')
    grid

    legend('Positive Discharges', 'Negative Discharges', 'Location', 'southeast')

end
```

Part of the code used to make Weibull plots of the data is a product of previous summer internship work at SINTEF Energy Research.

Appendix G PRPD Plots of PD at 6 kV Right Before Current was Turned Off

G.1 Joint 1

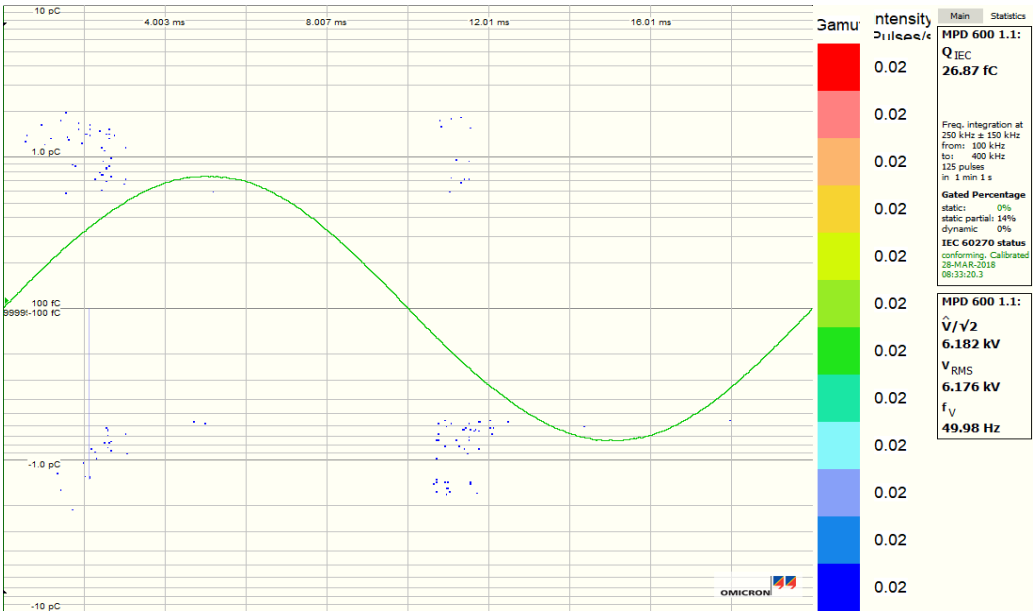

Figure 75: PRPDA-plot PD recorded in joint 1 at 6 kV at the end of the PD measurements in stage 2, at room temperature.

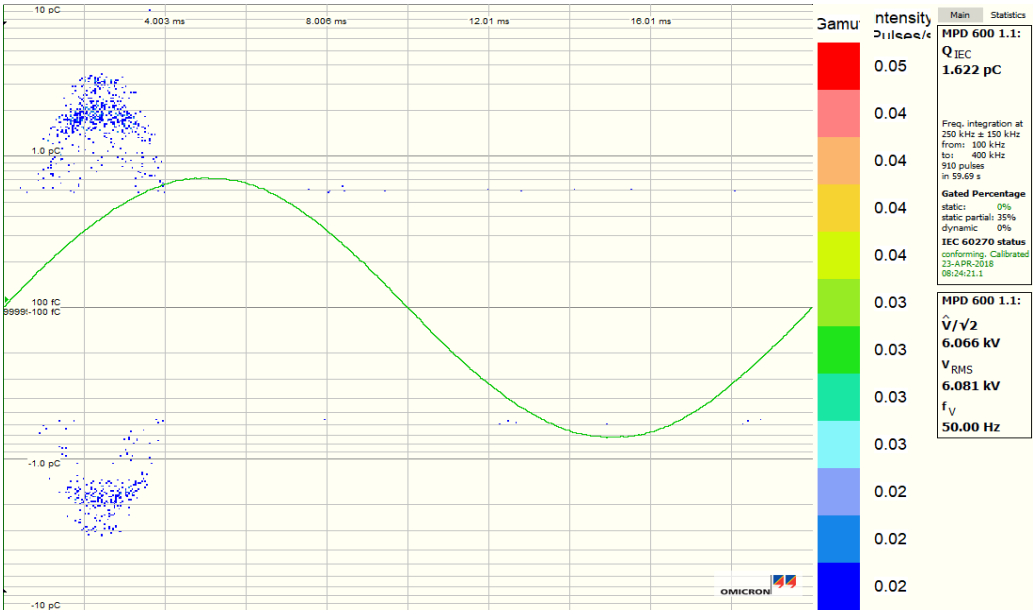

Figure 76: PRPDA-plot PD recorded in joint 1 at 6 kV at the end of the PD measurements in stage 2, at load cycling of 225 A.

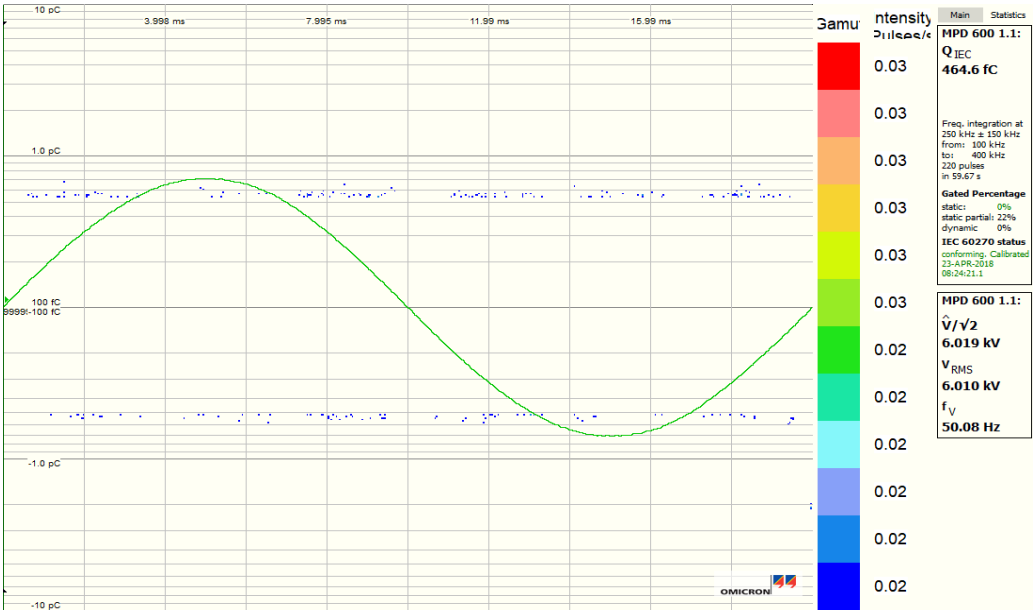

Figure 77: PRPDA-plot PD recorded in joint 1 at 6 kV at the end of the PD measurements in stage 2, at load cycling of 350 A.

G.2 Joint 2

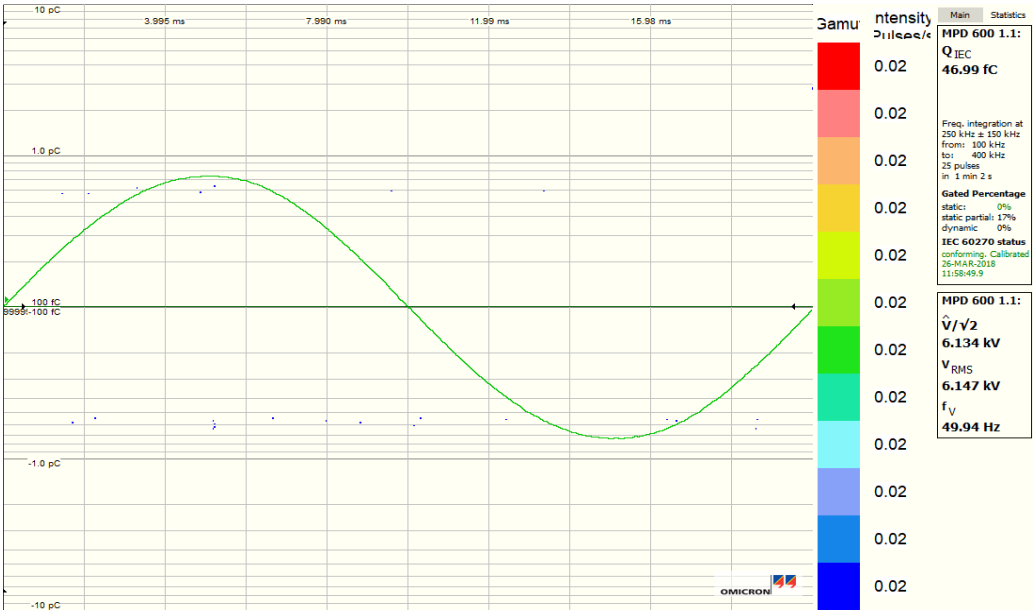

Figure 78: PRPDA-plot PD recorded in joint 2 at 6 kV at the end of the PD measurements in stage 2, at room temperature.

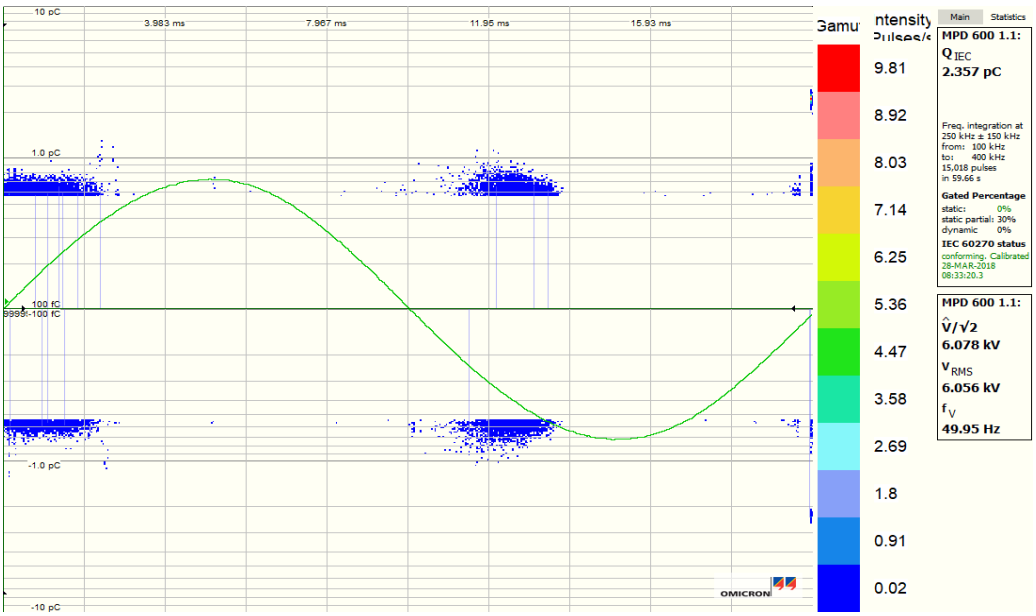

Figure 79: PRPDA-plot PD recorded in joint 2 at 6 kV at the end of the PD measurements in stage 2, at load cycling of 225 A.

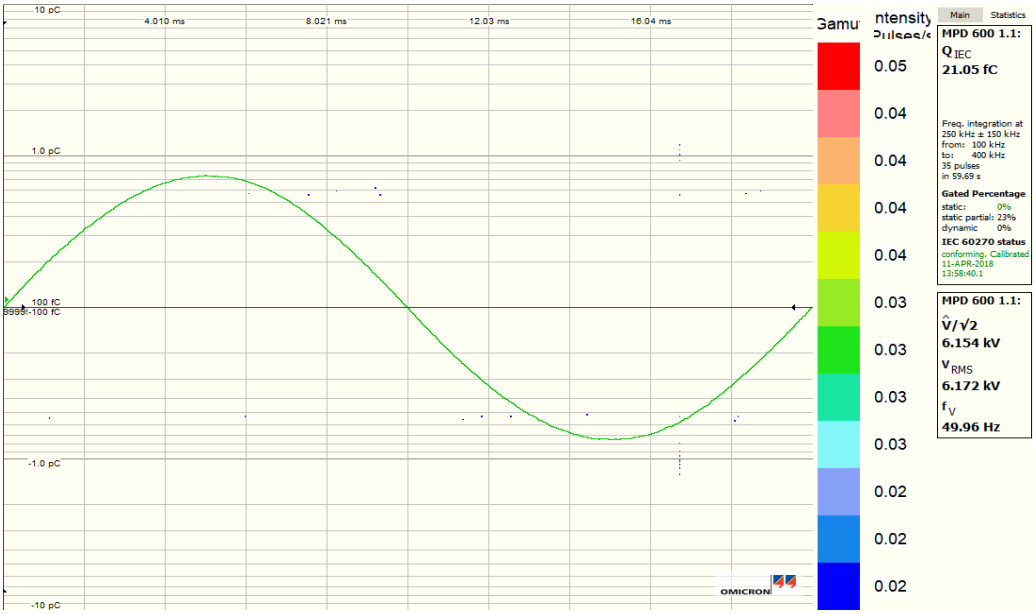

Figure 80: PRPDA-plot PD recorded in joint 2 at 6 kV at the end of the PD measurements in stage 2, at load cycling of 350 A.

G.3 Joint 3

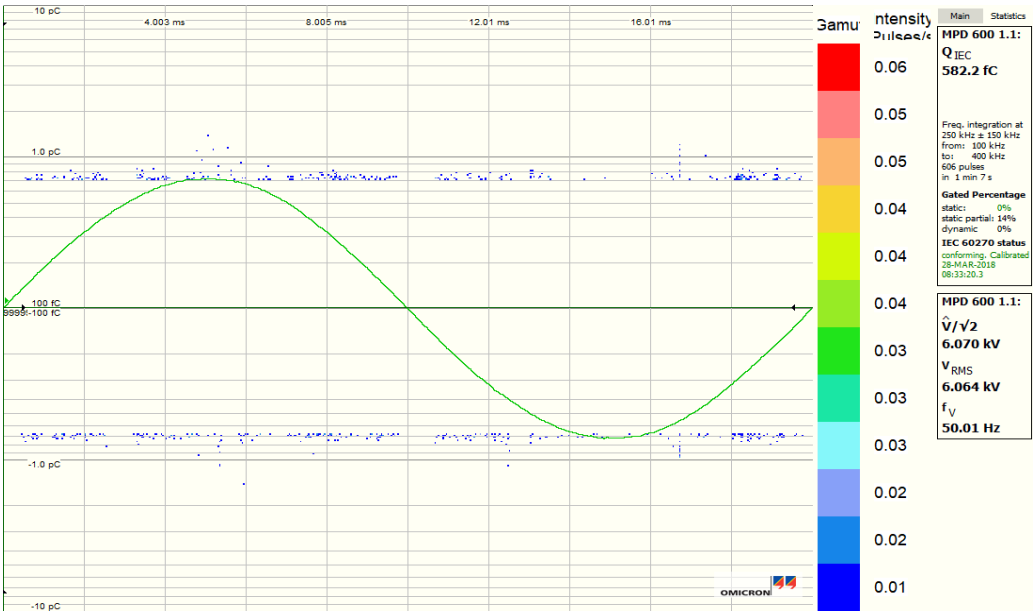

Figure 81: PRPDA-plot PD recorded in joint 3 at 6 kV at the end of the PD measurements in stage 2, at room temperature.

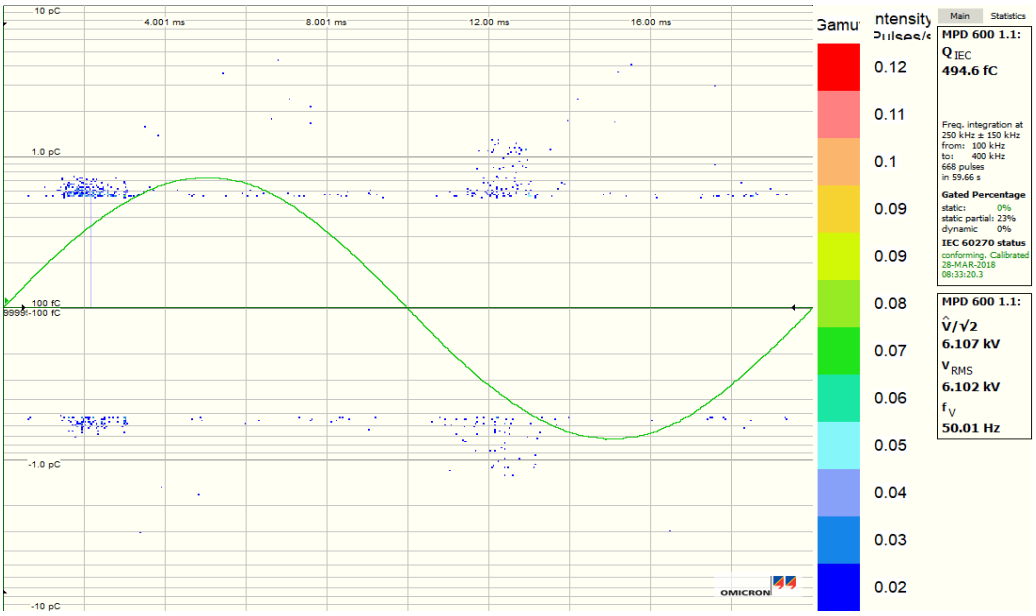

Figure 82: PRPDA-plot PD recorded in joint 3 at 6 kV at the end of the PD measurements in stage 2, at load cycling of 225 A.

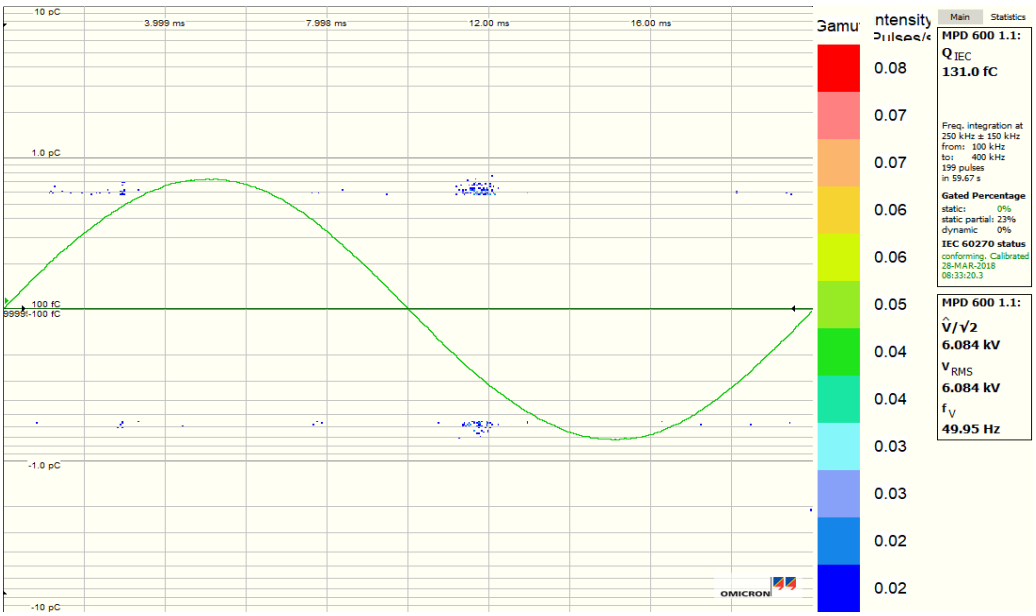

Figure 83: PRPDA-plot PD recorded in joint 3 at 6 kV at the end of the PD measurements in stage 2, at load cycling of 350 A.

Appendix H Weibull Plots of PDs Recorded during Cooling of the Test Objects

H.1 Joint 1

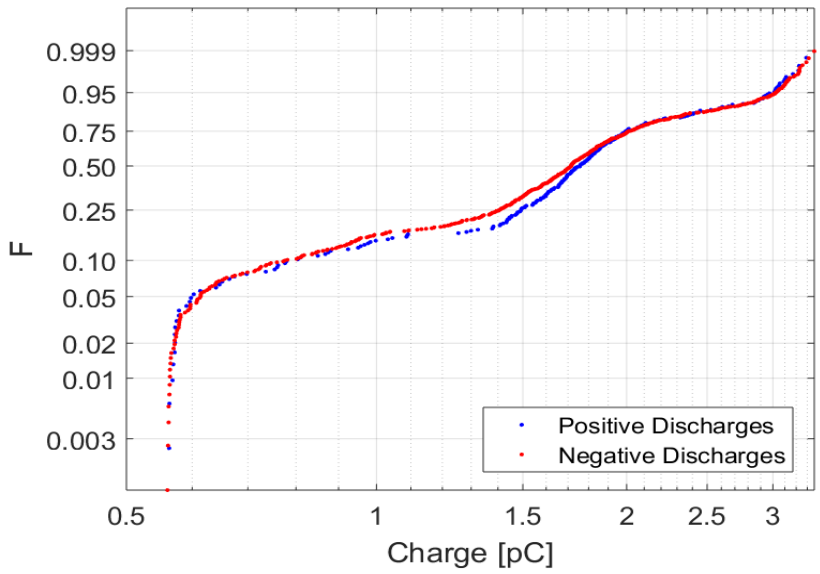

Figure 84: PD recorded in joint 1 at 6 kV, before load current was turned off. Estimated conductor temperature: 37 °C.

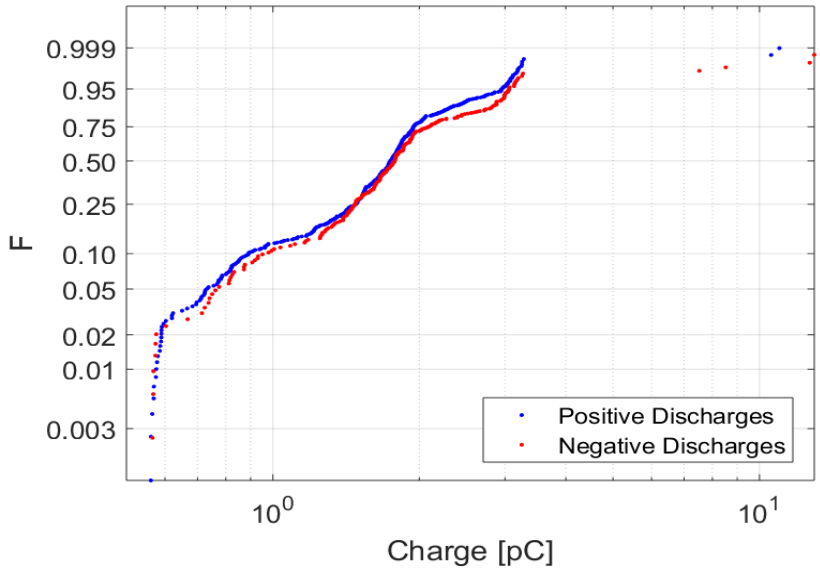

Figure 85: PD recorded in joint 1 at 6 kV, right after the load current was turned off. Estimated conductor temperature: 36.7 °C.

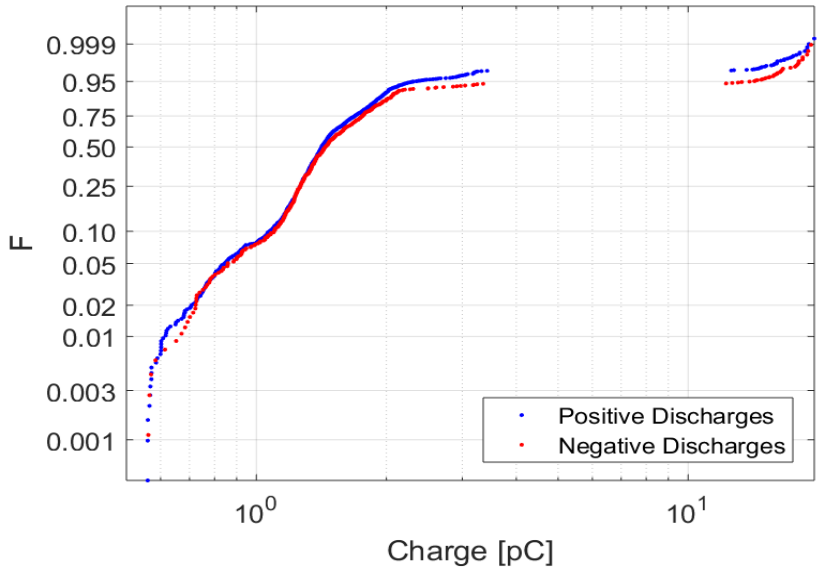

Figure 86: PD recorded in joint 1 at 6 kV, 8 minutes after the load current was turned off. Estimated conductor temperature: 34.9 °C.

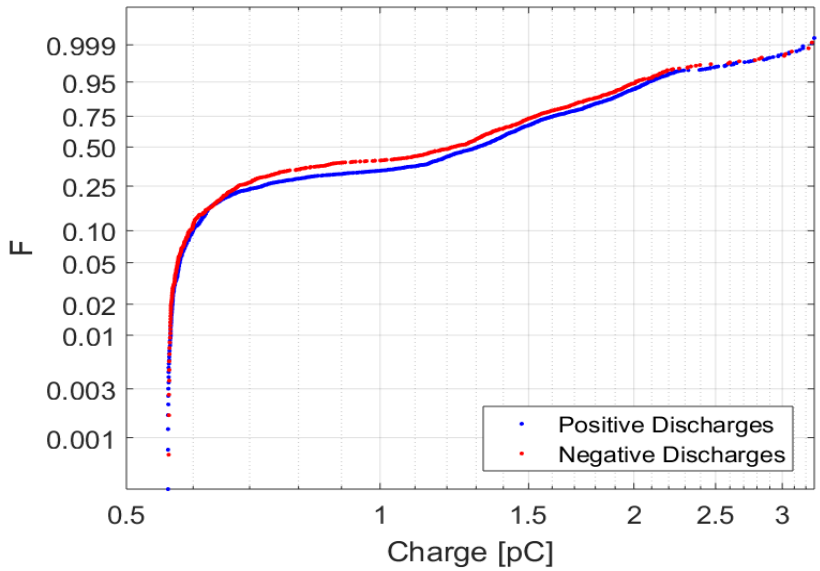

Figure 87: PD recorded in joint 1 at 6 kV, 16 minutes after the load current was turned off. Estimated conductor temperature: 33.7 °C.

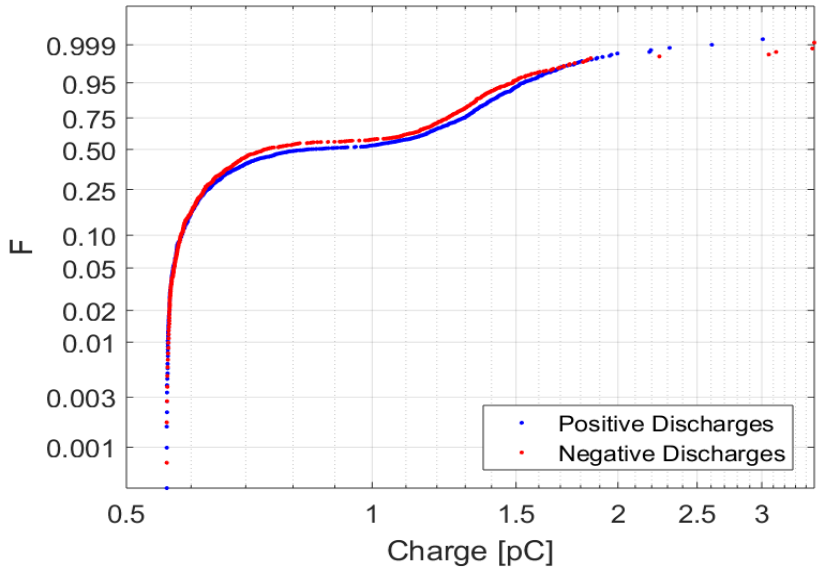

Figure 88: PD recorded in joint 1 at 6 kV, 24 minutes after the load current was turned off. Estimated conductor temperature: 32.7 °C.

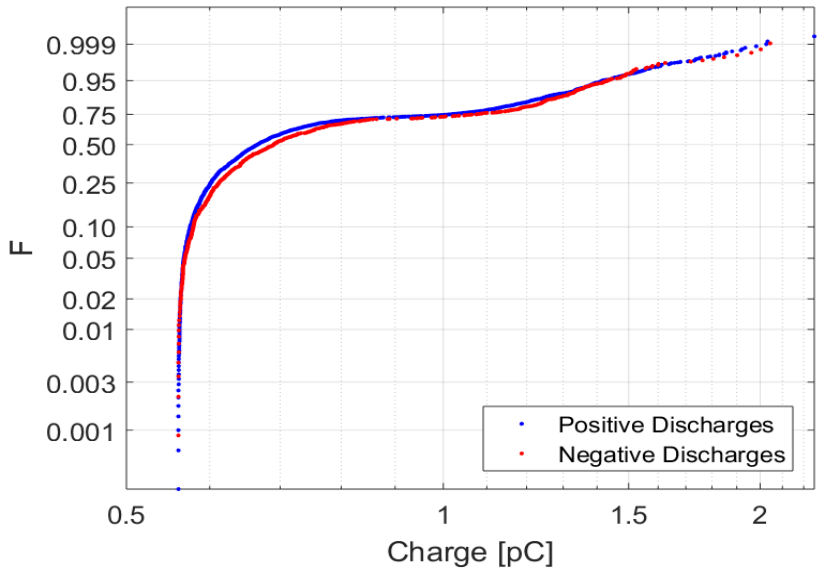

Figure 89: PD recorded in joint 1 at 6 kV, 32 minutes after the load current was turned off. Estimated conductor temperature: 31.8 °C.

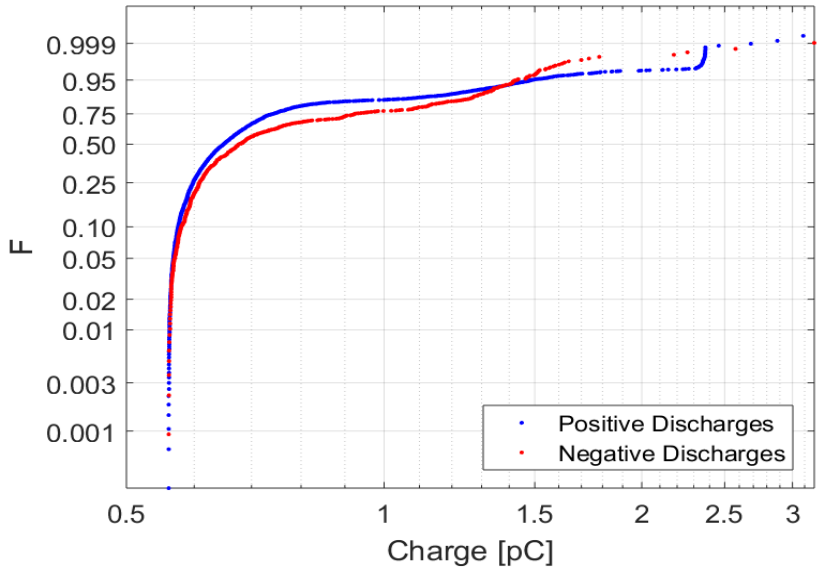

Figure 90: PD recorded in joint 1 at 6 kV, 40 minutes after the load current was turned off. Estimated conductor temperature: 31.2 °C.

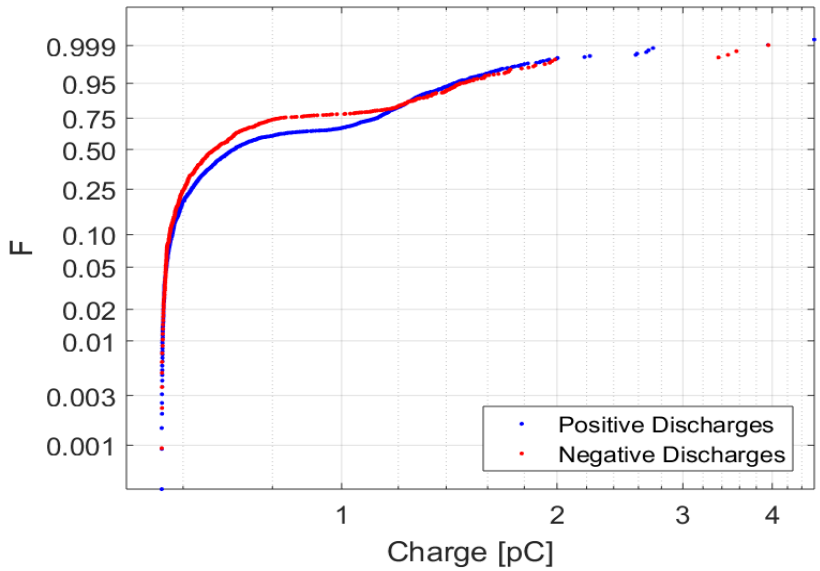

Figure 91: PD recorded in joint 1 at 6 kV, 48 minutes after the load current was turned off. Estimated conductor temperature: 30.6 °C.

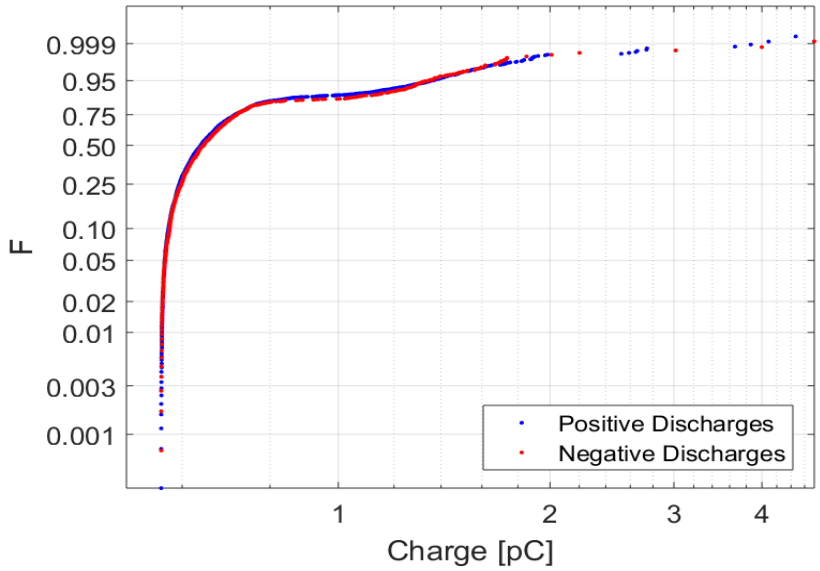

Figure 92: PD recorded in joint 1 at 6 kV, 56 minutes after the load current was turned off. Estimated conductor temperature: 30 °C.

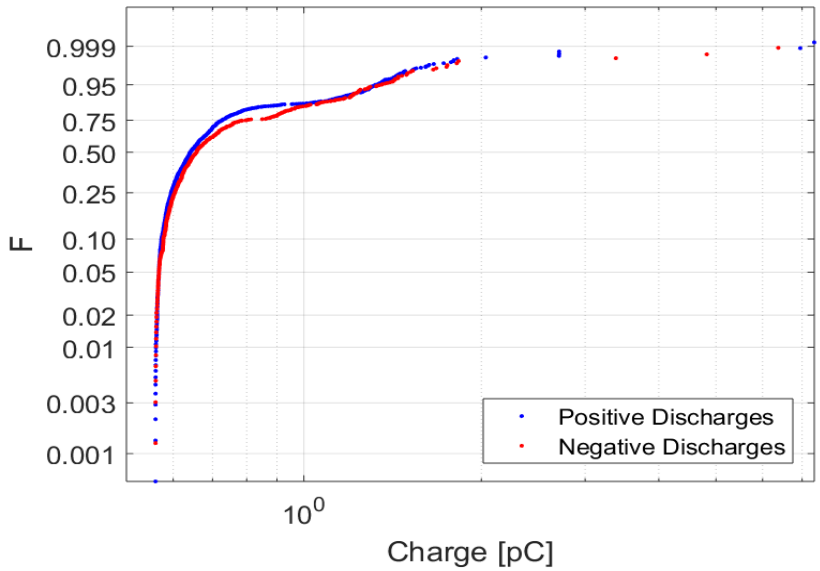

Figure 93: PD recorded in joint 1 at 6 kV, 1 hour and 4 minutes after the load current was turned off. Estimated conductor temperature: 29.3 °C.

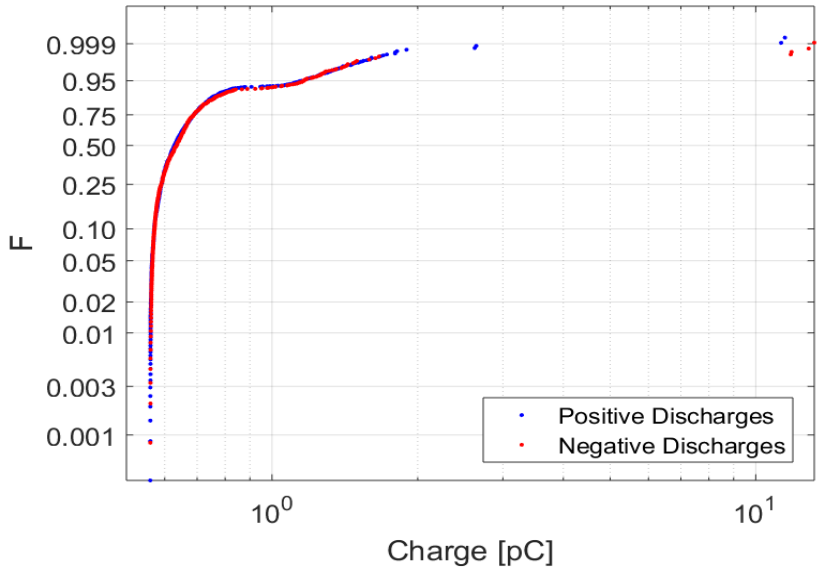

Figure 94: PD recorded in joint 1 at 6 kV, 1 hour and 12 minutes after the load current was turned off. Estimated conductor temperature: 28.8 °C.

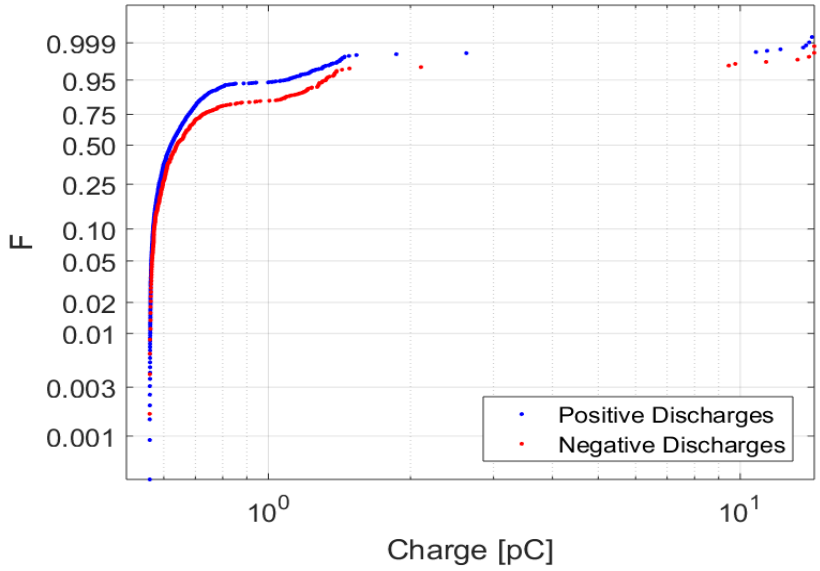

Figure 95: PD recorded in joint 1 at 6 kV, 1 hour and 20 minutes after the load current was turned off. Estimated conductor temperature: 28.2 °C.

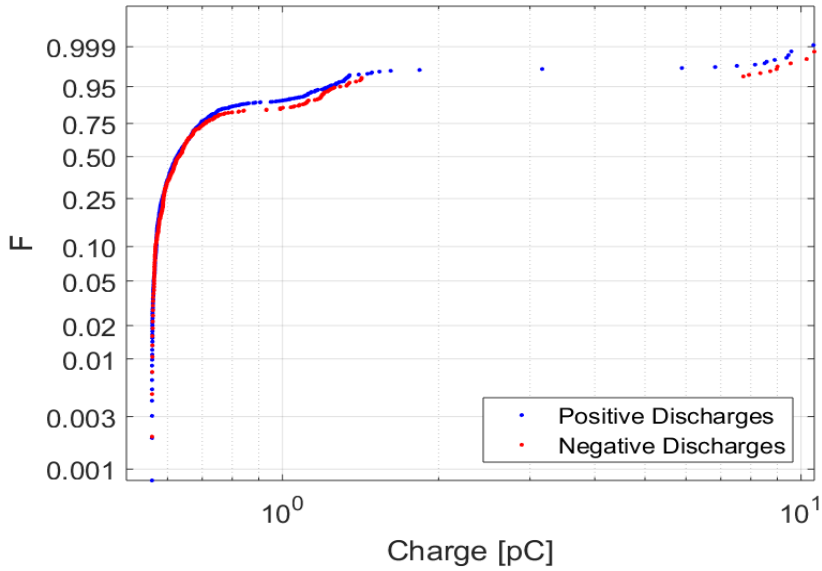

Figure 96: PD recorded in joint 1 at 6 kV, 1 hour and 28 minutes after the load current was turned off. Estimated conductor temperature: 27.7 °C.

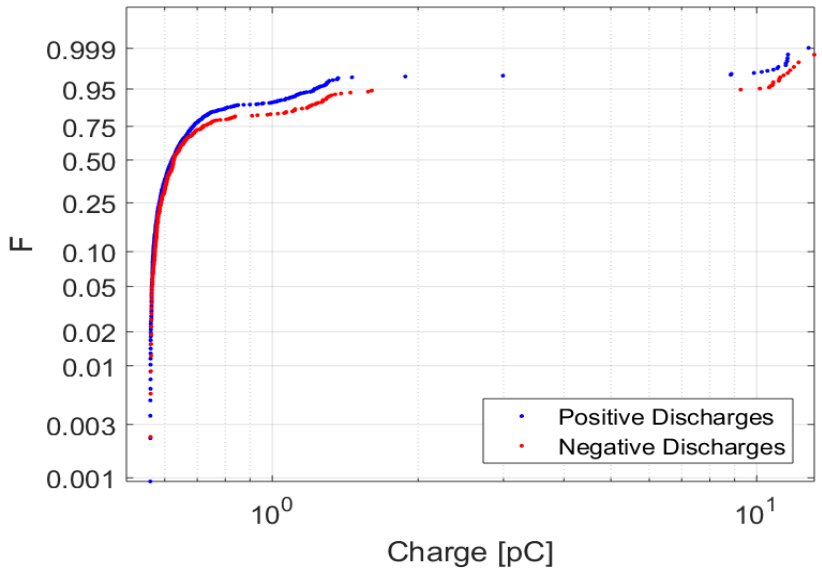

Figure 97: PD recorded in joint 1 at 6 kV, 1 hour and 36 minutes after the load current was turned off. Estimated conductor temperature: 27.3 °C.

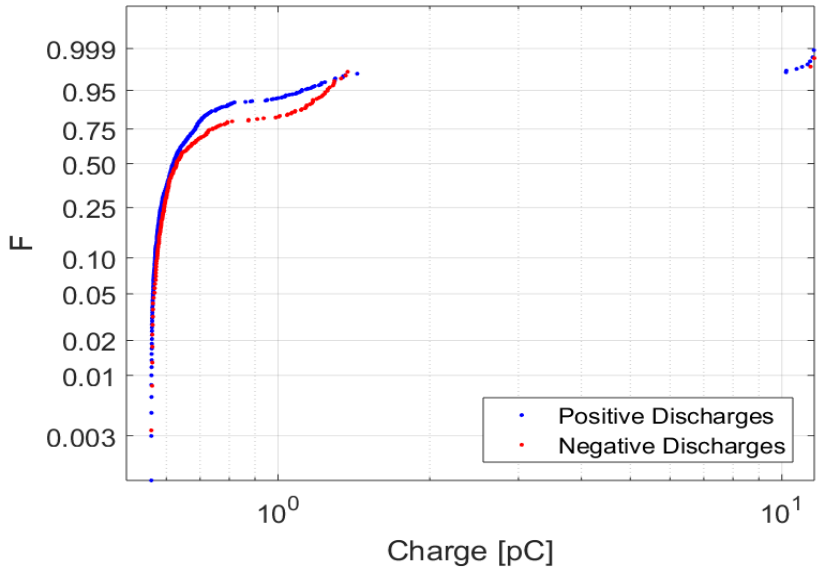

Figure 98: PD recorded in joint 1 at 6 kV, 1 hour and 44 minutes after the load current was turned off. Estimated conductor temperature: 26.9 °C.

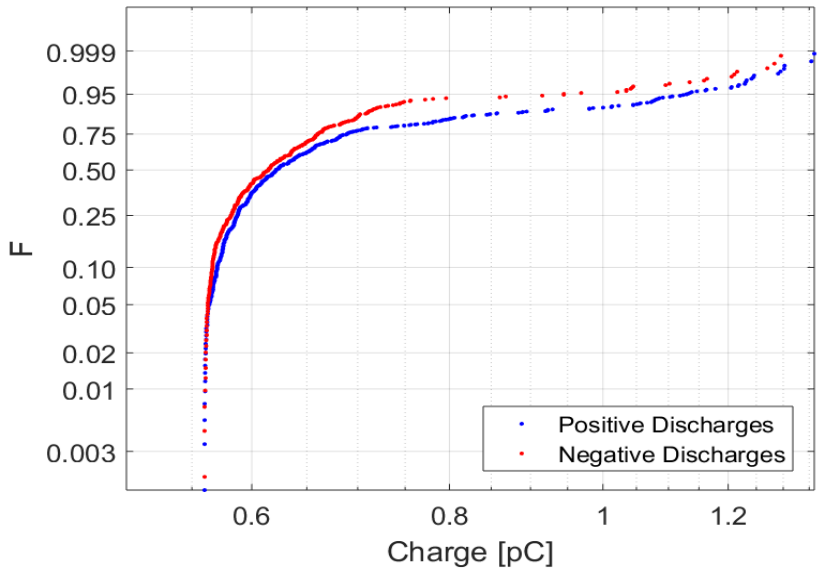

Figure 99: PD recorded in joint 1 at 6 kV, 1 hour and 52 minutes after the load current was turned off. Estimated conductor temperature: 26.6 °C.

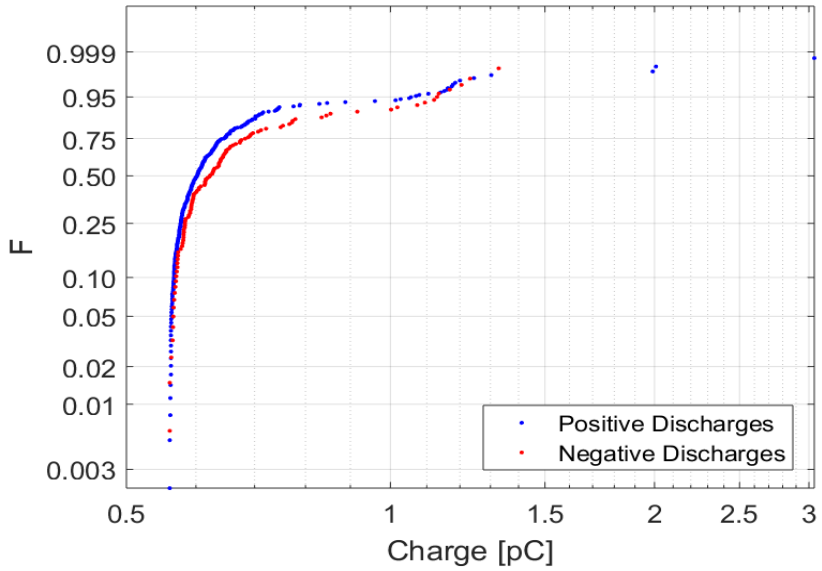

Figure 100: PD recorded in joint 1 at 6 kV, 2 hours after the load current was turned off. Estimated conductor temperature: 26.2 °C.

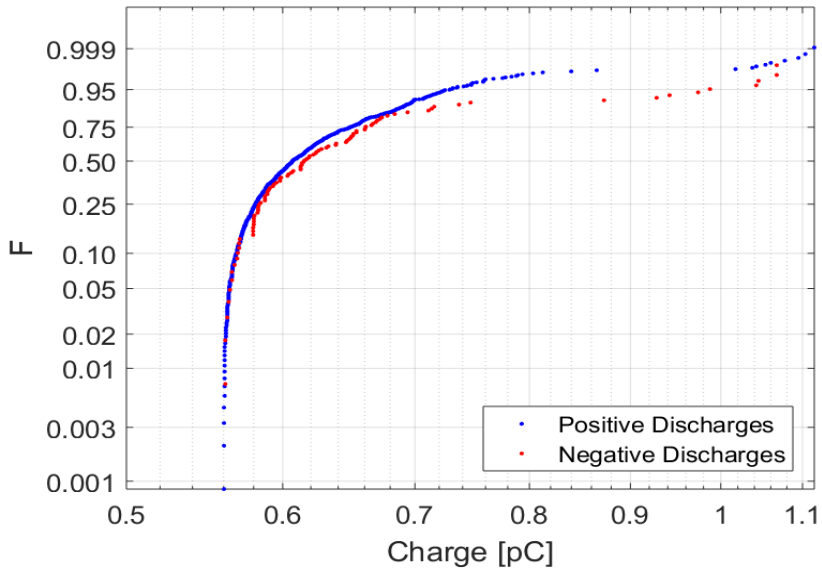

Figure 101: PD recorded in joint 1 at 6 kV, 2 hours and 8 minutes after the load current was turned off. Estimated conductor temperature: 25.8 °C.

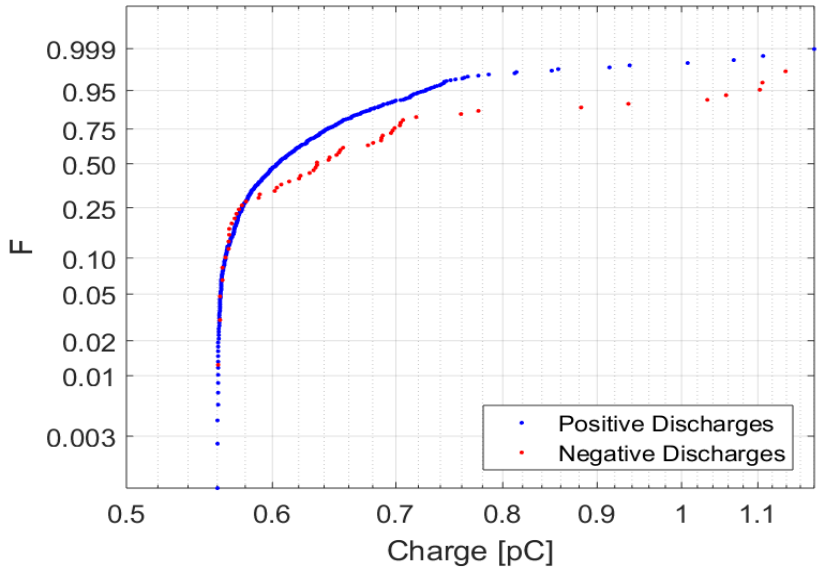

Figure 102: PD recorded in joint 1 at 6 kV, 2 hours and 16 minutes after the load current was turned off. Estimated conductor temperature: 25.4 °C.

H.2 Joint 2

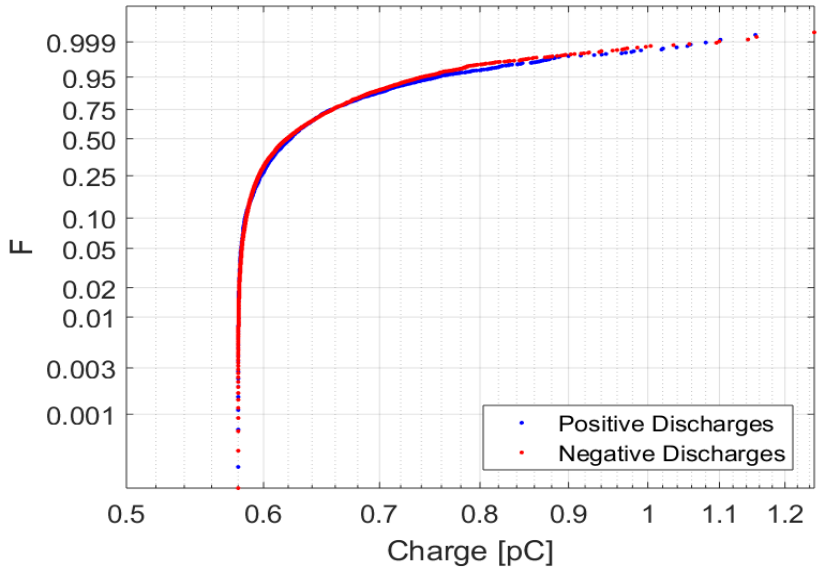

Figure 103: PD recorded in joint 2 at 6 kV, before load current was turned off. Estimated conductor temperature: 36.7 °C.

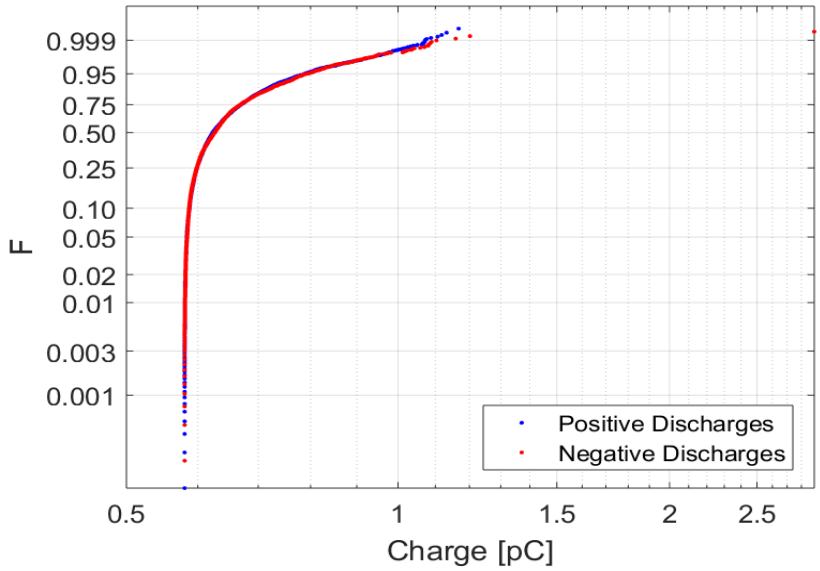

Figure 104: PD recorded in joint 2 at 6 kV, right after the load current was turned off. Estimated conductor temperature: 36.5 °C.

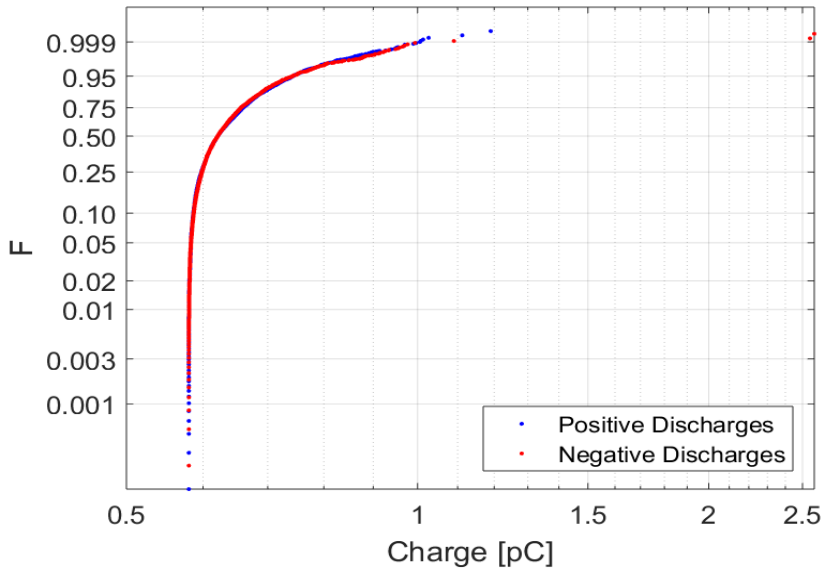

Figure 105: PD recorded in joint 2 at 6 kV, 8 minutes after the load current was turned off. Estimated conductor temperature: 35 °C.

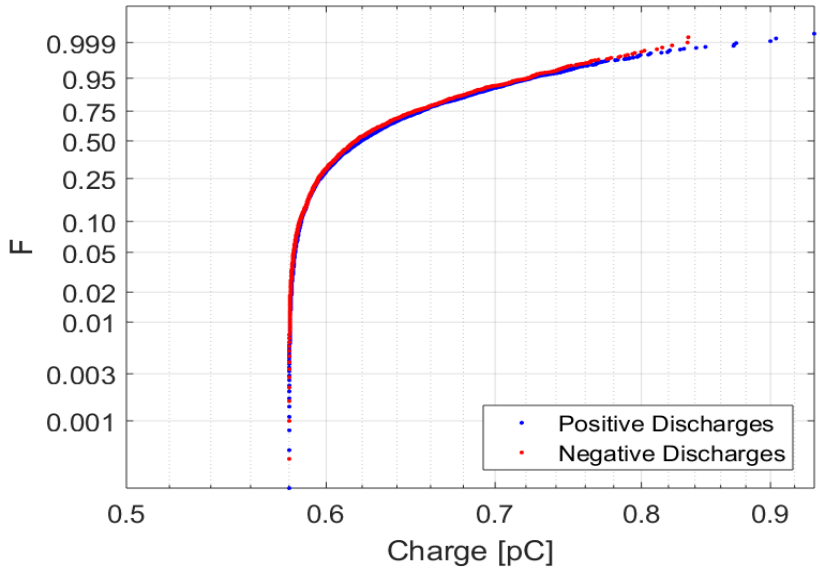

Figure 106: PD recorded in joint 2 at 6 kV, 16 minutes after the load current was turned off. Estimated conductor temperature: 33.9 °C.

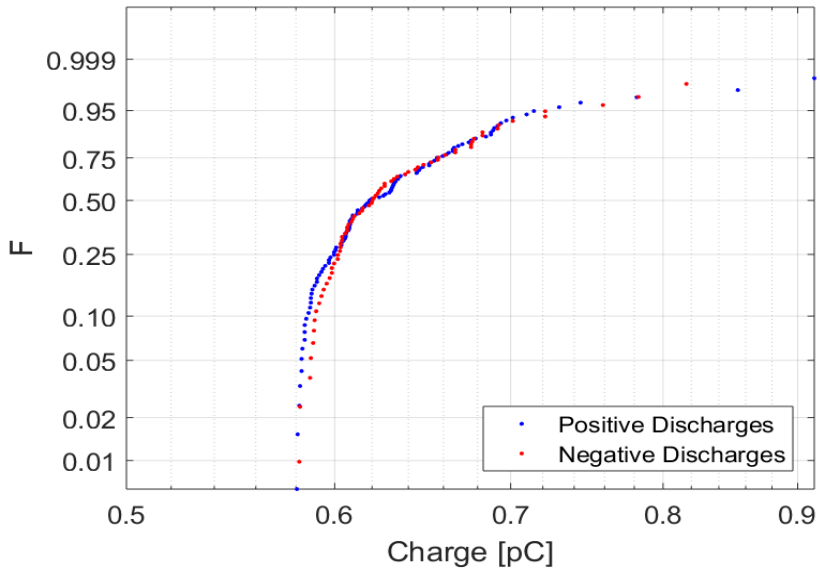

Figure 107: PD recorded in joint 2 at 6 kV, 24 minutes after the load current was turned off. Estimated conductor temperature: 32.8 °C.

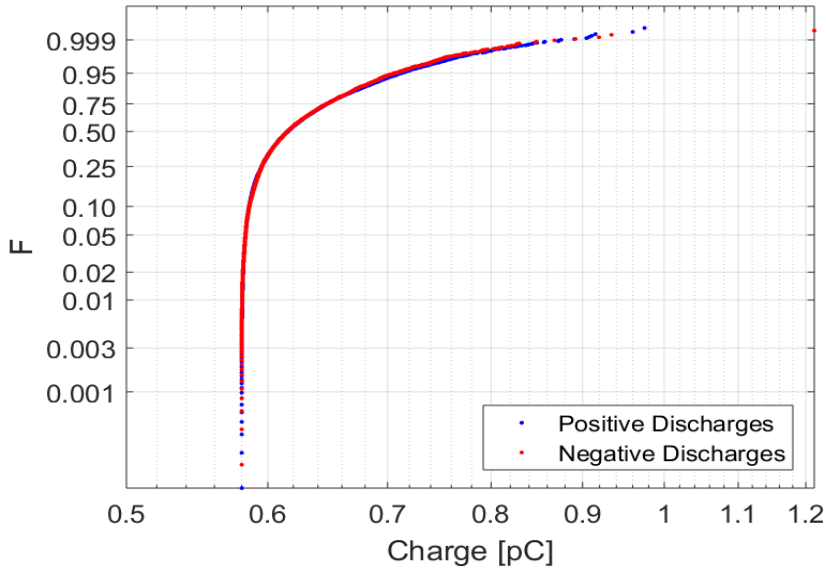

Figure 108: PD recorded in joint 2 at 6 kV, 32 minutes after the load current was turned off. Estimated conductor temperature: 31.8 °C.

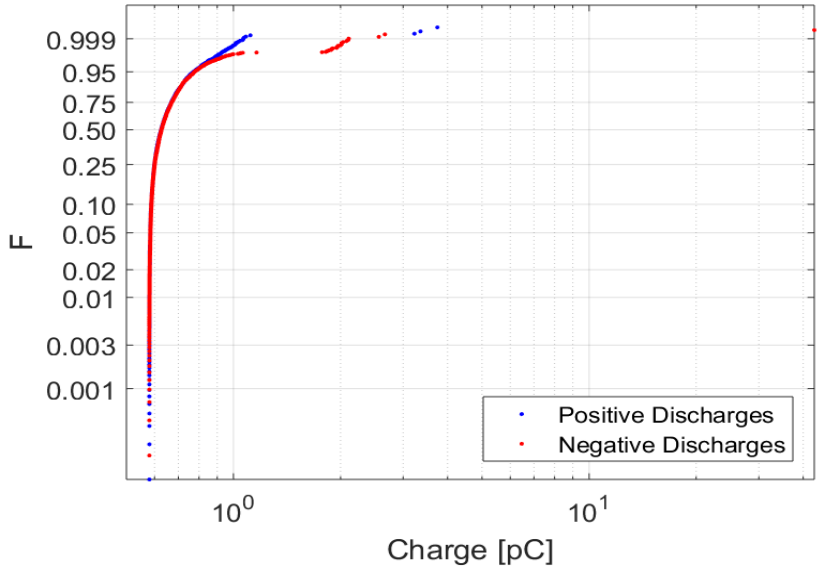

Figure 109: PD recorded in joint 2 at 6 kV, 40 minutes after the load current was turned off. Estimated conductor temperature: 31 °C.

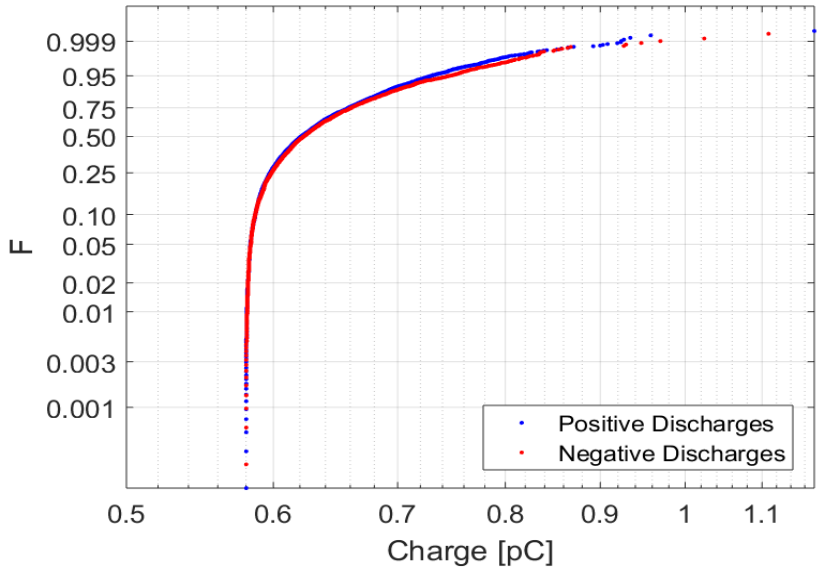

Figure 110: PD recorded in joint 2 at 6 kV, 48 minutes after the load current was turned off. Estimated conductor temperature: 30.3 °C.

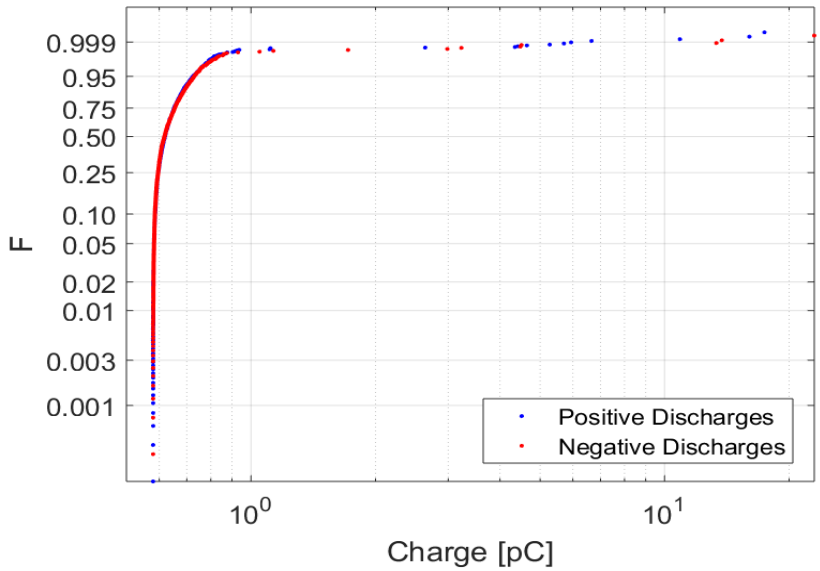

Figure 111: PD recorded in joint 2 at 6 kV, 56 minutes after the load current was turned off. Estimated conductor temperature: 29.6 °C.

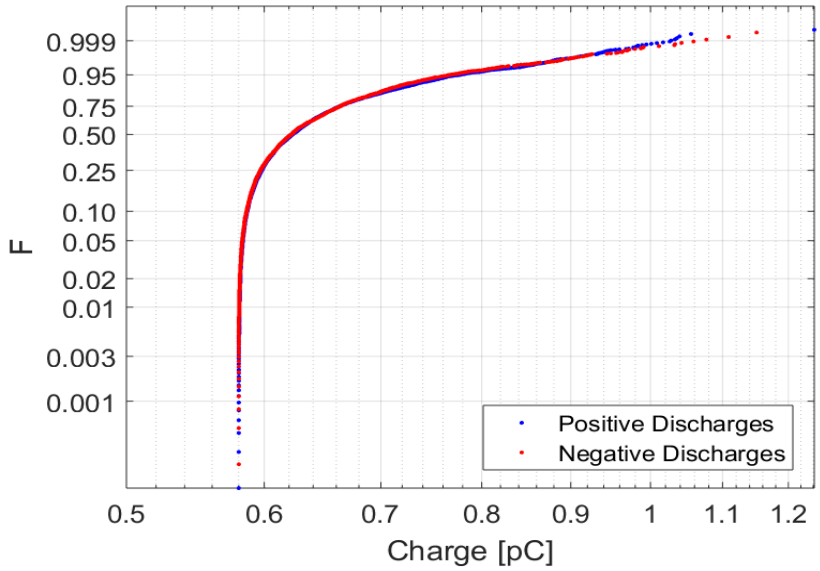

Figure 112: PD recorded in joint 2 at 6 kV, 1 hour and 4 minutes after the load current was turned off. Estimated conductor temperature: 28.9 °C.

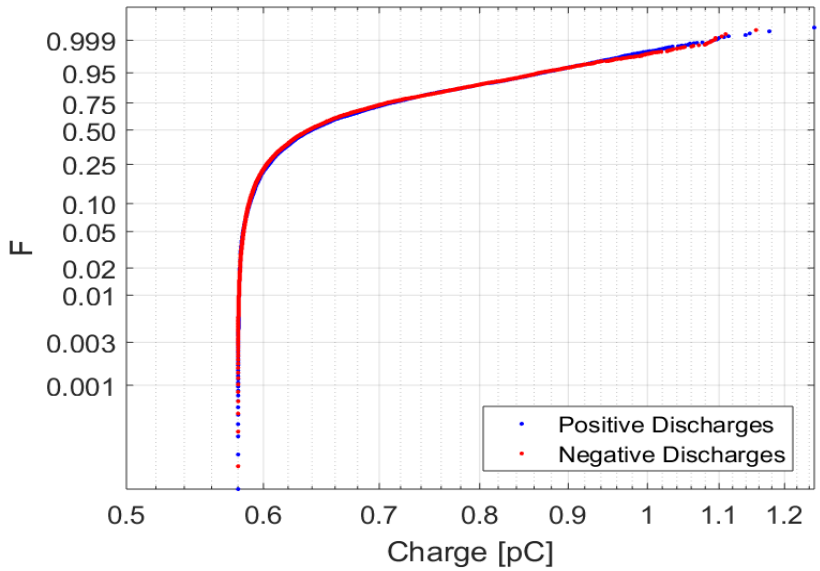

Figure 113: PD recorded in joint 2 at 6 kV, 1 hour and 12 minutes after the load current was turned off. Estimated conductor temperature: 28.3 °C.

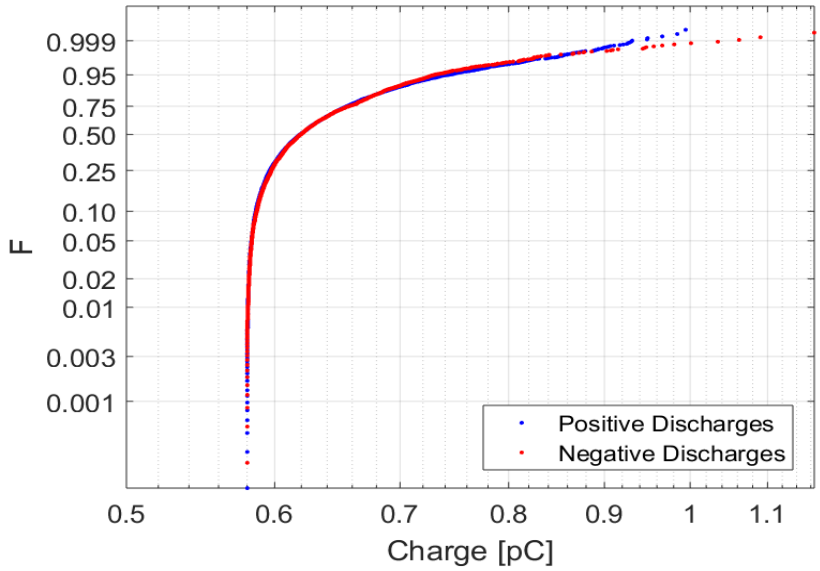

Figure 114: PD recorded in joint 2 at 6 kV, 1 hour and 20 minutes after the load current was turned off. Estimated conductor temperature: 27.7 °C.

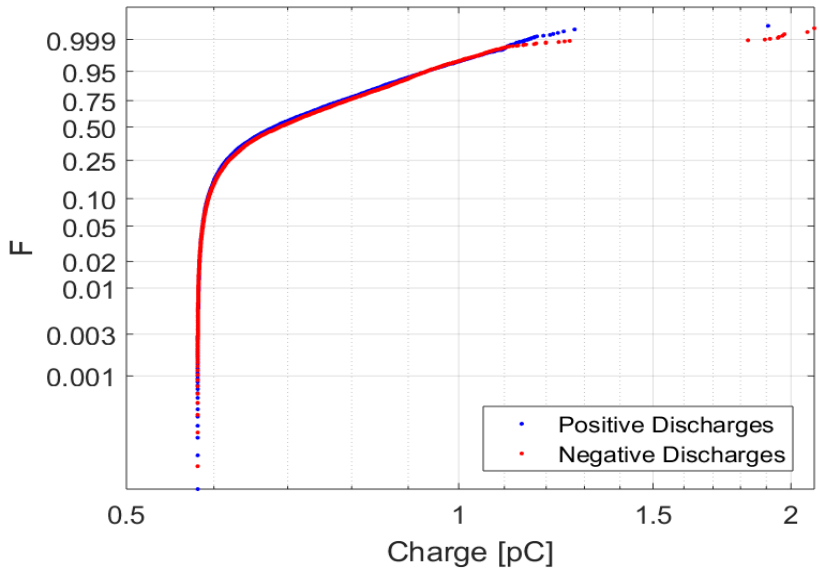

Figure 115: PD recorded in joint 2 at 6 kV, 1 hour and 28 minutes after the load current was turned off. Estimated conductor temperature: 27.3 °C.

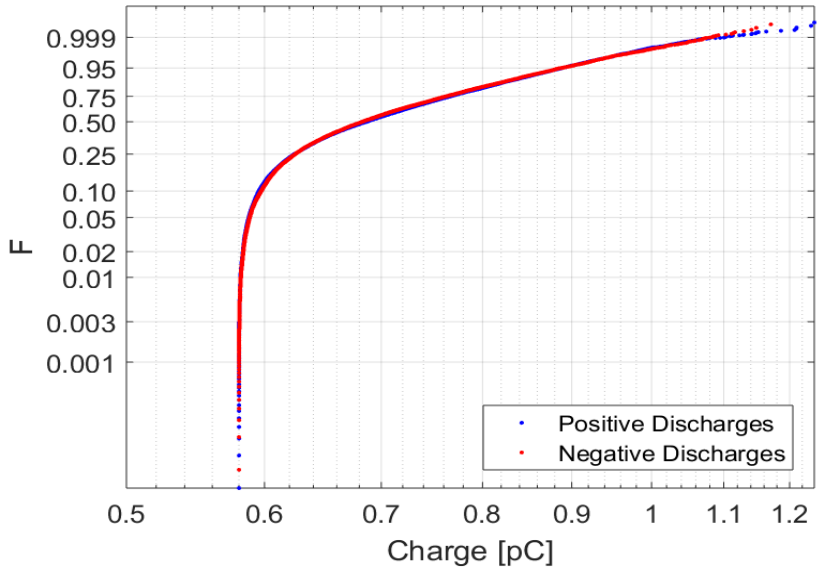

Figure 116: PD recorded in joint 2 at 6 kV, 1 hour and 36 minutes after the load current was turned off. Estimated conductor temperature: 26.9 °C.

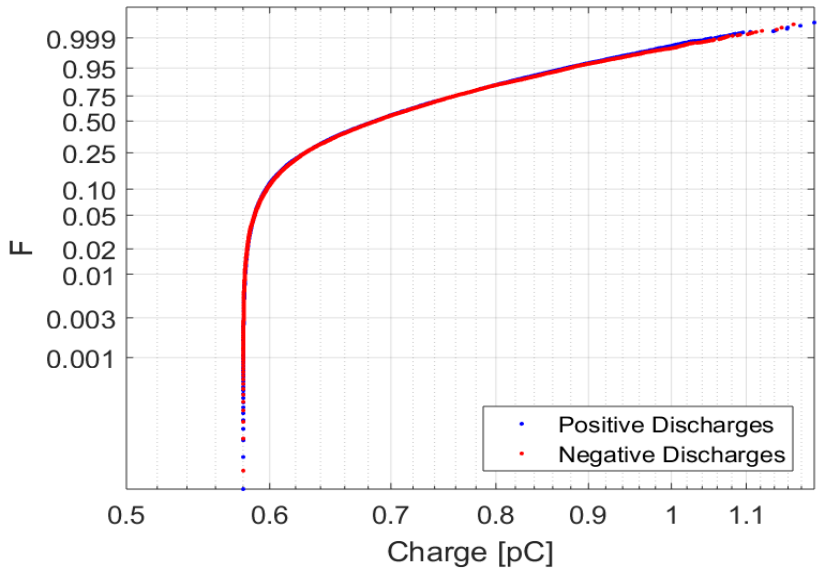

Figure 117: PD recorded in joint 2 at 6 kV, 1 hour and 44 minutes after the load current was turned off. Estimated conductor temperature: 26.4 °C.

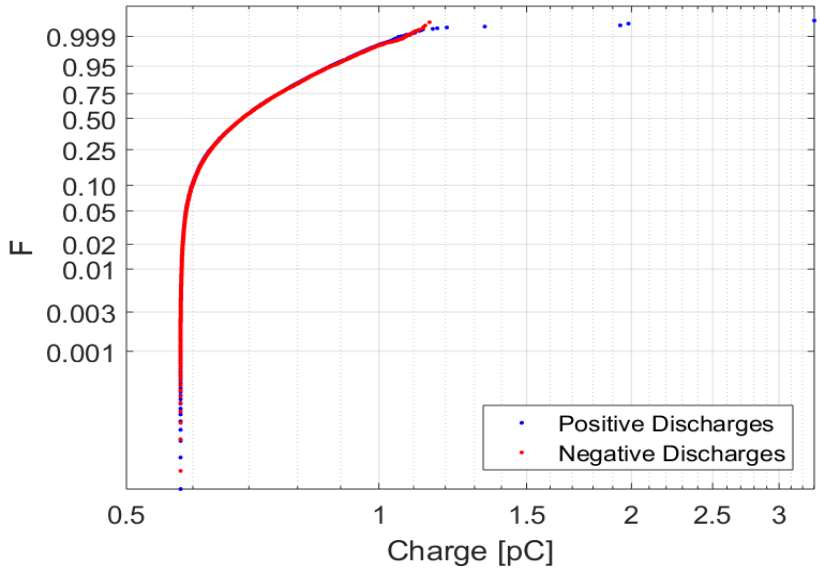

Figure 118: PD recorded in joint 2 at 6 kV, 1 hour and 52 minutes after the load current was turned off. Estimated conductor temperature: 26.1 °C.

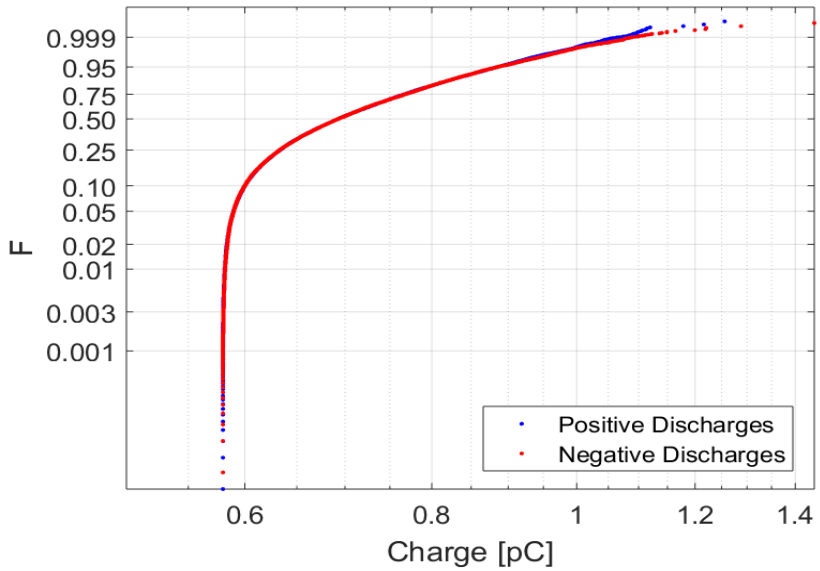

Figure 119: PD recorded in joint 2 at 6 kV, 2 hours after the load current was turned off. Estimated conductor temperature: 25.7 °C.

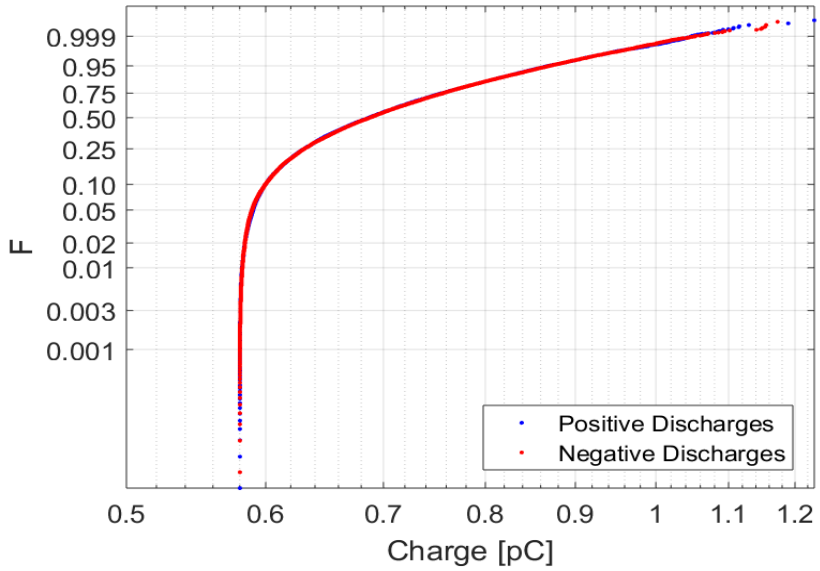

Figure 120: PD recorded in joint 2 at 6 kV, 2 hours and 8 minutes after the load current was turned off. Estimated conductor temperature: 25.4 °C.

H.3 Joint 3

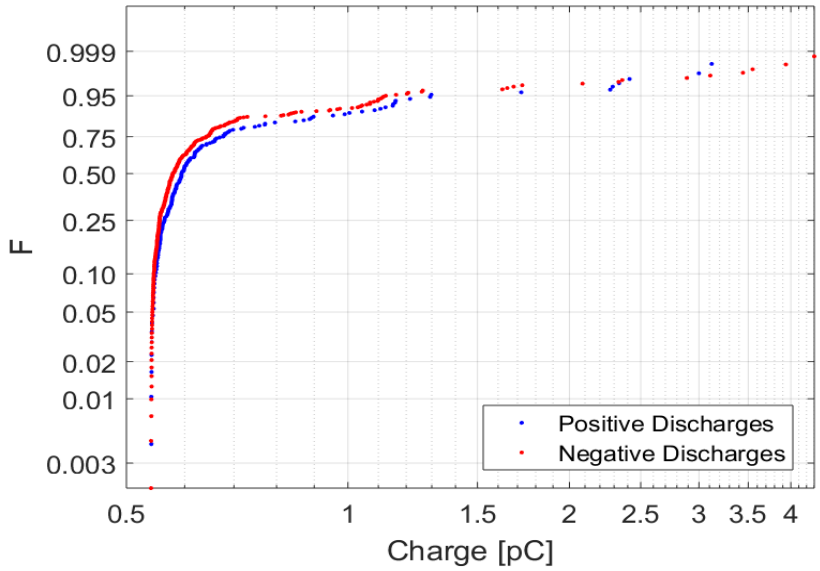

Figure 121: PD recorded in joint 3 at 6 kV, before load current was turned off. Estimated conductor temperature: 37 °C.

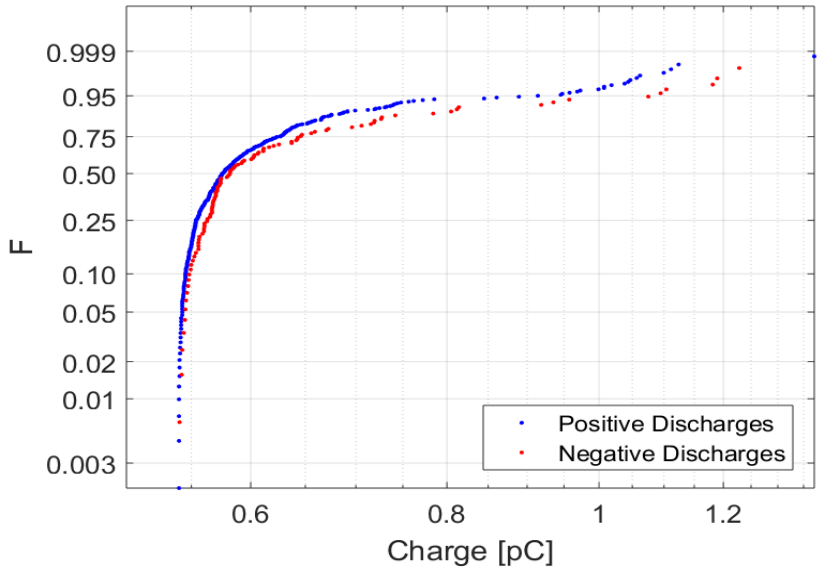

Figure 122: PD recorded in joint 3 at 6 kV, right after the load current was turned off. Estimated conductor temperature: 36.7 °C.

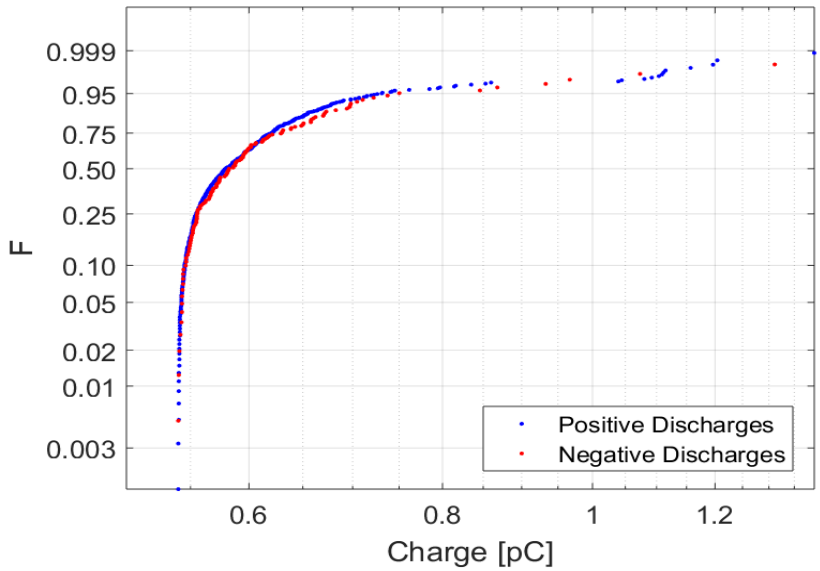

Figure 123: PD recorded in joint 3 at 6 kV, 8 minutes after the load current was turned off. Estimated conductor temperature: 35 °C.

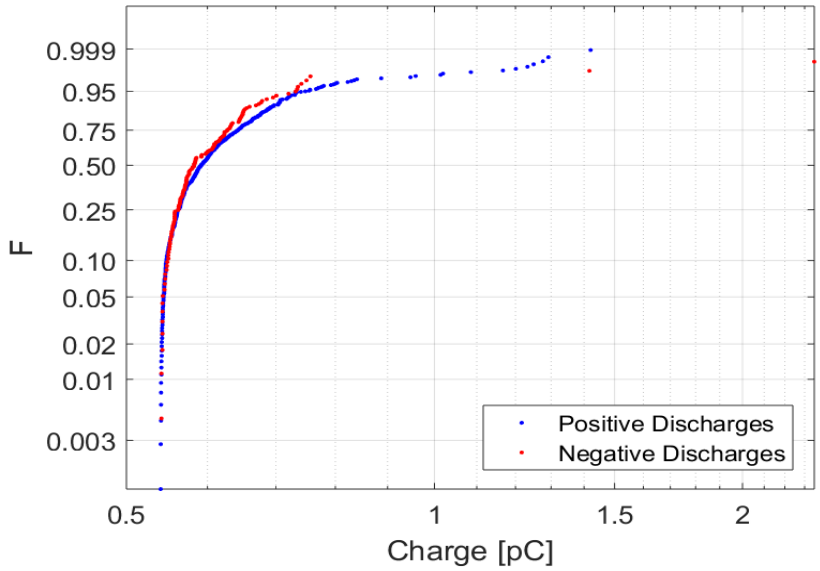

Figure 124: PD recorded in joint 3 at 6 kV, 16 minutes after the load current was turned off. Estimated conductor temperature: 33.8 °C.

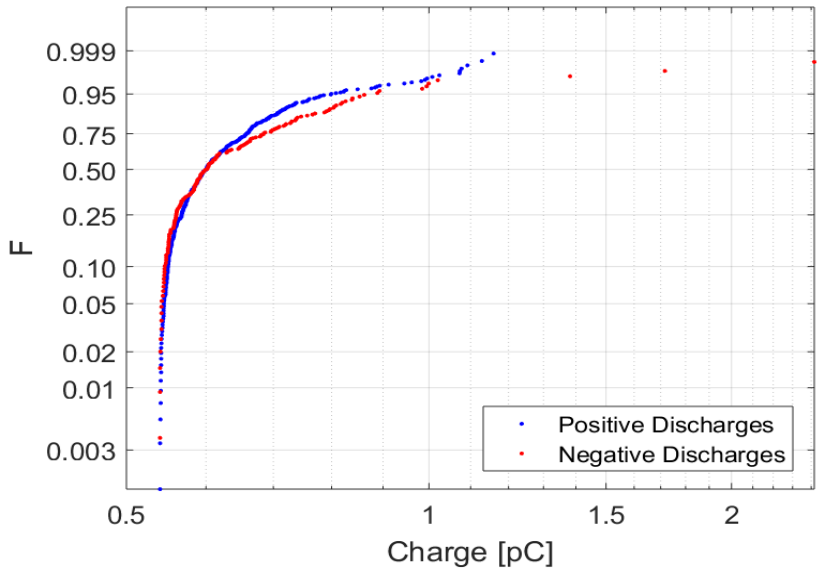

Figure 125: PD recorded in joint 3 at 6 kV, 24 minutes after the load current was turned off. Estimated conductor temperature: 32.7 °C.

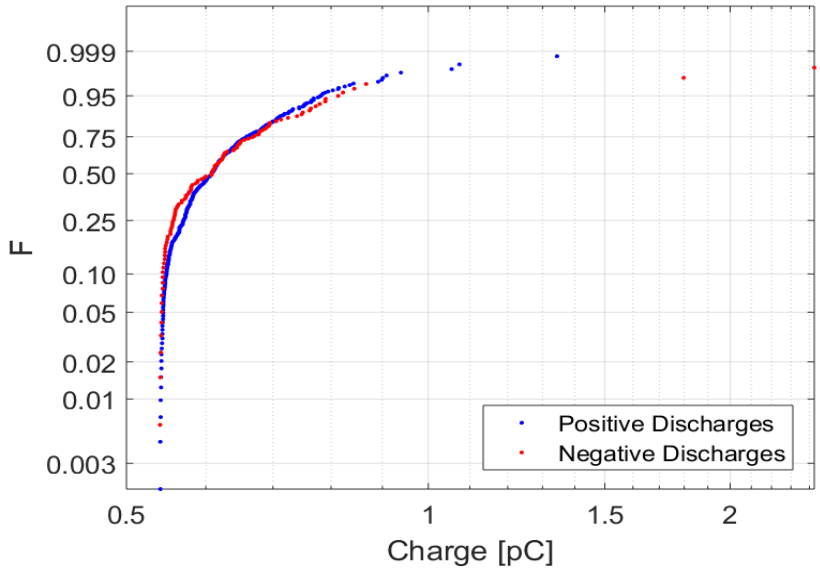

Figure 126: PD recorded in joint 3 at 6 kV, 32 minutes after the load current was turned off. Estimated conductor temperature: 31.8 °C.

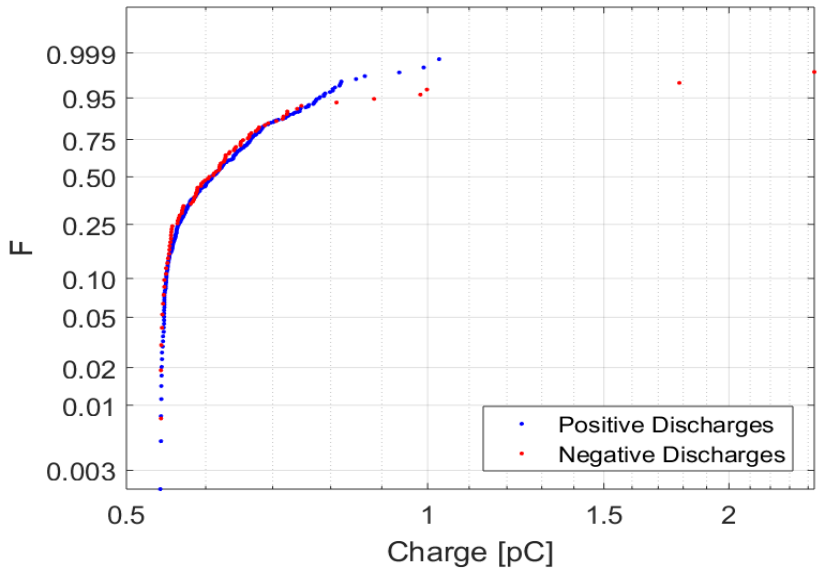

Figure 127: PD recorded in joint 3 at 6 kV, 40 minutes after the load current was turned off. Estimated conductor temperature: 31 °C.

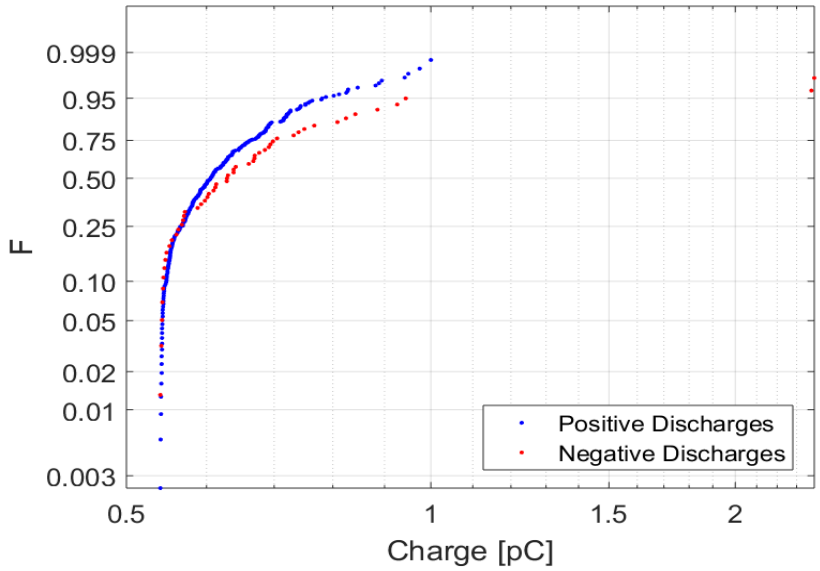

Figure 128: PD recorded in joint 3 at 6 kV, 48 minutes after the load current was turned off. Estimated conductor temperature: 30.2 °C.

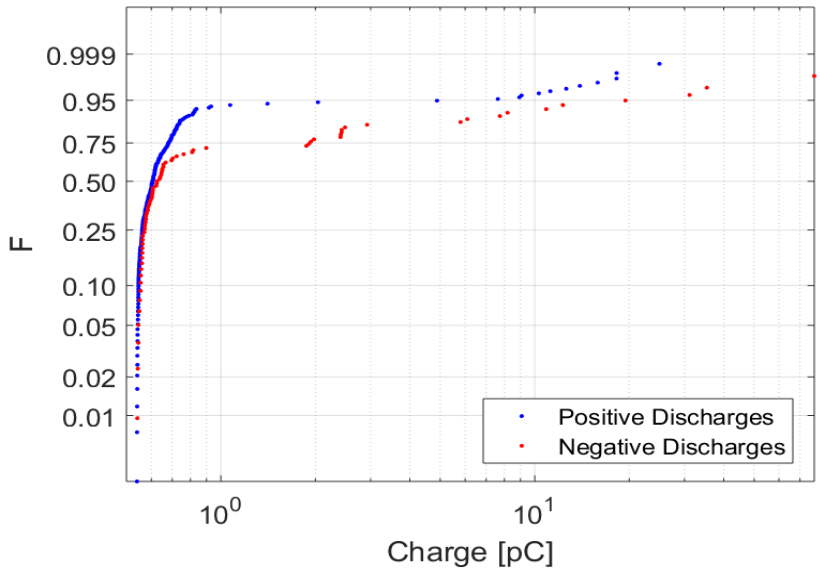

Figure 129: PD recorded in joint 3 at 6 kV, 56 minutes after the load current was turned off. Estimated conductor temperature: 29.6 °C.

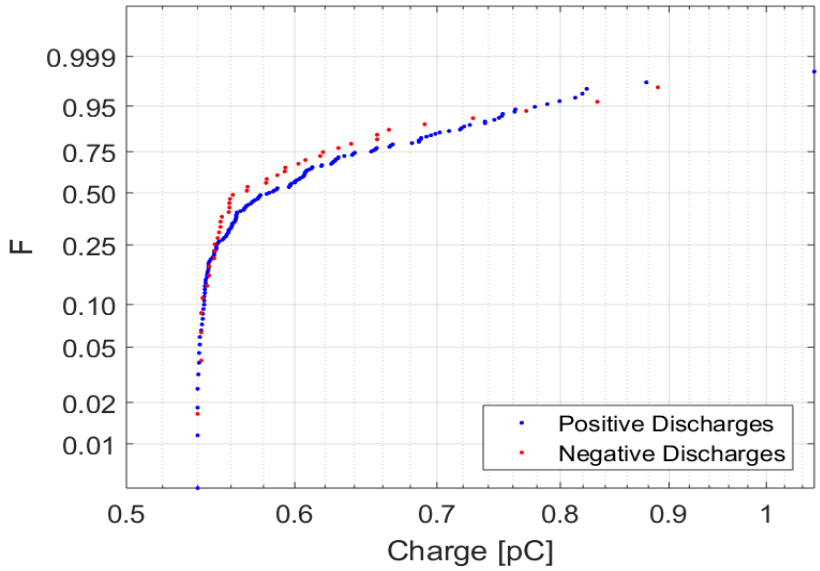

Figure 130: PD recorded in joint 3 at 6 kV, 1 hour and 4 minutes after the load current was turned off. Estimated conductor temperature: 29 °C.

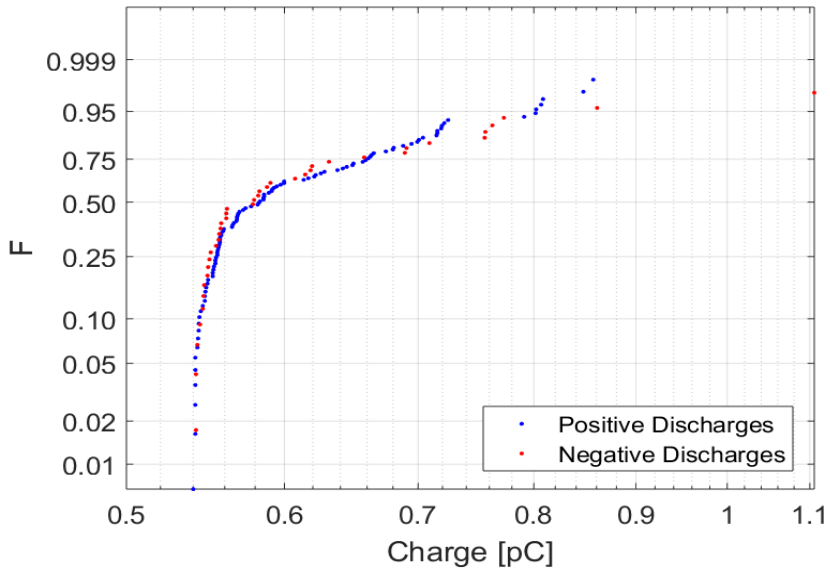

Figure 131: PD recorded in joint 3 at 6 kV, 1 hour and 12 minutes after the load current was turned off. Estimated conductor temperature: 28.4 °C.

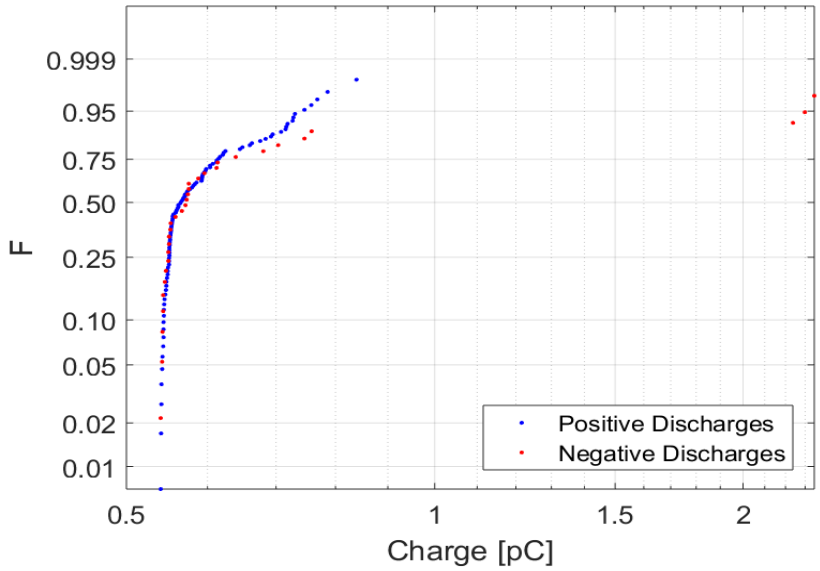

Figure 132: PD recorded in joint 3 at 6 kV, 1 hour and 20 minutes after the load current was turned off. Estimated conductor temperature: 27.9 °C.

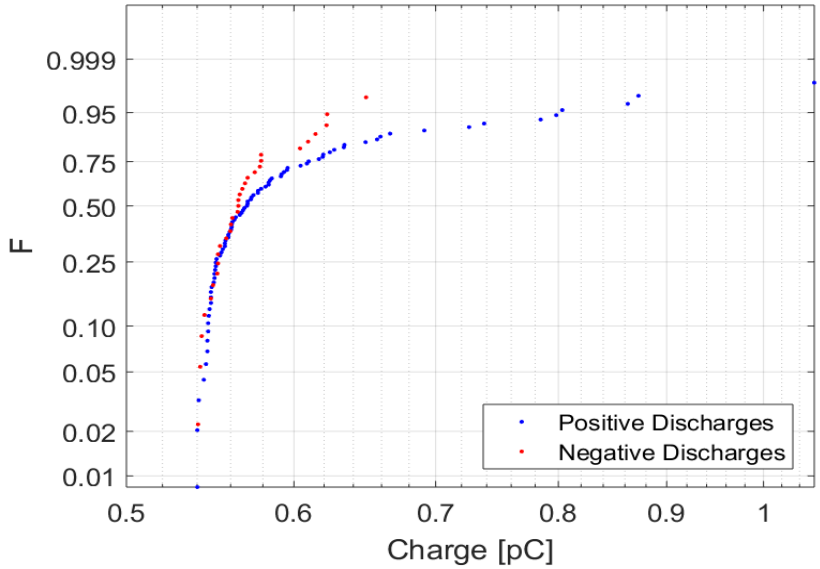

Figure 133: PD recorded in joint 3 at 6 kV, 1 hour and 28 minutes after the load current was turned off. Estimated conductor temperature: 27.4 °C.

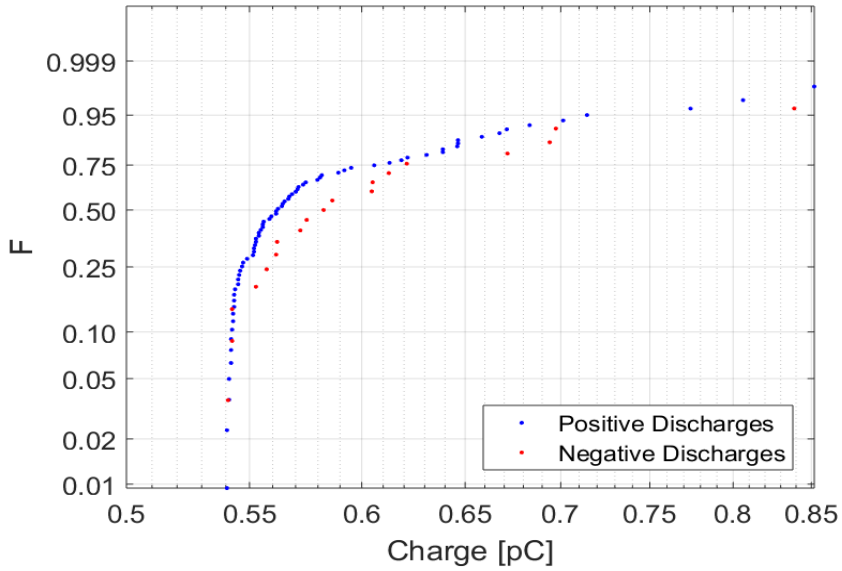

Figure 134: PD recorded in joint 3 at 6 kV, 1 hour and 36 minutes after the load current was turned off. Estimated conductor temperature: 27 °C.

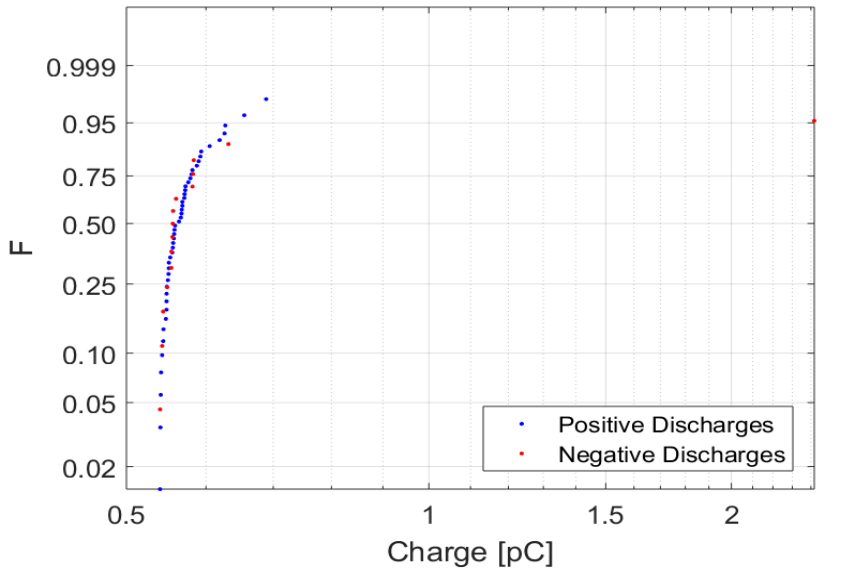

Figure 135: PD recorded in joint 3 at 6 kV, 1 hour and 44 minutes after the load current was turned off. Estimated conductor temperature: 26.6 °C.

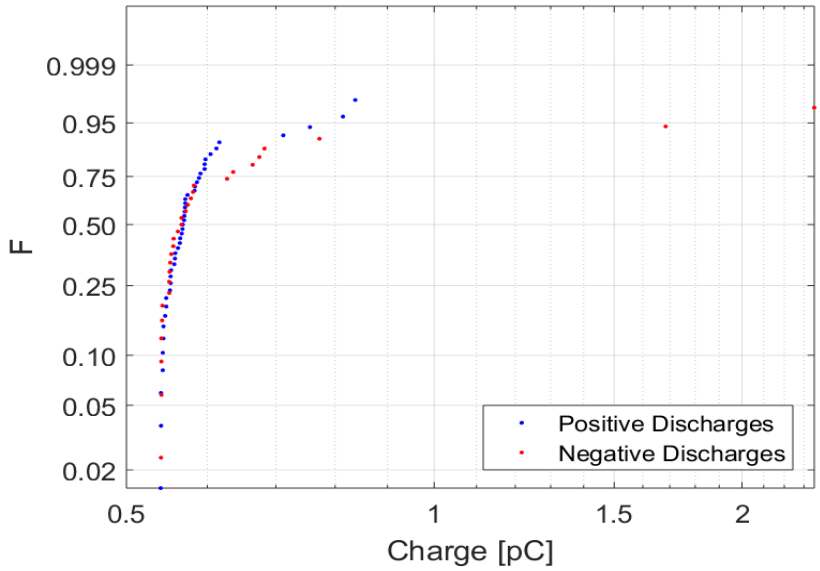

Figure 136: PD recorded in joint 3 at 6 kV, 1 hour and 52 minutes after the load current was turned off. Estimated conductor temperature: 26.2 °C.

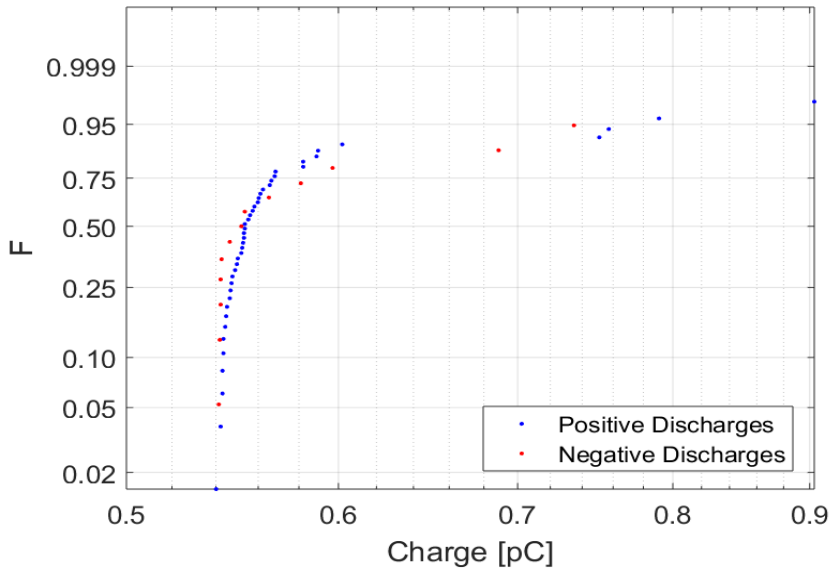

Figure 137: PD recorded in joint 3 at 6 kV, 2 hours after the load current was turned off. Estimated conductor temperature: 25.8 °C.

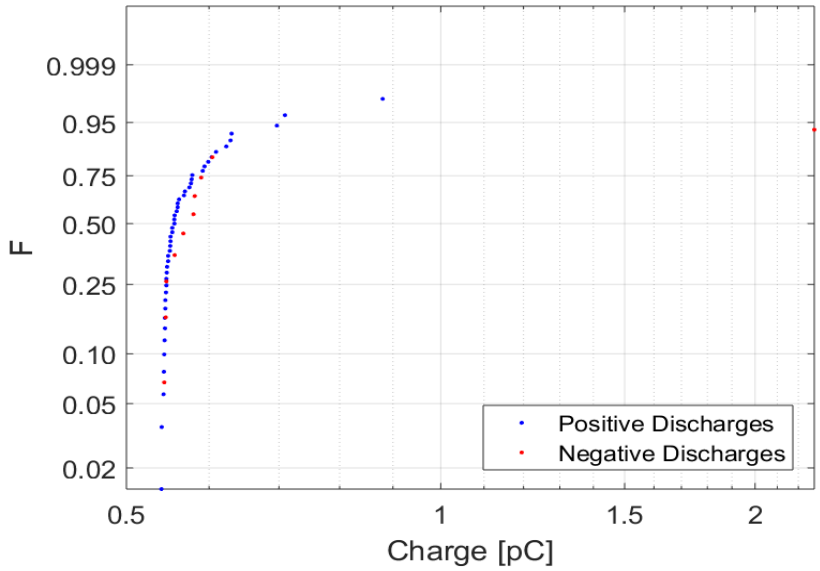

Figure 138: PD recorded in joint 3 at 6 kV, 2 hours and 8 minutes after the load current was turned off. Estimated conductor temperature: 25.5 °C.